

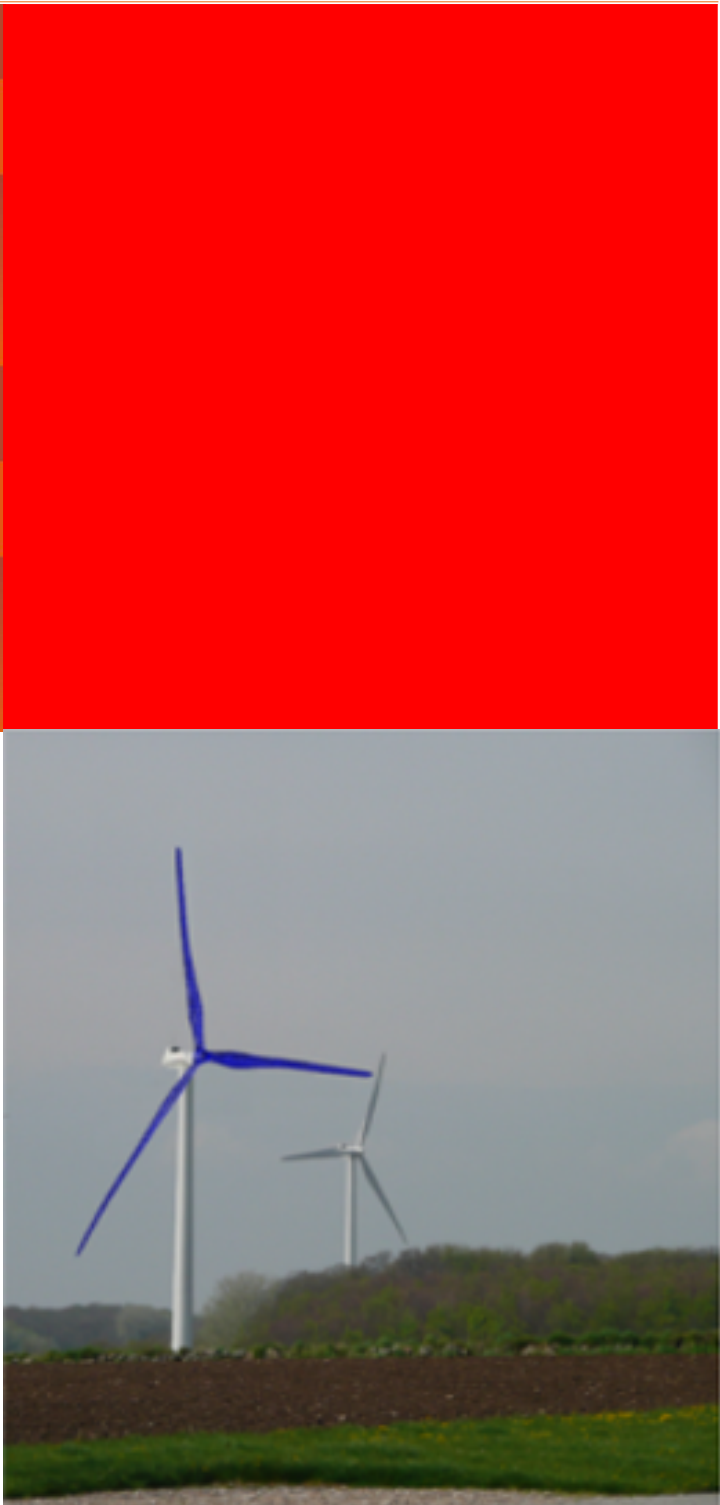
Aerodynamic and Aeroelastic Design of Low Wind Speed Wind Turbine Blades

Department of
Wind Energy
Master Report

C.A. Ramirez Gutierrez

DTU Wind Energy Master Thesis M-0055

17.08.2014



Title: Aerodynamic and Aeroelastic Design of Low Wind Speed Wind Turbine Blades

17.08.2014

Author: C.A. Ramirez Gutierrez

Department: European Wind Energy Master

Summary (max. 2000 characters):

This project is a continuation of the special course where the aerodynamic and aeroelastic performance of the reference wind turbine rotor provided by Mingyang has been made with the software of HAWC2 and Bladed. The final design of long blades for low wind speed wind turbine application is performed in this master project, based on the reference rotor with a rated power of 2.0MW and a diameter of 115 m..

Project Period:

2014.03.17 2014.08.17

ECTS:

30

Education:

Master of Science

Field:

Wind Energy

Supervisor:

Wen Zhong Shen

Supervisor (external):

W.A. Timmer

Peng Li

Wenfei Gao

Remarks:

This report is submitted as partial fulfilment of the requirements for graduation in the above education at the Technical University of Denmark.

Contract no.: -

Project no.:

DTU Wind Energy Master Thesis
M-0055

Sponsorship: -

CONACYT, Mexico

European Commission Erasmus Mundus

Ming Yang Wind Power ApS European Research Center

Front page:

Wind Turbine DTU image
Self-edit of photo by J. Davis

Pages: 143

Tables: 19

References: 72

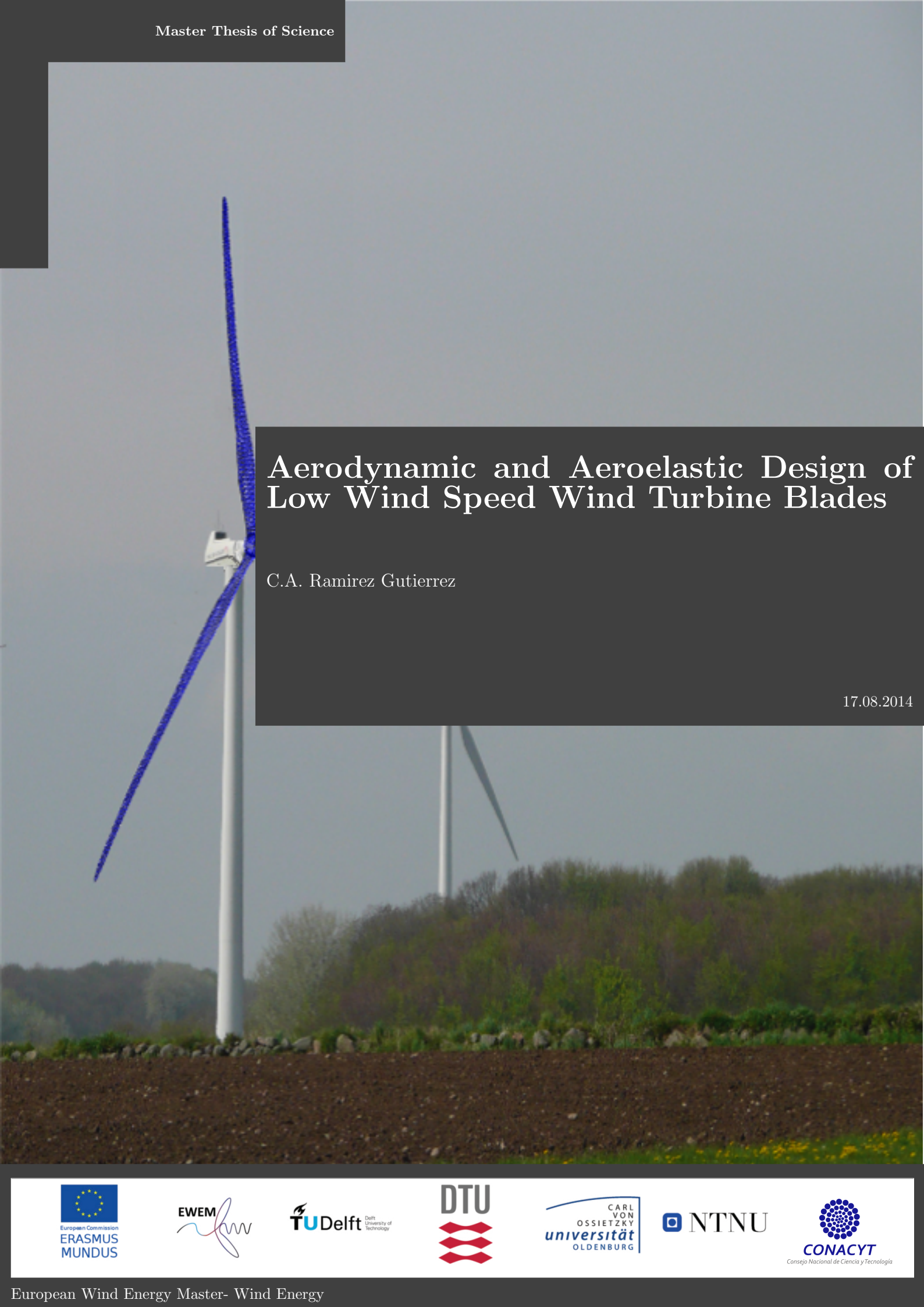
Danmarks Tekniske Universitet

DTU Vindenergi

Nils Koppels Allé

Bygning 403

2800 Kgs. Lyngby



Aerodynamic and Aeroelastic Design of Low Wind Speed Wind Turbine Blades

C.A. Ramirez Gutierrez

17.08.2014



Aerodynamic and Aeroelastic Design of Low Wind Speed Wind Turbine Blades

MASTER OF SCIENCE THESIS

For obtaining the degree of Master of Science in Engineering Wind Energy at Technical University of Denmark and in Aerospace Engineering at Delft University of Technology.

C.A. Ramirez Gutierrez

17.08.2014

European Wind Energy Master
Wind Energy Department, Technical University of Denmark
Faculty of Aerospace Engineering, Delft University of Technology



MINGYANG WIND POWER

The work in this thesis was supported by Mingyang Wind Power European RD Center ApS. Their cooperation is hereby gratefully acknowledged.



The master scholarship sponsors, who financially supported this venture, are thankfully acknowledged.



DTU Wind Energy
Department of Wind Energy

Copyright © C.A. Ramirez Gutierrez
All rights reserved.

EUROPEAN WIND ENERGY MASTER - EWEM
OF
ROTOR DESIGN TRACK

The undersigned hereby certify that they have read and recommend to the European Wind Energy Master - EWEM for acceptance a thesis entitled "**Aerodynamic and Aeroelastic Design of Low Wind Speed Wind Turbine Blades**" by **C.A. Ramirez Gutierrez** in partial fulfilment of the requirements for the degree of **Master of Science**.

Dated: 17.08.2014

Supervisor: _____
Shen, Wen Zhong of Technical University of Denmark

Supervisor: _____
Timmer, W.A. of Delft University of Technology

Reader: _____
Li, Peng of Ming Yang Windpower ApS

Reader: _____
Gao, Wenfei of Ming Yang Wind Power

Abstract

A large number of wind energy installations exist on rich wind resource sites. Nevertheless, estimates show that about 50% of the world's wind energy resource has a wind speed of $7\frac{m}{s}$ or less. For these low wind speed resource areas, low wind turbine technology is required. For this reason, this DTU Wind Energy master project, in cooperation with Ming Yang Wind Power European R&D Center ApS, looks into the design of a low wind speed wind turbine blade. The project's goal is to design a wind turbine blade for a *2 MW* wind turbine, with a rotor diameter of 115 meters. A site, in China, is also proposed for the wind turbine design.

The project focuses on the design of a blade for low wind speed wind turbine applications, on sites with a mean wind speed of about $7\frac{m}{s}$. The project includes several stages. First an introduction to the blade design and blade optimisation methods are introduced. Afterwards, the provided site in China is assessed and key parameters are selected for the next project stages. The next step, involves the wind turbine design, provided by Ming Yang Wind Power. This one is reviewed by doing an aerodynamic and aero-elastic performance analysis. With a cost of energy approach, a new wind turbine blade, for a wind turbine with a rated power of *2MW*, is designed. Finally, an aerodynamic and aero-elastic performance analysis of the new blade under different wind conditions is performed to assess its feasibility. The framework is carried out with HAWC2, developed by DTU, and compared to GH Bladed, at some of the design stages.

Acknowledgements

Joining this program was only possible with the sponsorship of the Erasmus Mundus European Commission and Conacyt. I am very thankful for this life opportunity. However, this was only possible through the acceptance to the EWEM master program. For this, I would like to first thank the EWEM board and coordinators of the rotor design track, Dr. Carlos Simão Ferreira and Dr. Jens Norkær Sørensen, for their support and vision. To plan and execute such an academic program for the first time, is a memorable task. DTU and TU Delft truly posses the tools and the people, that make this program a success.

I also would like to thank my supervisors, Wen Zhong Shen and Nando Timmer, for their support and patience. A new master program, like EWEM, requires a lot of support from both DTU and TU Delft supervisors. Peng Li, from Ming Yang Wind Power, was also very helpful providing information and also with the general logistics involved in this process.

Inspiring, supportive and talented colleagues and friends, were essential during this master program. Whether in DTU or in Delft, their example, work ethic and friendship, inspired me to improve in and outside student life.

I wish to thank my family for their never-ending love, support, inspiration and guidance. During these past 5 years in Europe, their hard work, example and sacrifice, have taught me important life lessons. Gracias mama, papa, Jonathan, Pierre y Stephanie! Special thanks to Hélène, my girlfriend, for her support and encouragement. Merci beaucoup!

Kgs. Lyngby, Denmark
17.08.2014

C.A. Ramirez Gutierrez

"I hear and I forget. I see and I remember. I do and I understand."
- Confucius -

Contents

Abstract	v
Acknowledgements	vii
List of Figures	xvi
List of Tables	xvii
Nomenclature	xix
1 Introduction	1
1.1 Motivation	1
2 State Of the Art	5
2.1 Optimization Methods	5
2.1.1 Optimization Tools	6
2.1.2 Optimization Formulation	7
2.2 Airfoil Design	7
2.3 Blade Design	9
2.3.1 Blade Element Momentum	9
2.3.2 Vortex Methods	12
2.3.3 Computational Fluid Dynamics	13
2.3.4 Blade Optimizations	14
2.4 Aeroelastic Design	15
2.4.1 HAWC2	17
2.4.2 GH Bladed	17
2.4.3 Aeroelastic Instabilities	18

2.4.4	Campbell Diagram	20
2.5	Site-specific Design	21
2.6	Cost of Energy Design	22
2.7	Discussion	22
3	Site Data	25
3.1	Site Description	25
3.2	Wind Resource	27
3.3	Wind Speed Probability	28
3.3.1	Hub Height Wind	30
3.4	Extreme Wind	31
3.4.1	Wind Turbine Class	32
4	Reference Wind Turbine	35
4.1	Wind Turbine Reference Values	36
4.2	Blade Geometry	37
4.3	Blade Properties	38
4.4	Tower Properties	40
4.4.1	Tower Clearance, Tilt & Cone Angle	41
4.5	Wind Turbine Performance, GH Bladed	42
4.6	Campbell Diagram	44
4.7	Summary	46
5	Aerodynamic Design	47
5.1	Objective Function	47
5.2	Constraints	50
5.2.1	Rotor Diameter	50
5.2.2	Airfoil Family	51
5.2.3	Other Constraints, w.r.t. Reference WT	57
5.3	Design Variables	58
5.3.1	Bézier Chord & Twist Distribution	59
5.4	HAWC2 Simulation Setup	61
5.5	Optimization Algorithm	63
5.5.1	Controller: Assumption	64
5.6	Results Overview	66
5.6.1	Blade Design #1 and #2	67
5.7	Design Assessment	68
5.7.1	Performance	69
5.7.2	Design Comparison, HAWC2 & GH Bladed	70
5.7.3	Code-Code Comparison	73
5.8	Discussion	74
5.9	Full Rotor Geometry	75

6 Aeroelastic Analysis	77
6.1 Aeroelastic Stability	77
6.2 Cambpell Diagram	79
6.2.1 Blade Eigenmodes	80
6.3 Blade Deflection Analysis, HAWC2	81
6.3.1 Runaway Case	81
6.3.2 Frequency Domain	82
6.3.3 Time Domain	85
6.4 Blade Deflection Analysis, GH Bladed	87
6.5 Discussion	88
7 Large Rotor Study	89
7.1 Results Overview	90
7.2 Discussion	91
8 Conclusions	93
A Airfoil Polar Data	95
A.0.1 DU00-W2-401	95
A.0.2 DU00-W2-350	96
A.0.3 DU93-W-210	96
A.0.4 DU00-W-212	97
A.0.5 DU96-W-180	97
A.0.6 NACA-64618	98
A.0.7 NACA-63215	98
A.0.8 CL/CD All Airfoils	99
B Structural Design Test	101
B.1 Structural Blade Design, BECAS	101
B.1.1 BECAS Input	102
B.1.2 Region Layout	103
B.1.3 Layout Results	104
C HAWC2 Structural Properties	105
D Blade Torsional Stiffness	109
D.0.4 Box Thickness	109
D.0.5 Torsional Stiffness	109
E Baseline Test: DU Airfoils	111
References	113

List of Figures

1.1	Annual mean wind speed across China. Taken from CMA [15]	2
2.1	Geometry Parameterization. Taken from Grasso [28]	7
2.2	GA, Crossover Operator. Taken from Jones [43]	8
2.3	Aerodynamic models in terms of increasing complexity. Taken from Schepers [60]	9
2.4	Velocity and Force Diagram for a Blade Element. Taken from Bak and Timmer [5]	10
2.5	Vortex methods, lifting surface modelling. Taken from Grasso F. [29]	12
2.6	Wake Geometry. Taken from Grasso F. [29]	12
2.7	Simulated wake behind the NTNU rotor. Taken from Ramos-Garca et al. [58]	13
2.8	Computational Fluid Dynamics Method	13
2.9	HAWTOPT: Program structure. Taken from Flemming Rasmussen [24]	14
2.10	Schematic of the field of aeroelasticity. Taken from Hodges and Pierce [37]	15
2.11	Simplified overview of aero-hydro-servo-elastic codes. Taken from Vorpahl et al. [69]	16
2.12	Multibody formulation. Taken from Kim et al. [45]	17
2.13	NREL 5MW Wind Turbine Visualizations	18
2.14	DOFs Terminology, Taken from Hansen [33] and Jureczko et al. [44]	19
2.15	Blade flutter mode illustrated by snapshots over one period of oscillation. Taken from Hansen [33]	20
2.16	Flutter phenomena explained. Taken from Holierhoek [38]	20

2.17	Ground-fixed natural frequencies. Lines denote approximations to the computed frequencies, and the center frequencies of the rotor whirling modes given $\pm \bar{\Omega}$, added to the ground-fixed natural frequencies. Taken from Hansen [33]	21
2.18	Sunderland's Cost Model Flowchart. Taken from Hau et al. [36]	22
2.19	Blade cost scaling relationship. Taken from Fingersh et al. [23]	23
3.1	Satellite Imagery	25
3.2	Wind Site Characteristics	26
3.3	Wind Speed & Power Density	28
3.4	Classes of wind power density. Taken from Elliott et al. [20]	28
3.5	Wind Speed & Wind Energy Frequency Distributions	29
3.6	Wind Direction & Wind Energy Rose: Annual Mean	29
3.7	Wind Profile & Weibull PDF	31
3.8	Cumulative Distribution, function of Wind Speed: At Site & IEC Standard Specific	32
4.1	Wind Turbine, GH Bladed	35
4.2	Principle behind PRVS Wind Turbines. Taken from Bak [4]	36
4.3	Blade Geometric Properties of the 2.0 MW wind turbine	37
4.4	Blade Planform of the 2.0 MW wind turbine	37
4.5	Blade Planform of the 2.0 MW wind turbine	38
4.6	Property Distributions of 2.0 MW wind turbine	38
4.7	Property Distributions of 2.0 MW wind turbine	39
4.8	Blade Geometry Overview	39
4.9	Tower Property Distributions of 2.0 MW wind turbine	40
4.10	Wall Thickness Distribution of 2.0 MW wind turbine	40
4.11	Tower Clearance	41
4.12	Deflections & Thrust Curves, Ref. WT	42
4.13	Operational Curves, Ref. WT	42
4.14	Bending Moment, C_p - λ Curves, Ref. WT	43
4.15	Controller Look-up Table	43
4.16	Campbell Diagram, Reference Wind Turbine	44
4.17	Visualization of Selected Eigenfrequencies	45
5.1	Power and site Weibull distribution	49
5.2	Blade Mass versus Rotor Diameter. Taken from Graue H. [30]	50
5.3	DU Wind Turbine Airfoils	51
5.4	NACA 6-Series Airfoils, Wind Turbine Application	52
5.5	Re Number, w.r.t. Radius	53

5.6	Computed limiting streamlines on a stall regulated wind turbine blade at a moderately high wind speed. Taken from Hansen [35]	54
5.7	DU97-W-300	55
5.8	DU91-W2-250	55
5.9	Static and dynamic values of lift w.r.t angle of attack. Taken from Holierhoek [39]	56
5.10	Distribution Description	57
5.11	Distribution of Cl/Cd_{design}	57
5.12	Cubic Bézier Curve Representation	59
5.13	GH Bladed to HAWC2 Converter	61
5.14	Blade Data Fitting	61
5.15	HAWC2 Program Structure. Taken from DTU [18]	62
5.16	HAWC2 Output Structure. Taken from DTU [18]	62
5.17	HAWC2, Constraint check: examples	63
5.18	Flow Diagram	64
5.19	HAWC2 Results	66
5.20	Blade Layout: Design # 1	66
5.21	Blade, Before Procedure	67
5.22	Blades, After Procedure	67
5.23	Power and Thrust Response. HAWC2	68
5.24	Wind Turbine, Operational Curves	69
5.25	Wind Turbine, Thrust and Bending Moments	69
5.26	C_p - λ Curve	70
5.27	Power Curve, Rough & Clean Cases	72
5.28	Wind Turbine Rotor, with Designed Blades	75
5.29	Wind Turbine Rotor, Top View	75
6.1	Aeroelastic frequencies, MYWP- 2MW	78
6.2	Flapwise mode excitation, on blade	78
6.3	Campbell Diagram, HAWC2	79
6.4	Campbell Diagram	79
6.5	Wind Turbine Blade Modes	80
6.6	Wind Turbine Blade Modes	80
6.7	Free Rotation	82
6.8	Tip Relative Velocity & Aeroelastic Twist	82
6.9	Out-of-Plane Tip Deflection	83
6.10	Out-of-Plane Root Bending Moment	83
6.11	In-Plane Tip Deflection	84

6.12 In-Plane Root Bending Moment	84
6.13 In-Plane Tip Deflection	85
6.14 In-Plane Root Bending Moment	85
6.15 Out-of-Plane Tip Deflection	86
6.16 Out-of-Plane Root Bending Moment	86
6.17 Out-of-Plane Deflections	87
6.18 In-Plane Deflections	87
7.1 Stiff and Soft Blade Cases	90
7.2 Blade Distribution	90
7.3 Power and Thrust Curves	91
A.1 DU00-W2-401 RFOIL	95
A.2 DU00-W2-350 RFOIL	96
A.3 DU93-W-210	96
A.4 DU00-W-212	97
A.5 DU96-W-180	97
A.6 NACA-64618	98
A.7 NACA-63215	98
A.8 DU00-W2-401, DU00-W2-350	99
A.9 DU97-W-300, DU91-W2-250	99
A.10 DU93-W-210, DU00-W-212	100
A.11 DU96-W-180, NACA-64618	100
A.12 NACA-63215 RFOIL	100
B.1 BECAS Algorithm	101
B.2 Airfoil Geometry Preparation	102
B.3 BECAS Region Layout	103
B.4 BECAS Region Layout	103
B.5 BECAS Blade Structure Results	104
B.6 BECAS Structural Property Distributions	104
C.1 St File, part 1	106
C.2 St File, part 2	107
D.1 Crossectional Box Section	109
E.1 MYWP Baseline & Baseline with DU Airfoils	111
E.2 MYWP Baseline & Baseline with DU Airfoils	111

List of Tables

2.1	Optimal and Conventional Design Process. Taken from Arora [3]	6
3.1	Assessment of Potential & Land, Guizhou Province	26
3.2	Provided Site Parameters	27
3.3	Power Law Reference Values	30
3.4	Estimate of 50-year extreme wind	32
4.1	Gross Properties for the MY 2.0-MW Reference Wind Turbine	36
4.2	Performance Indicators, 2 MW Reference WT	43
4.3	List of the first eigenmodes and their corresponding eigenfrequencies.	45
4.4	Summary of 2 MW reference wind turbine	46
5.1	Airfoil Requirement w.r.t. Blade Region	52
5.2	Constraint Comparison, Averaged Values. HAWC2	70
5.3	Constraint Comparison, Steady Values. GH Bladed	71
5.4	Blade Scenarios: Clean, Mixed & Rough	72
5.5	Code Comparison, GH Bladed, BEM & HAWC2 at 8 m/s	73
6.1	Wind Turbine with New Rotor, HAWC2 Eigenanalysis.	77
6.2	HAWC2 Blade Modal Analysis	81
7.1	Scale Laws for Blades, Structural Properties	89
7.2	Blade Scenario: Baseline & Large Blade	91
B.1	Typical Effective Material Properties for E-Glass / Carbon	102

Nomenclature

Latin Symbols

a'	tangential induction factor	[—]
\bar{U}	mean wind speed	[$\frac{m}{s}$]
ρ	air density	[$\frac{kg}{m^3}$]
$\bar{\frac{P}{S}}$	mean power density	[$\frac{W}{m^2}$]
v	wind speed	[$\frac{m}{s}$]
a	axial induction factor	[—]
C_d	drag coefficient	[—]
C_l	lift coefficient	[—]
C_t	thrust coefficient	[—]
C_n	normal coefficient	[—]
B	blade number	[—]
$c(r)$	chord length	[m]
e	eccentricity factor	[—]
x_θ	displacement of CG from EA	[m]
P	P	[kW]
D	rotor diameter	[—]
b_{rotor}	material cost constant	[—]
C_{rotor}	rotor cost	[—]
w_{rotor}	rotor mass	[kg]
H_{ref}	reference height	[m]
H	hub height	[m]

k	weibull shape parameter	[—]
A	weibull scale parameter	$[\frac{m}{s}]$
C	rayleigh scale parameter	$[\frac{m}{s}]$
C_p	power coefficient	[—]

Greek Symbols

α_o	shear exponent	[—]
$\Gamma(x)$	gamma function	[rad]
ϕ	inflow angle	[deg]
α	angle of attack	[deg]
σ	solidity factor	[—]
ζ	damping	[—]
δ	logarithmic decrement	[—]
λ	tip speed ratio	[—]
θ_{cone}	coning angle	[deg]
θ_{tilt}	tilt angle	[deg]
ζ	damping ratio	[—]

Abbreviations

$pdf_{W,R}$	Weibull or Rayleigh probability density function
AC	Aerodynamic center
AEP	annual energy production
AOE	Annual operating expenses
BEM	Blade Element Momentum
CDF	Cumulative distribution function
CFD	Computational fluid dynamics
CF	capacity factor
CG	Center of gravity
COE	Cost of Energy
DAKOTA	Design Analysis Kit for Optimization and Terascale Applications
DEM	digital elevation map
DLC	design load case
DU	Delft University
EA	Elastic center

FCR	Fixed charge rate
FEM	Finite element method
FFT	Fast fourier transform
FVW	Free vortex wake
GA	Genetic algorithm
GUI	Graphic user interface
ICC	Initial capital cost
IEC	International Electrotechnical Commission
LER	leading edge roughness
MFD	Method of feasible descent
MYWP	Ming Yang Wind Power
NASA	National Aeronautics and Space Administration
NREL	National Renewable Laboratory
OpenMDAO	Open Multidisciplinary Design Analysis and Optimization
PRVS	Pitch regulated variable speed
PSO	Particle swarm optimization
rpm	revolutions per minute
SNL	Sandia National Laboratories
SQP	Sequential quadratic programming
SSW	South-southwest
SW	Southwest
WT	wind turbine

Chapter 1

Introduction

With this master project a study for the design of low wind speed wind turbine blades takes place. The design of a low wind speed blade for a 2 MW wind turbine with a rotor diameter of 115 m is found. A suitable aerodynamic and aeroelastic performance of the designed blade is a key requirement for this project. The analysis includes investigations on blade deflection and other effects, with the use of aeroelastic simulations, based in different wind speed conditions.

Before the study takes place, in Chapter 2, the state of the art in wind turbine blade design is presented. It is important to review the different, existing design and optimization methods for wind turbine blade design. The blade design is site-specific and the site data for the proposed location is described and analyzed, in Chapter 3. The thesis targets the design of a new blade, meaning the design of other components is not necessary. In Chapter 4, a description of the reference wind turbine is provided, along with the wind turbine blade's design and its aerodynamic and aeroelastic performance. Chapter 5, presents the optimization procedure, the design of the wind turbine blade and its aerodynamic and aeroelastic performance. The same design is then compared with two aeroelastic codes, and some results are presented in the same chapter. Finally, a large rotor case is studied in Chapter 7 and the conclusions outlining the results and further design opportunities for this project, are presented in Chapter 8.

1.1 Motivation

Areas with a low wind speed energy resource require low wind speed wind turbine technology. The trend in the industry is to develop wind turbines that make such low wind speed sites viable for energy generation. Low wind speed wind turbine technology opens a new market in countries where wind energy was not considered before. Many of the rich, inland wind resource sites decline in numbers. About 50%

of the world's wind energy resource is classified as low wind, with winds of $7.5 \frac{m}{s}$ or less¹. Approximately 70% of China experiences low wind speed conditions, Elliott et al. [20]. Figure 1.1 includes a map of the available Chinese wind resource.

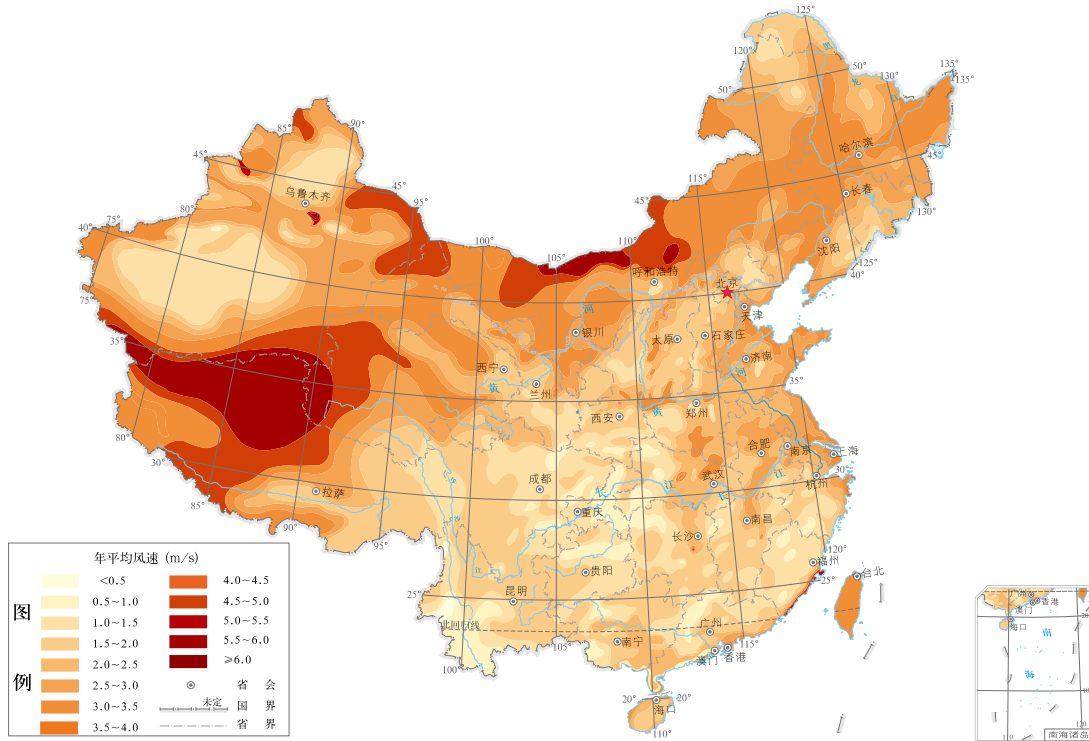


Figure 1.1: Annual mean wind speed across China. Taken from CMA [15]

Low wind speed regions play an important role for the wind energy industry. With the purpose of expanding into this low wind speed regions, this thesis aims to answer the following question:

What is an optimal low wind speed blade design that minimizes the cost of energy? and under what conditions is the blade aeroelastically stable?

To solve this, a cost of energy (COE) optimization is developed to determine the blade's geometry. Once a design is identified, aeroelastic simulations take place for the identification of any instabilities. The optimization targets energy yield maximization specific to the proposed site.

¹NREL. TP-500-32781 Wind Energy Resource Atlas of Southeast China

The following steps were the basis for the project's development and completion.

1. State of the Art / Understand Project's Context
2. Analyze Reference Wind Turbine / Site
3. Design 115 m Blade for a 2MW Wind Turbine
4. Choose Optimization i.e. Cost of Energy.
5. Implement Design in Simulation (i.e. GH Bladed/HAWC2/BEM)
6. Perform Aeroelastic Simulation
7. Validate & Assess Design
8. Report Results

Chapter 2

State Of the Art

The increasing demand for wind energy and the decreasing availability of high wind speed areas, push the industry to develop low wind speed wind turbines. Ming Yang Wind Power (MYWP) initiates a feasibility study for the design of such a turbine, with the cooperation of Denmark Technical University (DTU). The baseline for this feasibility study is provided in Chapter 4.

Developing a blade design is a time consuming task, where ease of manufacture and structural integrity are equally important with respect to the blade's aerodynamic performance. The wind turbine's site influences the design process as well, due to cost of energy targets. There are numerous design methods and tools for blade design. In this thesis, the use of the aeroelastic tools HAWC2, created by DTU, and GH Bladed, created by DNV GL, are used to create a site specific and cost of energy blade design optimization. The main focus being the aerodynamics and the aeroelastic design, where the latter is highly dependent of the provided structural model.

Important design steps or tools to explore the potential of low wind speed energy are: site specific design, wind turbine blade optimization procedures, airfoil usage and the implementation of aeroelastic codes. One size does not fit all, and only a limited number of wind turbine designs are adequate for the same site. It is important to review current blade design methods and optimization methodologies. Some findings include current blade design optimization methods, focused in the cost of energy (COE), rather than optimal aerodynamic performance. Other interesting findings mention the coupling of aeroelastic calculations with cost of energy models and the benefits site-specific wind turbine blade design has to offer.

2.1 Optimization Methods

A wide variety of optimization methods exist for the optimization of a blade design. This palette of algorithms are classified as gradient-based methods and gradient-

free methods. Some gradient-based methods include conjugate gradient method, method of feasible descent (MFD) and sequential quadratic programming (SQP). Gradient-based methods make use of function gradients. Some gradient-free methods include genetic algorithms, Nelder-Mead simplex and particle swarm optimization (PSO). The Matlab optimization toolbox is a powerful tool as well. Countless publications make reference to the use of the `fmincon` function. This function finds the minimum for a constrained multivariable function, MathWorks [50]. This popular function is a gradient based, minimization solver. Some of these listed algorithms have been implemented and are currently used in wind turbine blade and airfoil design. The steps involved in a conventional and an optimal design process, in table 2.1, highlight the benefit of using an optimization method during an engineering design process.

Table 2.1: Optimal and Conventional Design Process. Taken from Arora [3]

Optimal Steps	Conventional Steps
1. Specifications	1. Specifications
2. Baseline	2. Baseline
3. Analysis	3. Analysis / Experiment
4. Constraint Check	4. Performance / Failure Check
5. Optimal conditions satisfied?	5. Satisfactory design?
6. Yes, then stop process - End	6. Yes, then stop process - End
7. No, Change parameters: Optimization	7. No, Change parameters: Intuition
8. Return to Step 3. Analysis	8. Return to Step 3. Analysis

2.1.1 Optimization Tools

One of the latest optimization tools, used for an engineering design process, is an Open Multidisciplinary Design Analysis and Optimization framework. OpenMDAO was developed by NASA. With this optimization tool, diverse disciplines are coupled and optimized in unison with respect to specific goals. This tool is an open source framework written in Python. It allows the user to link different codes together for an integrated design analysis, NASA [53]. This is essential to tackle engineering problems. Among some of the OpenMDAO users are TU Delft and DTU. NREL and DTU are currently working together to develop an OpenMDAO plugin for the integrated analysis of wind turbine systems.

Another available optimization tool is DAKOTA or Design Analysis Kit for Optimization and Terascale Applications . The DAKOTA project, developed by Sandia National Laboratories (SNL), is a multilevel parallel object-oriented framework for design optimization. In the same manner as an OpenMDAO, this tool couples codes together for an iteratively analysis method, which results in an optimized design, SNL [64].

2.1.2 Optimization Formulation

Regardless of the optimization method chosen, most design optimization problems are formulated in the following manner: problem description, data/information collection, design variable definition, optimization criteria and constraint formulation.

Following this formulation, the problem is defined in Section 1.1. The necessary blocks of information for the wind turbine model and site model, are provided by MYWP. This information is reviewed in Chapters 3 and 4. When performing an optimization with HAWC2, discussed in Section 2.4.1, selecting convenient design variables is an important step. Design variables in blade design, usually describe the airfoil and the rotor's shape, i.e. lift coefficient, drag coefficient, angle of attack, rotor diameter, chord, twist, relative thickness and shell thickness, Wang et al. [70]. The chosen design variables must be independent of each other, if this is not the case, some constraints must exist between them. The design degrees of freedom are determined by the number of independent design variables. The design variables are reviewed in Section 5.3. In this thesis, the optimization criteria used to compare blade designs, is the minimization of the objective function presented in Section 5.1. Finally, the optimization restrictions (constraints) used to verify performance requirements, are discussed in Section 5.2.

2.2 Airfoil Design

As mentioned earlier, one example of optimization methods are genetic algorithms (GA). The Energy Research Center of the Netherlands (ECN) used Rfoil with a genetic algorithm to design low-wind speed airfoils, which resulted in an airfoil family with predictable and favourable characteristics, Grasso [28]. For the implementation of the optimization, the airfoil geometry was represented and controlled by four Bezier curves, figure 2.2.

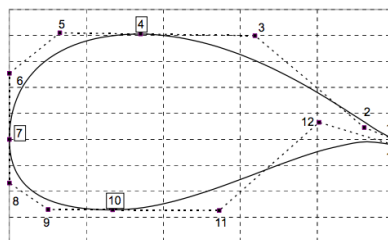


Figure 2.1: Geometry Parameterization. Taken from Grasso [28]

Most genetic algorithms consist of chromosome populations, fitness selection and crossover for new offspring production/mutation. Chromosomes may be seen as one of many possible solutions within a search domain. A fitness function determines the fitness of each candidate within the existent population. After mutations of the best candidates take place, a new population is created. The fitness score is dependent on the candidate's ability to solve the specified problem. Basic genetic algorithms

involve a selection, crossover and mutation operators. Selection operators select the best candidates for reproduction. A crossover operator exchanges information between two candidates to create two offspring. Finally, mutation changes some small piece of information of a chromosome in a random manner, Jones [43].



Figure 2.2: GA, Crossover Operator. Taken from Jones [43]

CENER (National Renewable Energy Center) implemented an evolutionary algorithm for the design of an airfoil family for large blades. Genetic algorithms are a type of evolutionary algorithm and are not exactly the same optimization method. An evolutionary algorithm has a selection operator, where a candidate is excluded from a new generation (extinctive). A genetic algorithm selects candidates for a new generation, while preserving the rest.

Both optimizations require the good selection of an objective function and made use of Xfoil/Rfoil. In the first optimization case, the design driver was increasing energy capture with respect to loading, to reduce the cost of energy. In the second optimization case, a number of individual objective functions made up a compound objective function. The design driver, in this case, were low lift related loads, low sensitivity to roughness and a high torque coefficient, Mendez et al. [52]. Risø National Laboratory and the Department of Wind Energy at DTU, have also targeted the cost of energy with optimization methods applicable for airfoil design, but also for blade design, [10], [25], [72]. Some are discussed in the next section.

Airfoil design has focused in aerodynamic performance. However additional to this requirement, the increasing blade length trend requires an optimal structure. The increasing importance of structural stiffness and aerodynamic performance requires different design approaches. Recently Bak et al. [6], implemented an airfoil optimization which aimed for a high design lift, while respecting specific structural constraints. This optimization approach made use of AirfoilOpt, an airfoil design tool developed at Risø-DTU. Targeting the same structural trend Zahle et al. [71], use an OpenMDAO framework. In this case, airfoil performance and structural constraints are met by linking the OpenMDAO to XFOIL and EllipSys2D during the optimization.

Other airfoil developments include the study of airfoil characteristics at low and high Reynolds numbers. In DTU, an NREL airfoil, designed for a Re of 100,000, is tested in a wind tunnel. This test is compared to large eddy simulations (LES) performed with Ellipsys3D, Chivaeet al. [14]. On the other hand, tests at high Re numbers were performed at the DNW-HDG and TU-Delft LST wind tunnels, [46]. These were used to assess the maximum lift and angle of attack effects.

This thesis does not cover airfoil design, which are the building blocks of a wind turbine blade. The methods reviewed in this section, show the continuous develop-

ment of airfoils and their benefits for blade design. For this reason, airfoil choice is extremely important. With traditional airfoils there is no simple technique to obtain a concrete reduction in the cost of energy, Fuglsang and Madsen [25]. This is a key factor to be aware of during the development of the blade. Whether DU airfoils or other airfoils are implemented, the structural integrity of the blade must be kept.

2.3 Blade Design

There are several wind turbine blade design methods, figure 2.3. Some of them are more traditional than others, however there are blade design methods, which stand out due to their approach and results. Some of the traditional design and optimization methods involve the choice of an objective function targeting maximum energy production (AEP) and minimal cost of energy (COE), [25].

Whether a traditional method is used or not, blade element momentum (BEM) theory is the backbone for wind turbine design methods, Shen et al. [61]. This is due to quality approximations resulting from BEM calculations, [61].

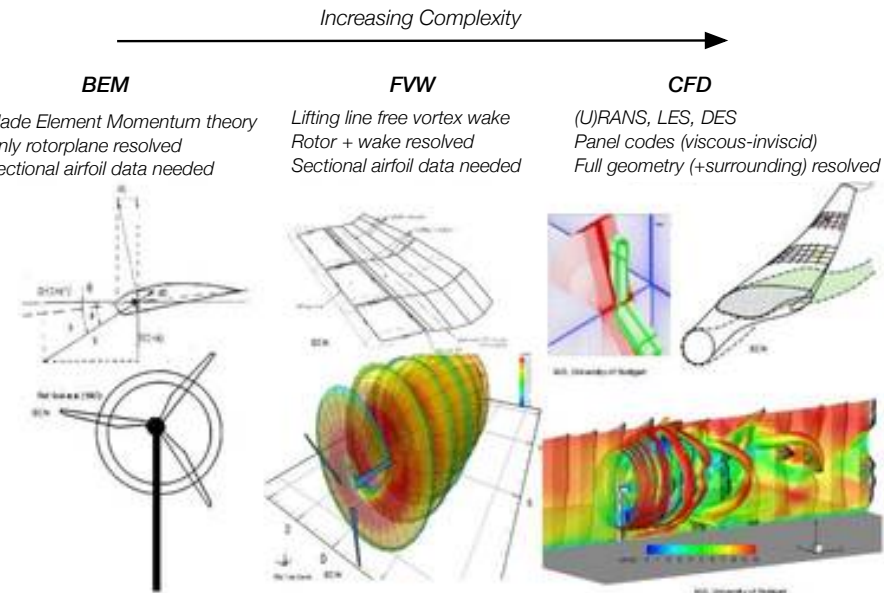


Figure 2.3: Aerodynamic models in terms of increasing complexity. Taken from Schepers [60]

2.3.1 Blade Element Momentum

Blade Element Momentum theory, is the standard method of calculating or estimating wind turbine loads, thrust and power. This is done for different wind speed,

rotational speed and pitch angle settings. Assumptions in BEM theory are: no interaction between radial elements and a constant force of the blades on the flow, which is corrected with Prandtl's tip loss correction.

One approach, on how to model rotor aerodynamics using the Blade Element Momentum, is explained below:

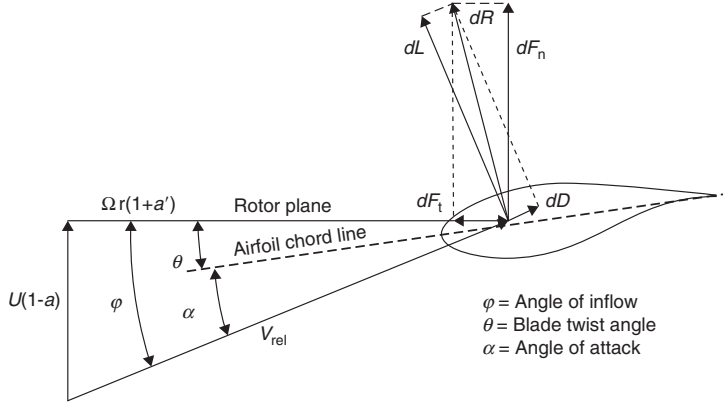


Figure 2.4: Velocity and Force Diagram for a Blade Element. Taken from Bak and Timmer [5]

The first step is to estimate a value for the axial and tangential induction factors, respectively a and a' . These values go through a loop in order to calculate necessary parameters. The first step in the loop is to calculate the flow angle, ϕ :

$$\phi = \tan^{-1} \left(\frac{V_o(1-a)}{(1+a')\omega r} \right) \quad (2.1)$$

and Prandtl's tip loss correction,

$$F = \frac{2}{\pi} \cos^{-1} \left(\exp \left(-\frac{0.5B \cdot (R-r)}{\sin \phi} \right) \right) \quad (2.2)$$

Using the angle of attack, Eq. 2.3, the airfoil's lift and drag coefficients are known, C_l and C_d . For a geometrical description of the angles, see figure 2.4.

$$\alpha = \phi - (\theta + \beta) \quad (2.3)$$

With these airfoil coefficients, the thrust, C_t , and normal coefficients, C_n , are determined:

$$C_n = C_l \cos \phi + C_d \sin \phi \quad (2.4)$$

$$C_t = C_l \sin \phi - C_d \cos \phi \quad (2.5)$$

To update the induction factors, the solidity, σ , is required. This is given by:

$$\sigma(r) = \frac{Bc(r)}{2\pi r} \quad (2.6)$$

where B is the number of blades and $c(r)$ is the chord length over the radius of the blade. The tangential induction factor is finally updated with the following equation:

$$a' = \frac{1}{\left(\frac{4F \sin \phi \cos \phi}{\sigma C_t} - 1\right)} \quad (2.7)$$

In order to compute the new a , the Glauert correction is applied.

$$a = \frac{1}{\left(\frac{4F \sin^2 \phi}{\sigma C_n} + 1\right)} \quad (2.8)$$

This correction involves the calculation of the local thrust coefficient, C_{Tl} :

$$C_{Tl} = \frac{\sigma(1-a)^2 C_n}{\sin^2 \phi} \quad (2.9)$$

When this meets the criteria $C_{Tl} \leq 0.96$, the axial induction factor, a , is calculated as follows:

$$a = \frac{1}{\left(\frac{4F \sin^2 \phi}{\sigma C_n} + 1\right)} \quad (2.10)$$

Finally, a and a' are inserted back into the loop until convergence, within a set tolerance, is reached. Once convergence is met, the final distributions for the angle of attack, α , thrust and torque coefficients are known. With this, per segment blade loads are determined.

It is important to understand that BEM theory has some limitations. BEM cannot model accurately the flow at the root and tip sections of the blade, Dssing et al. [19]. For this, reason tip loss corrections among other corrections are studied. Although the Prandtl tip loss correction exists, this one overestimates loading at the tip section, so further corrections must be made, Shen et al. [61]. Other corrections involve wake expansion and rotation, which obtain more accurate BEM results at the root and tip blade sections, Dssing et al. [19]. BEM corrections for inflow with shear, also provide better approximations to be used on aeroelastic tools, Madsen et al. [48]. This is relevant as large rotor diameters experience significant wind shear due to differences in height.

2.3.2 Vortex Methods

Vortex methods use a better approach to model the physics behind rotor aerodynamics. Within vortex methods, there are various methods available, figure 2.5.

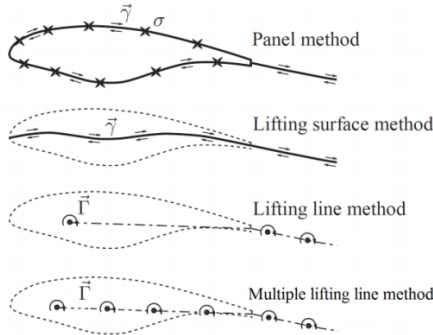


Figure 2.5: Vortex methods, lifting surface modelling. Taken from Grasso F. [29]

One of this methods is the lifting line method, figure 2.6. Methods, like this one, are useful to make better estimations of blade loads and wind turbine aerodynamic performance. Unlike BEM, these methods are valid in turbulent wake states, where BEM theory is no longer valid. In figure 2.3, another vortex method is mentioned. Free vortex wake methods (FVW) are more computationally expensive than vortex methods with a prescribed wake. To assess the physical solutions, resulting from these methods, experimental data is important and very valuable.

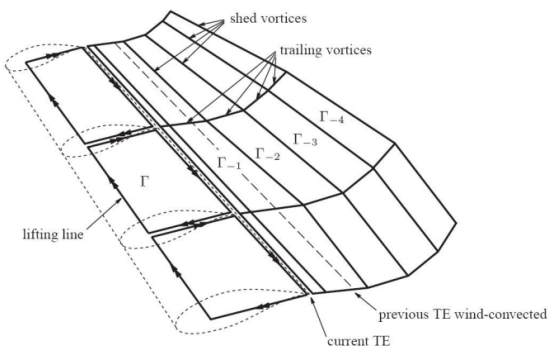


Figure 2.6: Wake Geometry. Taken from Grasso F. [29]

Panel methods are also mentioned in figure 2.5. This method solves the potential flow over 2D or 3D geometries, represented by panels. Each of these panels posses their own circulation, a condition necessary for the flow not to pass through the panels. Therefore, the flow may be represented in a more realistic manner. Recently developed at DTU, MIRAS is a three-dimensional panel method capable of predicting the aerodynamics of wind turbine blades and their wakes, Ramos-Garca et al. [58]. Methods like this one, reduce the uncertainty of predictions done with codes like BEM, mentioned earlier. MIRAS was validated with experimental data

and other computationally expensive methods, like CFD. A MIRAS rotor wake simulation is included in figure 2.7.

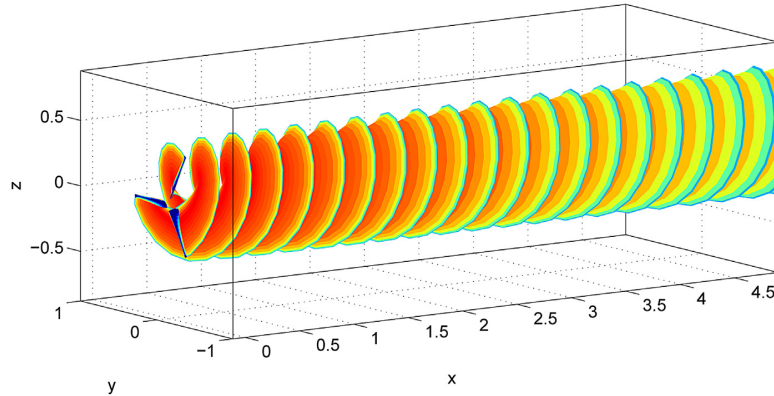
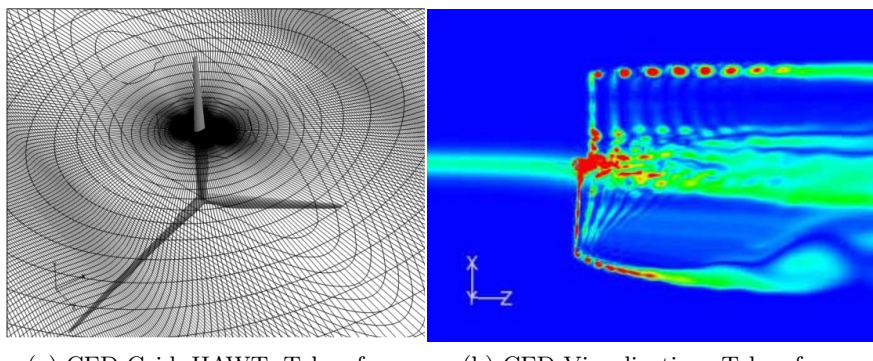


Figure 2.7: Simulated wake behind the NTNU rotor. Taken from Ramos-Garcia et al. [58]

2.3.3 Computational Fluid Dynamics

Computational fluid dynamics (*CFD*) methods increase the complexity of a problem in comparison to BEM or vortex methods, see figure 2.3. This method is continuously developed in order to reduce the uncertainty of the loads predicted with the use of BEM, Snel [63]. CFD solves the Navier-Stokes equations for the flow around a rotor's blade. It is very accurate, however, this accuracy is time dependent, which make CFD methods a time-expensive approach. Depending on one's available processing power, the computational time for methods like BEM or vortex methods, may range from few minutes to hours. For CFD, this may take a couple of days or even more. Below, in figure 2.8, one can observe the mesh used to solve the flow around the rotor. A very fine or coarse mesh do affect the computational time, mentioned earlier.



(a) CFD Grid, HAWT. Taken from Barlas et al. [8] (b) CFD Visualization. Taken from Barlas et al. [8]

Figure 2.8: Computational Fluid Dynamics Method

The Technical University of Denmark and Riso have developed an in-house flow

solver called EllipSys3D. This improved Reynolds-averaged Navier-Stokes solver is actively used for wind turbine applications and development, Sorensen et al. [66]. Other CFD commercial codes are available, but are not further discussed in this thesis.

2.3.4 Blade Optimizations

The increasing complexity of modelling blade aerodynamics is also coupled to optimization techniques. A recent example of this, is the implementation done by Alpman [2], where BEM theory and a genetic algorithm are linked together. Some relevant findings are the definitions used for the chord, twist distributions and control point number.

Another recent development is done by Bottasso et al. [13]. In this approach, an SQP algorithm is used. By specifying aerodynamic and structural constraints, one obtains an optimized design and assesses the cost of energy. In this case, the blade layout is optimized, but the airfoil shapes remain fixed. By using this approach, the annual energy production and the cost of energy are significantly improved.

Some other available optimization tools include HARP-Opt [54], from NREL, and HAWTOPT [26], from DTU-Risø. These are wind turbine optimization tools, which use genetic or SLP algorithms to optimize rotor performance. HARP-Opt utilizes a BEM theory code to predict rotor performance. However, HAWTOPT has the possibility to include various tools, i.e. BEM, aeroelastic calculations, etc.

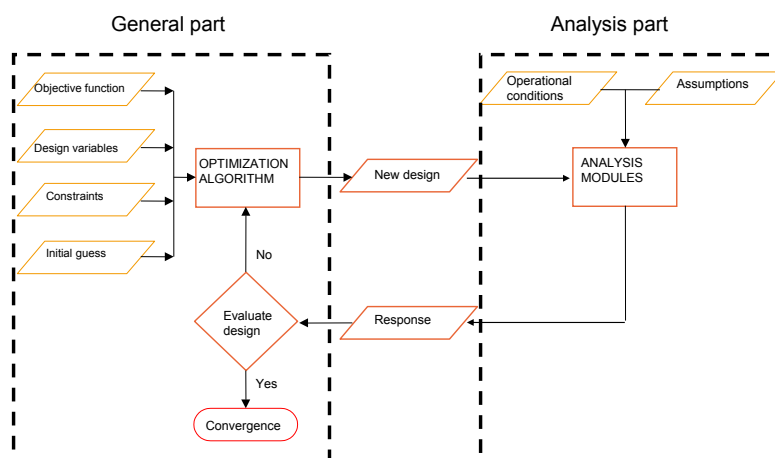


Figure 2.9: HAWTOPT: Program structure. Taken from Flemming Rasmussen [24]

These are relevant blade optimization methods or tools, however the effects of aeroelasticity need to be taken into account. Coming up with a design that increases energy production might not be enough for a final blade design. The aeroelastic effects on a blade, while in operation, determine whether such a blade design performs in a stable manner or not. It is important to study the effects of aeroelasticity and the occurrence of aeroelastic instabilities on wind turbine blades.

2.4 Aeroelastic Design

The introduction of aeroelastic codes, has further developed current blade design methods. In several aeroelastic codes, the aerodynamics of a rotor are modelled with an extension of the blade element-momentum theory. Aeroelastic codes or aeroelasticity deal with the interaction between the fields of elasticity, dynamics and aerodynamics, figure 2.10.

A wind turbine vibrates and operates in turbulent conditions, but it is also subject to inertial, gravitational and centrifugal forces. For such a case, it is important to model the deformation due to the loads and the loads due to the deformation. To solve this coupled problem, there is a large range of aeroelastic codes. The present study makes use of the Horizontal Axis Wind turbine simulation Code 2nd generation or HAWC2. This is an aeroelastic code developed by the Aeroelastic Design research group at DTU Wind Energy, for the calculation of wind turbine response in the time domain. HAWC2 does not have a GUI, which makes it the perfect tool for an optimization loop.

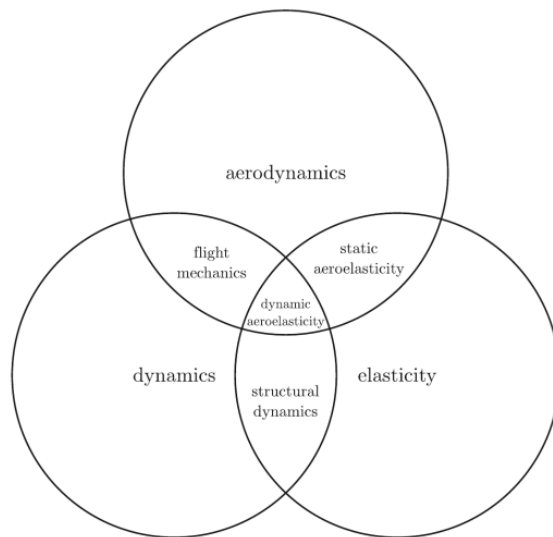


Figure 2.10: Schematic of the field of aeroelasticity. Taken from Hedges and Pierce [37]

Using aeroelastic codes, BEM and a cost model allows to optimize blade design in terms of blade deflections, loads and rotor lifetime, [44], [1]. There is indeed benefits as well for the tower and gearbox in terms of material and cost, Wang et al. [70]. Coupled optimizations allow to minimize the cost of energy and maximize energy production. A number of test cases have been done and compared to experimental values, proving the benefits of this optimization method, [70]. Aeroelastic codes are a key tool in this thesis.

MYWP makes use of an aeroelastic code called GH Bladed, developed by DNV-GL. Other existing aeroelastic codes are mentioned in figure 2.11. Both HAWC2 and GH Bladed are to be used at different stages of this thesis.

Code	Developer	OC3 participant	Aerodynamics (aero)	Hydrodynamics (hydro)	Control (servo)	Structure (elastic)
Adams	MSC + NREL + LUH	NREL + LUH ^a	BEM or GDW + DS	Airy ^{str.} or UD + ME, Airy + PF + ME	DLL, UD	Turbine: MBS, Moorings: QSCE, UDFD
ADCos-Offshore ⁵	ADC + IWES	IWES	BEM + DS	Airy ^{str.} or UD or Stream + ME	DLL, UD	FEM
ANSYS-WaveLads ^{6,7}	ANSYS + LUH	LUH ^a	None	Airy ^{str.} or UD or Stream + ME	None	FEM
BHawC ^c	Risø DTU + Siemens	Siemens	BEM or GDW + DS	Airy ^{str.} or UD + ME	DLL, UD	MBS / FEM
Bladed ⁸	GH	CENER + GH	BEM or GDW + DS	Airy ^{str.} or UD or Stream + ME	DLL	Turbine: FEM ^P + Modal / MBS, Moorings: UDFD
Bladed Multibody ⁹	GH	GH	BEM or GDW + DS	Airy ^{str.} or UD or Stream + ME	DLL	MBS
FAST ¹⁰⁻¹²	NREL	NREL + CENER + POSTECH	BEM or GDW + DS	Airy ^{str.} or UD + ME, Airy + PF + ME	DLL, UD, SM	Turbine: FEM ^P + Modal / MBS, Moorings: QSCE
FLEX5	Risø DTU	DONG + SWE + Vestas	BEM or GDW + DS	Airy ^{str.} or UD or Stream + ME	DLL, UD	FEM ^P + Modal / MBS
FLEX5-Poseidon ^{13,14}	Risø DTU + SWE + LUH	SWE ^b	BEM or GDW + DS	Airy ^{str.} or UD or Stream + ME	DLL, UD	FEM + Modal / MBS
HAWC ^{15,16}	Risø DTU	DNV + Risø DTU	BEM or GDW + DS	Airy ^{str.} or UD + ME	DLL, UD	FEM
HAWC2 ¹⁷	Risø DTU	Risø DTU	BEM or GDW + DS	Airy ^{str.} or UD + ME	DLL, UD, SM	Turbine: MBS / FEM, Moorings: UDFD
SESAM/DeepC ¹⁸	DNV	Acciona + NTNU	None	Airy ^{str.} + ME, Airy + PF + ME	None	Turbine: MBS, Moorings: QSCE, FEM
Simo ¹⁹	MARINTEK	MARINTEK	BEM	Airy + PF + ME	DLL	Turbine: MBS, Moorings: QSCE, MBS
SIMPACK	SIMPACK	SWE	BEM or GDW + DS	None	DLL, UD	MBS
3Dfloat ²⁰	IFE-UMB	IFE-UMB	BEM or GDW	Airy + ME	UD	Turbine: FEM, Moorings: FEM, UDFD

Figure 2.11: Simplified overview of aero-hydro-servo-elastic codes. Taken from Vorpahl et al. [69]

In this thesis, no changes are done to the blade's structural design, which limits the scope of the aeroelastic design phase. For both softwares, the structural design is a known input.

2.4.1 HAWC2

A wind turbine model in HAWC2 is divided into various subcomponents. The structural model for each of these components is represented by Timoshenko beam elements and the classical Timoshenko beam properties. The multi-body formulation allows each component to have its own coordinate system and with the movement of a coordinate system in space, the internal inertial loads are known.

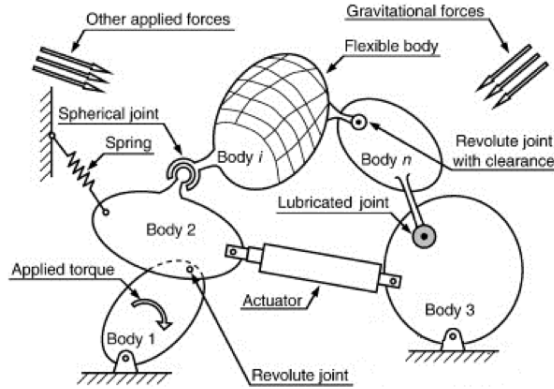


Figure 2.12: Multibody formulation. Taken from Kim et al. [45]

The multi-body formulation allows the wind turbine system to be represented as the assembly of many bodies, each with specific constraints. The constraints determine the type of interaction between wind turbine elements, figure 2.12. With this formulation, one can simulate a wind turbine's response. The multi-body formulation also accounts for large rotations or translations at the coupling points. Small deflections, within objects, are also assumed, due to the linear formulation inside each body, Kim et al. [45].

2.4.2 GH Bladed

The aeroelastic code GH Bladed, also uses an extension of blade element-momentum theory to model rotor aerodynamics. Like in other aeroelastic codes, corrections to BEM are implemented, Cordle and Jonkman [16]. In the past, GH Bladed modelled the wind turbine as a single dynamic system made up of a rotor and a tower, which coupled the tower modes and the rotor modes. With the code's development, the modal and multi-body formulations were combined. Just like in HAWC2, the structure is now represented by several separate bodies, with their individual properties. A Timoshenko beam, is the FEM model used, to calculate the modal properties for each of these bodies. To model flexible elements, like the blades or the tower, a modal representation is used. Tower and blade mode shapes depend on several body-specific details, i.e. stiffness distribution, mass distribution. These modes are then coupled with the equations of motion to perform a dynamic response analysis, Bossanyi [12].

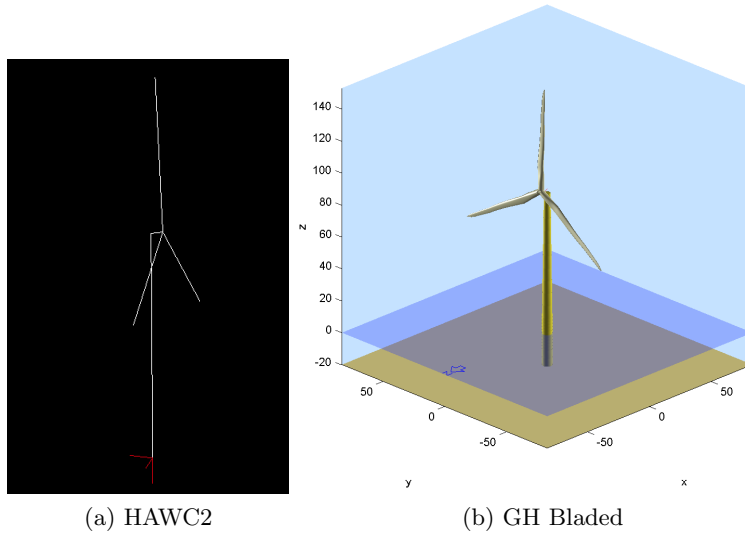


Figure 2.13: NREL 5MW Wind Turbine Visualizations

2.4.3 Aeroelastic Instabilities

It is important to analyse the interaction between the blade's structure and its aerodynamic properties. In this thesis, the reference structural properties are used, an important assumption. Dynamic modelling is essential to analyze the natural and excitation frequencies of the blade.

Degrees of Freedom

The terminology used to describe wind turbine dynamics, facilitates the understanding of aeroelastic instabilities, see figure 2.15 (a). Some of the most relevant degrees of freedom are: tower bending described by fore-aft and side-to-side movements, yaw and shaft rotation in the azimuthal direction. Additionally, in pitch regulated wind turbines, the blades can rotate in pitch, about the pitch axis, to control the angle of attack. With respect to the blades, important degrees of freedom are described by flap-wise and edge-wise directions, Hansen [33].

With regards to a blade section, the degrees of freedom are: rotation about the elastic axis, edge- and flap-wise translations, see figure 2.15 (b). The elastic center, EA , the point where blade rotation occurs, lies apart from the aerodynamic center by a distance of $e \cdot c$. Here, e , denotes the eccentricity factor. The aerodynamic center, AC , is the point where the blade section experiences aerodynamic lift and is assumed to be at $1/4$ of the chord length, c . The center of gravity, CG , lies behind the elastic center, by a distance of $x_\theta \cdot b$. Here x_θ represents the displacement of the CG from the EA . The variable, b , is equal to $c/2$.

Aeroelastic codes are powerful tools for the analysis of wind turbine aeroelastic instabilities. The Campbell diagram is a useful tool as well, but it covers the effects

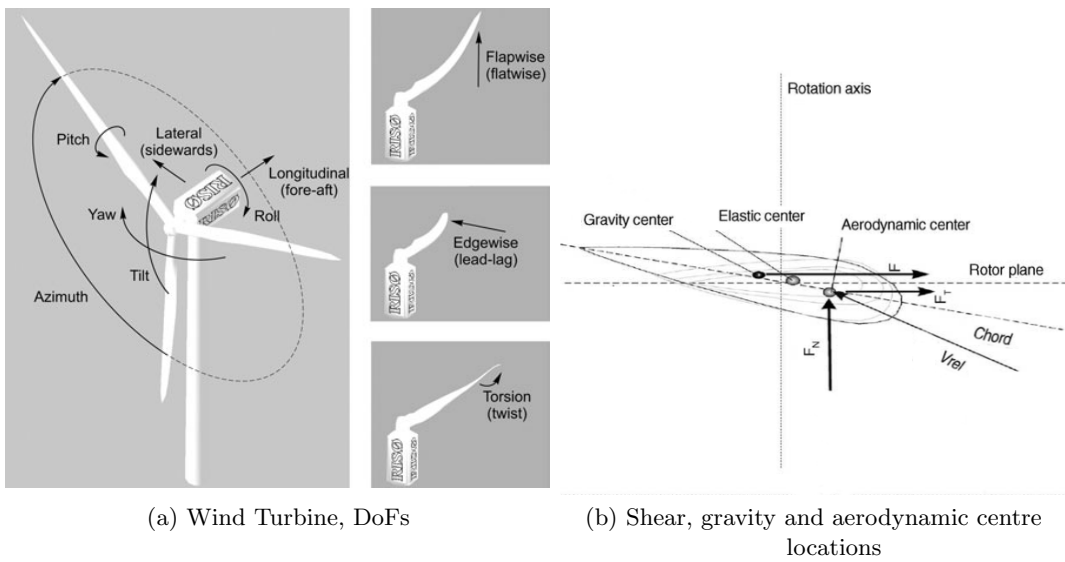


Figure 2.14: DOFs Terminology, Taken from Hansen [33] and Jureczko et al. [44]

of resonance. Aeroelastic instabilities and resonance are not synonyms. Resonance occurs when an external excitation has an equal frequency to one of the system's natural frequencies. Some sources of excitations are turbulence, wind shear, yaw misalignment and pitching. In such cases, vibration adds energy to the system with catastrophic effects. When an aeroelastic instability occurs, the aerodynamic forces are responsible for the added energy to the system. Frequency coincidence is not responsible for this effect, as in the resonance case.

Stall-Induced Vibrations

Stall-induced vibrations are relevant for stall-regulated wind turbines. There are three main aspects that determine whether a wind turbine is at risk of experiencing stall-induced vibrations. These aspects are: airfoil characteristics, direction of vibration and structural damping. In the case of airfoil characteristics, airfoils, with a steep change in the stall region, increase the vibration risk. The direction of vibration is affected by the airfoil characteristics. Some vibrations, relative to the rotor plane, have a higher risk than others. In the end, structural damping may counteract stall-induced vibrations. In the case of flutter, the structural damping cannot counteract the effects of negative damping.

Flutter

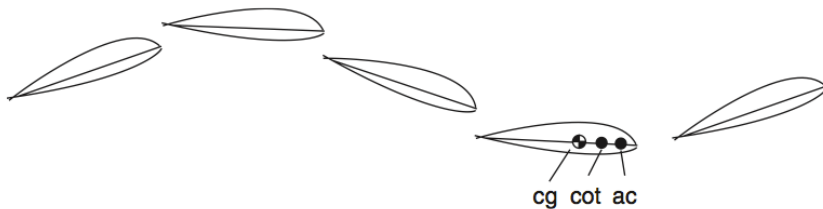
Wind turbine flutter instabilities are more violent than stall-induced ones. Classical flutter was not a driving design factor for wind turbines. However, with the upscaling of wind turbines, slender flexible blades need to be designed to avoid this instability. When flutter occurs, aerodynamic forces cause the blade's torsional mode to couple with the flapwise bending mode into a flutter mode. These torsional

movements affect the angle of attack and consequently the lift force is unfavourably affected, Hansen [33]. The flutter mode has a negative damping that cannot be compensated by structural damping. It has been predicted MW-sized wind turbines' flutter speed is approximately twice the rotor's operational speed, Lobitz [47].



Figure 2.15: Blade flutter mode illustrated by snapshots over one period of oscillation. Taken from Hansen [33]

This effect is clearly explained by Holierhoek [38], in figure 2.16, below.



Classical flutter of an aerofoil. If the centre of gravity (cg) is behind the aerodynamic centre, a flapping motion will result in a twisting moment due to inertia as well as due to the change in the aerodynamic forces. Twisting of the blade will result in a change in flap deformation due to the change in aerodynamics and inertia. The coupling can result in a cycle of twisting and flapping as illustrated, which under certain circumstances can increase in amplitude.

Figure 2.16: Flutter phenomena explained. Taken from Holierhoek [38]

2.4.4 Campbell Diagram

Designers use a powerful tool for the analysis of possible resonance effects in rotational systems, the Campbell Diagram. In this diagram, the turbine modes are placed along the y-axis, while in the x-axis, the rotational speed, is given. Resonance occurs when one of the eigenfrequencies intercept the rotor speed curve or multiples of it. Since the wind turbine has 3 blades, only multiples of these frequencies transfer loads into the hub system: 1P, 3P, 6P, etc.

When using a multi-blade coordinate transformation, one has a symmetric and backward/forward whirling modes for each blade mode. These last two have a shift of $\pm \Omega$ for each blade and increase with rotational speed due to centrifugal stiffening, Hansen [33] and Holierhoek [38]. This is illustrated in figure 2.17.

The Campbell diagram analysis is crucial in order to understand whether or not the rotor operates at rotational speeds, where resonance may occur. In the case of the reference wind turbine, the Campbell diagram is obtained with GH Bladed.

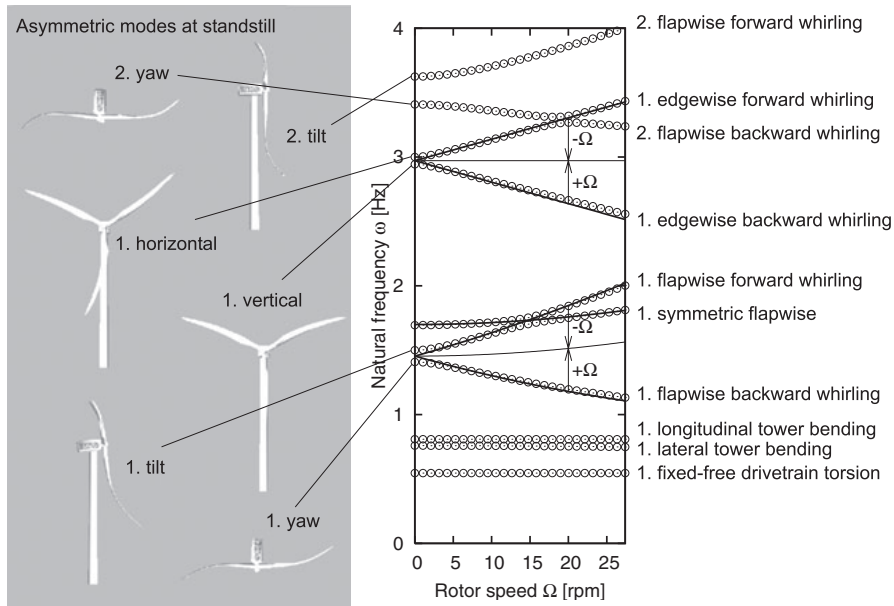


Figure 2.17: Ground-fixed natural frequencies. Lines denote approximations to the computed frequencies, and the center frequencies of the rotor whirling modes given $\pm\Omega$, added to the ground-fixed natural frequencies. Taken from Hansen [33]

HAWCStab2 is also an alternative tool for aeroelastic analysis and works with the same inputs as HAWC2. In Chapter 4, the reference wind turbine GH Bladed project file is provided and is the obvious choice for the eigenfrequency analysis.

2.5 Site-specific Design

On-site wind resources impose wind turbine blade design challenges as well. For example, in China, inland wind resource is generally low, Elliott et al., Song et al. [20, 65]. China's wind resource map confirms this, figure 1.1. In such cases, site specific design is feasible and offers clear advantages, Fuglsang and Thomsen [27]. With respect to blade design optimization, there are various existing methodologies, like GA mentioned earlier. For this thesis, relevant methodologies include the coupling of aeroelastic calculations with a cost of energy model, [26, 57, 70].

The low wind speed sector has been approached with methods that consider the sites in the wind turbine design procedure. These studies reviewed wind turbine design for an onshore and offshore site. Predictions made with an aeroelastic code and a cost model, show site-specific design is feasible. The study is extended by considering more wind climates and scenarios, where specific wind turbine components are modified, [26], [27]. The use of HAWC2 and a cost model, proved a site specific wind turbine design has a lower cost of energy, rather than using a generic wind turbine for all wind climates, Fuglsang et al. [26]. Design loads and annual energy yield are other benefits related to site-specific design.

2.6 Cost of Energy Design

By observing Sunderland's cost of energy model, it is clear many design variables affect the components' costs of a wind turbine, Hau et al. [36]. Below in figure 2.18, Sunderland's cost model flowchart is included. With the use of several wind turbine data sets, the Sunderland's cost model was validated, in order to observe the upscaling trend between rotor diameter and weight.

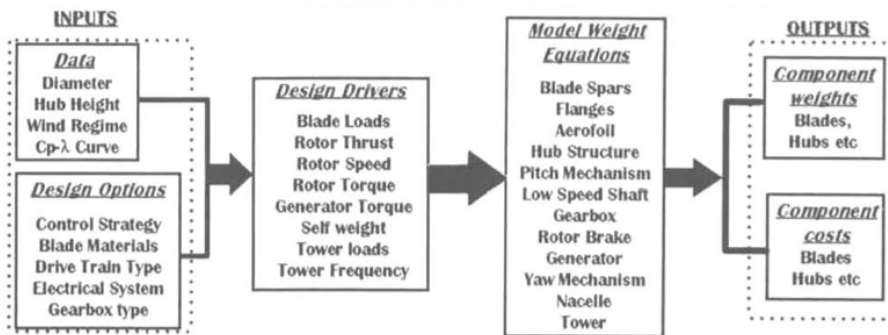


Figure 2 : Flowchart showing operation of the cost model

Figure 2.18: Sunderland's Cost Model Flowchart. Taken from Hau et al. [36]

Some years after Sunderland's cost model, NREL also developed a wind turbine cost and scaling model, Fingersh et al. [23]. The cost model contained updated relations between cost and mass for various wind turbine components. The main output of this cost model is the levelized cost of energy, Eq. 2.11

$$COE = \frac{FCR \times ICC}{AEP_{net}} + AOE \quad (2.11)$$

To approximate blade cost, NREL used information obtained from other wind turbine development projects. This resulted in blade mass and cost scaling laws for baseline or more advanced blade designs, figure 2.19.

In this thesis, blade length is not considered a design variable and remains as the baseline used. Therefore, it cannot be used to approximate the blade's cost. This requires the use of a cost model that consistently considers the changes in the chord distribution and its consequences on total mass. For this reason, the rotor cost model, proposed by Wang et al. [70], provides a relative rotor cost value. This is a sufficient approach for a cost of energy optimization. The cost model is described in Section 5.1.

2.7 Discussion

The use of site conditions, for wind turbine blade design, and the coupling of optimization methods, with aeroelastic simulations, back up the feasibility of low wind

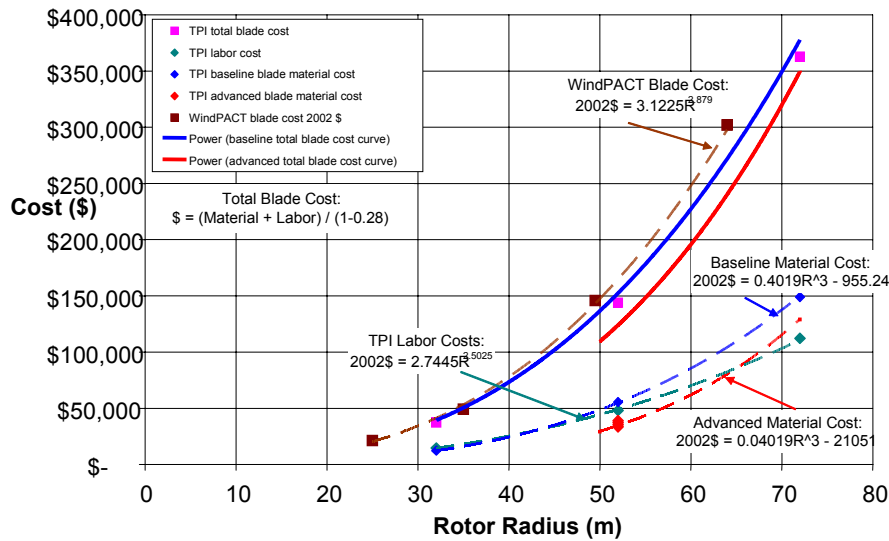


Figure 2.19: Blade cost scaling relationship. Taken from Fingersh et al. [23]

speed wind turbine design. The results from the analysis performed by NREL, on the development of low wind speed technology, summarize the developments needed for this sector to grow, [42]. Later on, NREL performed a wind resource analysis that confirmed most of the Chinese wind resource is predominantly of low wind speeds, Elliott et al. [20]. This means the market has great potential for growth. Therefore, the low wind speed wind turbine design market relies on further developments, whether from industrial or academic groups, J. et al. [42].

The coupling of aeroelastic codes with cost of energy models and the benefits from site-specific design are indeed a starting point to consider for the design of a low wind speed wind turbine blade. Nevertheless, optimization methods do not only affect the blades, but other wind turbine components as well.

Chapter 3

Site Data

3.1 Site Description

The wind turbine is meant for a site in the southwest of China, Guizhou Province, ($25^{\circ}49'N$ - $104^{\circ}25'E$), with an elevation of 2,445 meters above sea level, see figure 3.1. Wind data has been collected from 2010.11.1 to 2011.10.31 at 70 m, as a reference height. The wind resource data is provided by MYWP. An assessment performed by NREL is also referenced for additional details on the Guizhou Province, Elliott et al. [20].,

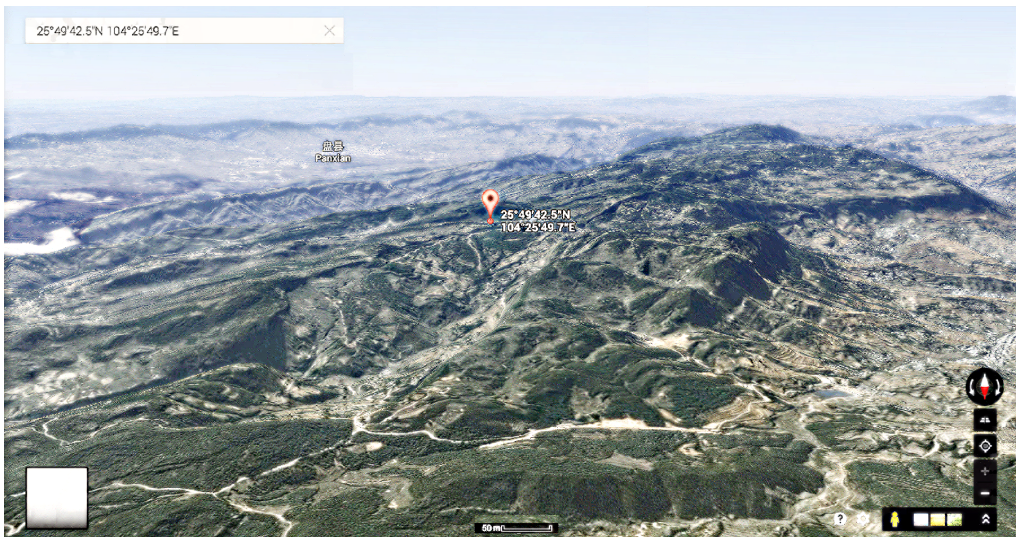


Figure 3.1: Satellite Imagery

Section 3.2 involves the wind data provided by MYWP, with some further complementary analysis. This, to understand whether the site matches the wind turbine specifications given by MYWP.

The Guizhou province has ridge crests and elevated terrain features that affect the wind resource. This is confirmed by observing figure 3.1. Adjustment of the wind data is required, as the uncertainty of the measured wind resource may lead to low or high power predictions. This is important, but outside the scope of this thesis. In Table 3.1, some conclusions on the site analysis by NREL.

Table 3.1: Assessment of Potential & Land, Guizhou Province

Province	Area (km^2)	Mapped Area	Class 3	Class 4	Class 5
Guizhou	142,734	10,037	151 km^2	12 km^2	1 km^2

The study done by NREL covers less than 10% of the province area, which limits the use of any site information provided by NREL's site assessment. However, by knowing the wind turbine's site, other features may be assessed by observing a digital elevation map, *DEM* [41] or by accessing a global weather conditions visualizer[9], as in figure 3.2. From these observations, conclusions can be drawn on the site's wind resource interaction with the terrain. This provides additional details necessary for further stages in the wind turbine development project, i.e. logistics, construction, grid layout, etc.

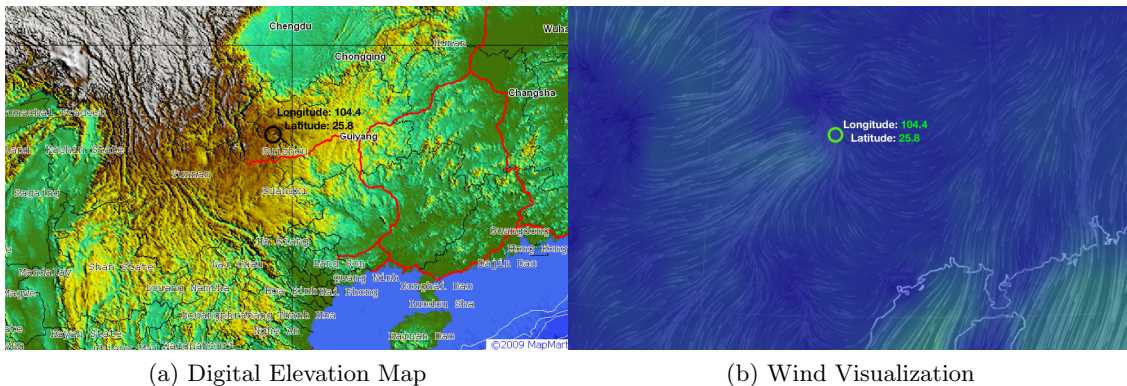


Figure 3.2: Wind Site Characteristics

3.2 Wind Resource

To proceed with the site analysis, the wind resource is studied. The mean wind speed distribution provided for the period of one year and 24 hours, is shown in figure 3.3.

Table 3.2: Provided Site Parameters

\bar{U} [m/s]	A [m/s]	k [-]
6.85	7.4	1.61

The provided site characteristics also include, the Weibull distribution parameters, in table 3.2. These parameters are needed when performing AEP calculations. For now, with the Weibull parameters, the mean wind speed is verified as follows,

$$\bar{U} = A\Gamma\left(1 + \frac{1}{k}\right) \quad (3.1)$$

Where $\Gamma(x)$ is the gamma function equal to $\int_0^\infty e^{-t} t^{x-1} dt$. The mean wind speed, \bar{U} of 6.63 m/s approximates the provided average value, table 3.2. Another parameter, used to assess the wind resource measurements and the potential of wind power per square meter, is the power density, $\frac{\bar{P}}{S}$, defined as follows;

$$\frac{\bar{P}}{S} [\text{W/m}^2] = \frac{1}{2n} \sum_{i=1}^n \rho \cdot v_i^3 \quad (3.2)$$

where n is the number of data points to be averaged, ρ is air density and v the wind speed.

The averaged power density values are also provided. The relations described above are found in, Manwell et al. [49]. Figure 3.3, shows the hourly and monthly average data for mean wind speed, \bar{U} , and power density. The wind speed, and thus the power density, change with the season and the time of the day, as expected. Due to this, a higher energy production occurs during certain periods of the year.

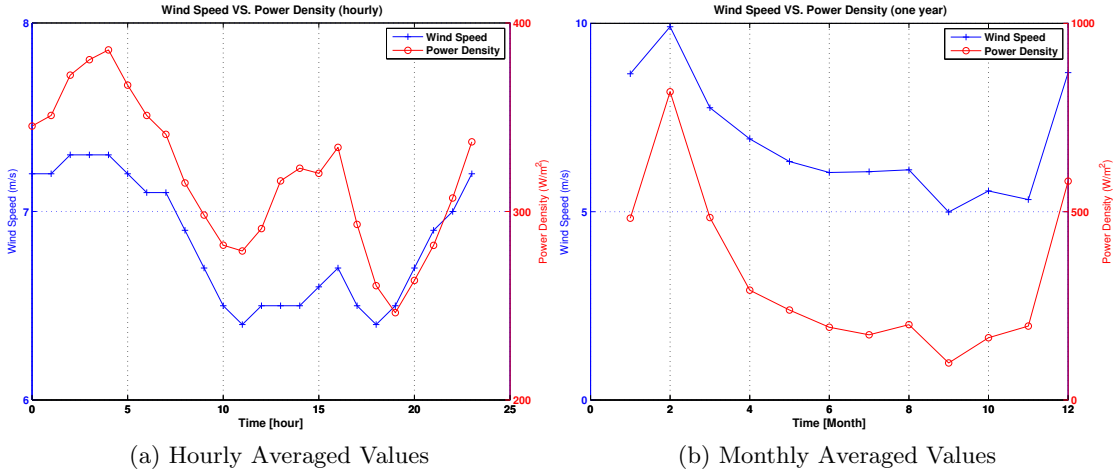


Figure 3.3: Wind Speed & Power Density

From the power density distribution, it is visible the site has a marginal to moderate resource potential. One third of the time, the power density is quite good in comparison to the rest of the year, see figure 3.4.

Class	Resource Potential	Wind Power Density (W/m ²) @ 30 m agl	Wind Speed (m/s) @ 30 m agl
1	Marginal	100 – 200	4.4 – 5.6
2	Moderate	200 – 300	5.6 – 6.4
3	Good	300 – 400	6.4 – 7.0
4	Good	400 – 500	7.0 – 7.5
5	Excellent	500 – 700	7.5 – 8.4
6	Excellent	700 – 1000	8.4 – 9.6
7	Excellent	> 1000	> 9.6

Figure 3.4: Classes of wind power density. Taken from Elliott et al. [20]

3.3 Wind Speed Probability

The trend for wind speed and power density are clear, however the probability of their occurrence is very useful. The wind speed and wind energy frequency distributions are included in figure 3.7. With the use of the Weibull and Rayleigh distributions, one verifies which distribution describes the site most accurately. The Weibull and Rayleigh wind distributions are determined with the scale, A or C , and shape, k , parameters as follows;

$$pdf_W = \frac{k}{A} \left(\frac{U}{A} \right)^{k-1} \exp \left(-\left(\frac{U}{A} \right)^k \right) \quad (3.3)$$

$$pdf_R = \frac{\pi}{2} \frac{U}{\bar{U}^2} \exp\left(\frac{\pi}{4}\left(\frac{U}{\bar{U}^2}\right)\right) \quad (3.4)$$

Below, in figure 3.7 a, the wind speed and energy probability show how some energy outputs and wind speeds are more likely than others. In figure 3.7 b, the fitted Rayleigh and Weibull distributions are graphed. It is clear the fitted Rayleigh distribution is closer to the provided site distribution (in black).

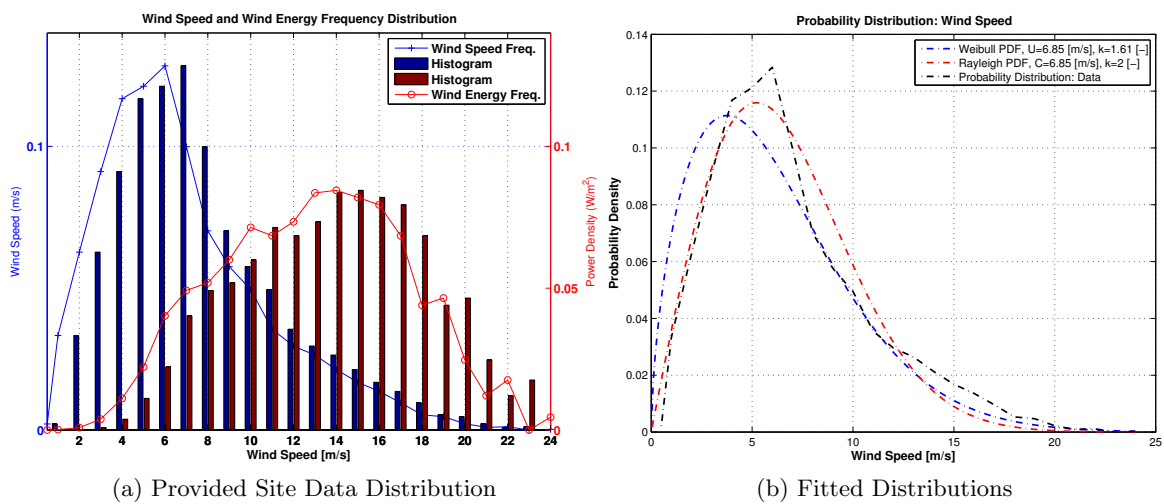


Figure 3.5: Wind Speed & Wind Energy Frequency Distributions

From figure 3.2, it is obvious the site is inland-type. The Weibull shape parameter, k , is less than 2, which is a typical value for this kind of sites. As mentioned earlier, according to Eq.(3.1), the mean wind speed is $\bar{U} = 6.63$ m/s.

As for the wind direction, the yearly wind direction is *SW* and *SSW*. The wind rose, figure 3.6, shows the annual mean value. The monthly averages follow the same trend. It is quite interesting how the wind comes predominantly from one direction. This can be caused by site orographic features, figure 3.1.

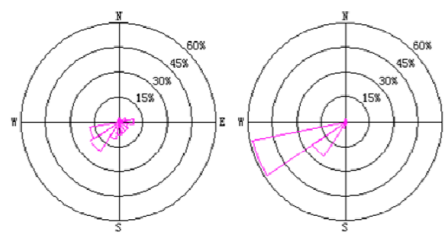


Figure 3.6: Wind Direction & Wind Energy Rose: Annual Mean

3.3.1 Hub Height Wind

Concerning the site's wind resource, the data concerns a reference height of $H_{ref} = 70\text{ m}$. Now, $H_{ref} = 60\text{ m}$ is used, as the shear exponent and mean wind speed for this height are both known. Transforming the resource data to hub height is standard procedure, before using the relations discussed in previous sections. Assuming neutral atmosphere conditions, wind speed at hub height is approximated with the power law, using table 3.3.

$$u(H) [\text{m/s}] = U_{ref} \times \left(\frac{H_{hub}}{H_{ref}} \right)^\alpha \quad (3.5)$$

The hub height for the wind turbine model is defined as, $H = 90\text{ m}$. The shear exponent, α_o , varies with season, elevation, time of the day, terrain's nature, wind speed, temperature, etc. In the end, the exponent value, best fitting the wind site data, is chosen. MYWP provided the reference value.

Table 3.3: Power Law Reference Values

\bar{U}_{Ref} [m/s]	H_{Ref} [m]	α [-]	\bar{U}_{Hub} [m/s]
6.56	60	0.2806	7.35

The site's Weibull distribution is extrapolated to the wind turbine's hub height by using the power law. The method is taken from Gualtieri and Secci [31]. It is important to have an accurate wind resource with respect to the wind turbine's hub height.

$$c_2 = c_1 \left(\frac{h_2}{h_1} \right)^n \quad (3.6)$$

$$k_2 = k_1 \left(\frac{1 - 0.881 \ln(h_1/h_r)}{1 - 0.881 \ln(h_2/h_r)} \right) \quad (3.7)$$

where c_1 and k_1 are the known Weibull parameters at height h_1 . The parameters are extrapolated to height h_r , by using the n -exponent from Eq. 3.8.

$$n = \alpha \left(\frac{1 - \ln(c_1)/\ln(v_h)}{1 - \alpha \ln(h_1/h_r)/\ln(v_h)} \right) \quad (3.8)$$

The results of the extrapolation show a small variation in the Weibull parameters, figure 3.7 (b). This is due to the extrapolation done from 70 m to 90 m , where the wind profile shows a slight change, figure 3.7 (b). Another reason is the extrapolation method used, where other methods could be used to make a comparison. This is beyond the scope of this thesis.

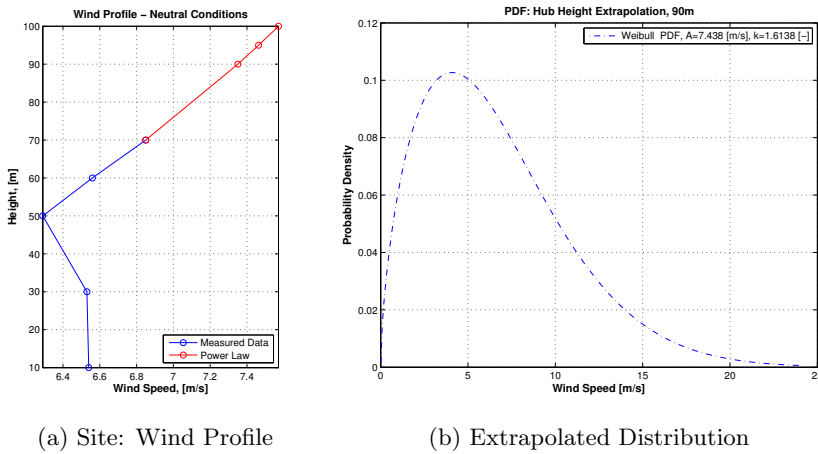


Figure 3.7: Wind Profile & Weibull PDF

3.4 Extreme Wind

Apart from the wind speed distribution, it is also necessary to determine the extreme wind cases, in order to define the class of the wind turbine. A first approximation, often used as a rule of thumb, states the 50-year extreme wind speed is five times the mean wind speed at the site;

$$U_{50} = 5 \cdot \bar{U} \quad (3.9)$$

Although it is a straight forward rule, the difference with more sophisticated methods is surprisingly small. However, in order to verify the previous rule, a Weibull based model is used to approximate the 50-year extreme wind, given by the following formula;

$$U_{50} [\text{m/s}] = \alpha_{50} \ln(50) + \beta_{50} \quad (3.10)$$

Where α_{50} and β_{50} are approximated as follows, according to [11]

$$\alpha_{50} = \frac{A}{k} (\ln(n))^{-1+1/k} \quad (3.11)$$

$$\beta_{50} = A(\ln(n))^{1/k} \quad (3.12)$$

Where $n = 0.483 \cdot N_U$, where N_U is equal to the number of 10-min averaged measured. In this case N_U is limited due to the amount of averaged values provided. Table 3.4, shows a comparison of the results obtained through the previous methods introduced.

Table 3.4: Estimate of 50-year extreme wind

Method	U_{50} [m/s]
Rule of Thumb	34.25
Weibull Estimate	24.97

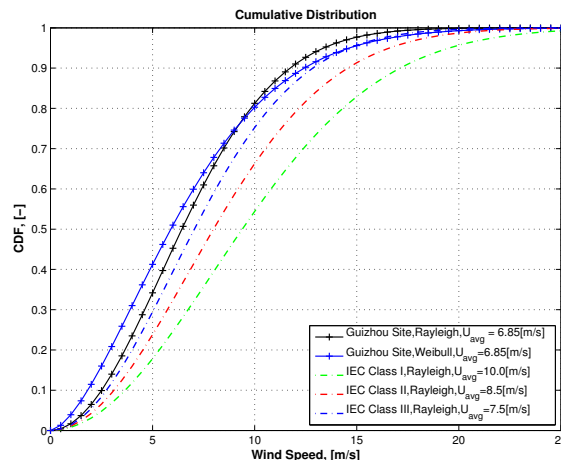
3.4.1 Wind Turbine Class

There is a distinct difference between the values in Table 3.4, because the wind data used to compute the previous parameters, is based in few mean values during one year, where 10-min data should be used for higher accuracy. The site 50-year extreme wind is to be closer to the first value from Table 3.4, leading to a **IEC class III**, [40]. This value matches the extreme wind speed, 37.5 [m/s], determined by MYWP's design requirements.

According to MYWP's site report, this inland site possess a turbulence intensity of 18.93 %. According to IEC, [40], this is a high turbulence characteristic, which corresponds to **A**. Therefore, the class of this wind turbine should be:

III-A

However, design requirements mentioned turbulence characteristics corresponding to **C**. Additionally in figure 3.8, the cumulative distributions for the existing wind turbine classes are graphed, together with the Rayleigh and Weibull distributions matching the provided site parameters. It is clear the site's wind distribution is closer to that of a **IEC class III** wind turbine.

**Figure 3.8:** Cumulative Distribution, function of Wind Speed: At Site & IEC Standard Specific

From this site analysis, the wind model input, for HAWC2, is completed. It is also interesting to note, low wind speed sites have wind speeds of ≈ 6 m/s. However, the site provided has a slightly higher wind speed, ≈ 7.5 m/s, which is used for the optimization. Now, with the site's characteristics, the design of a site-specific wind

turbine design begins in Chapter 5. However, before developing a new design, the input reference wind turbine is studied in Chapter 4.

Chapter 4

Reference Wind Turbine

After the site assessment, one reviews the reference wind turbine and its overall characteristics. Both the site and the reference wind turbine serve as a baseline for the creation of the HAWC2 model. In this chapter, the reference turbine model taken from GH Bladed, is briefly studied. This provides an insight into the elements, the dimensions, and the operational characteristics taken from the baseline.

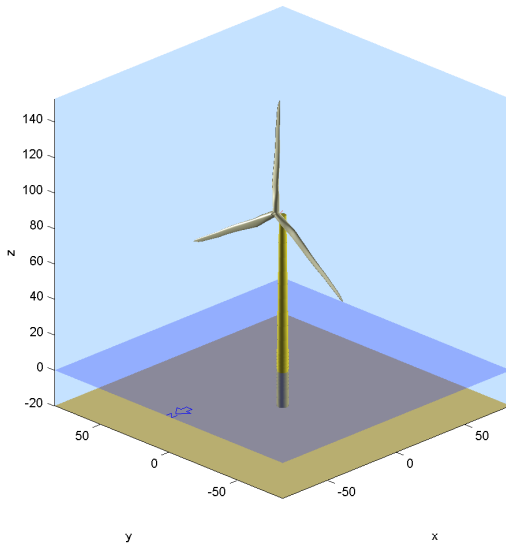


Figure 4.1: Wind Turbine, GH Bladed

4.1 Wind Turbine Reference Values

In this section, the specifications of the reference turbine referred to as the 'MY 2.0MW baseline wind turbine' are given. The wind turbine consists of three blades and is a conventional upwind variable-speed, variable blade-pitch-to-feather-controlled turbine. A table with the properties of the 2.0-MW wind turbine is shown below:

Table 4.1: Gross Properties for the MY 2.0-MW Reference Wind Turbine

Design Class	III-C
Rating	2.0 [MW]
Rotor Orientation, Configuration	Upwind, 3 Blades
Control	Variable Speed, Pitch Regulated
Drive train	Three-stage gearbox
Gearbox Ratio	131.38 [-]
Rotor, Hub Diameter	115 [m], 2.2 [m]
Airfoil Family	In-house [-]
Hub Height	85 [m]
Cut-In, Rated, Cut-Out Wind Speed	4 [m/s], 9.5 [m/s], 18 [m/s]
Cut-In, Rated Rotor Speed	8.375 [rpm], 13.3 [rpm]
Rated Tip Speed	75 [m/s]
Overhang, Shaft Tilt, Conning	3.24 [m], 5 [deg], -3.5 [deg]
Blade Prebend	2.75 [m]
Rotor Mass	55,508 [kg]
Nacelle Mass	86,600 [kg]
Tower Mass	205,573 [kg]

Some aspects to highlight are the design class of the wind turbine and the unknown airfoil family. It is also important to understand the constraints involved when designing a rotor, which must remain compatible to other wind turbine components that are not part of the design phase. Below, figure 4.2 shows the principle of operation for a pitch regulated variable speed wind turbine (PRVS).

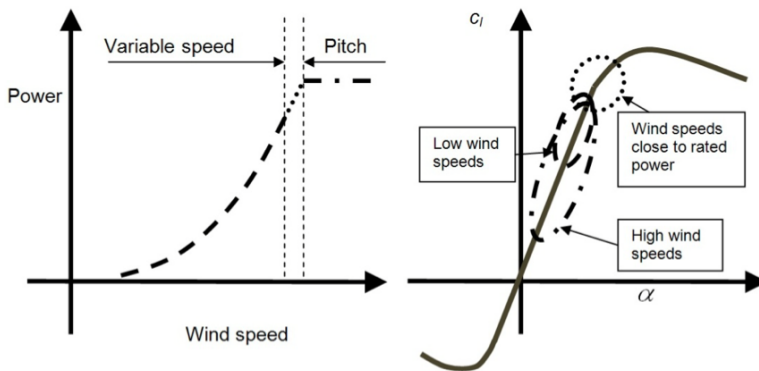


Figure 4.2: Principle behind PRVS Wind Turbines. Taken from Bak [4]

4.2 Blade Geometry

Blade geometrical properties are shown in this section. The data sets, obtained from the Bladed project file, contain most of the blade's properties. Below, an overview of the chord and twist distribution of the 2.0-MW wind turbine is given, figure 4.3. The chord distribution is smooth. On the other hand, the twist distribution has regions where changes occur with a constant slope. A smoother distribution is more beneficial with regards to manufacturing. In this case, no sudden changes in twist angle are present, which is good for material lay-up, avoiding stresses in-between layers.

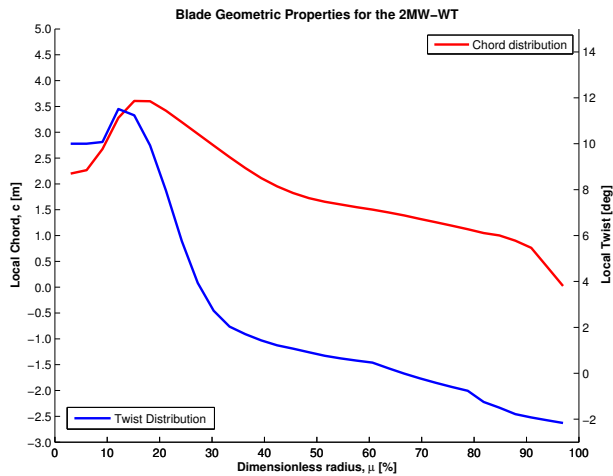


Figure 4.3: Blade Geometric Properties of the 2.0 MW wind turbine

The blade's planform shape is shown in figure 4.4. The given reference shape remains unchanged for the new design, from the location of the largest chord to the root. The blade also has a prebend of 2.75 meters at the tip. In the figure, the blue arrow indicates the region, where changes take place. Unlike the red arrow, indicating the opposite.

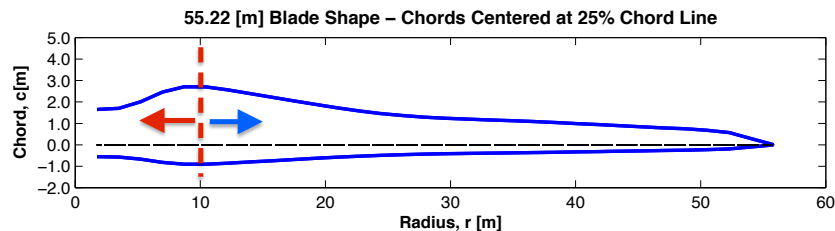


Figure 4.4: Blade Planform of the 2.0 MW wind turbine

The current airfoil layout is sketched, figure 4.5. The regions in yellow, contain airfoils resulting from an interpolation between the nearest pair of airfoil profiles. In the regions, between the yellow areas, airfoil profiles keep their shape, while being scaled to match the geometric specifications. From the reference blade geometry,

smooth transitions along the blade are appreciated. This is partially valid for the twist distribution. There is a compromise between performance and manufacturing, which is essential and kept in mind for the next stages.

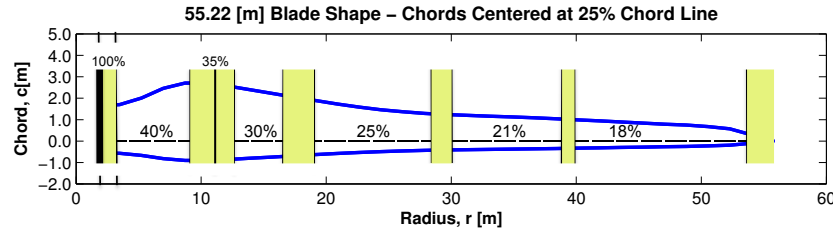


Figure 4.5: Blade Planform of the 2.0 MW wind turbine

4.3 Blade Properties

Important blade structural properties are included in figures 4.6 & 4.7. The structural integrity of the blade increases in importance from tip to root. In this case, the blade root and the largest chord section up to 10 m ensure an adequate flap-wise stiffness, driven by bending moments and blade deflection. The largest chord section has a larger flap-wise stiffness and a lower mass in comparison to the sections near the root. The use of materials like carbon fibre could create such an effect.

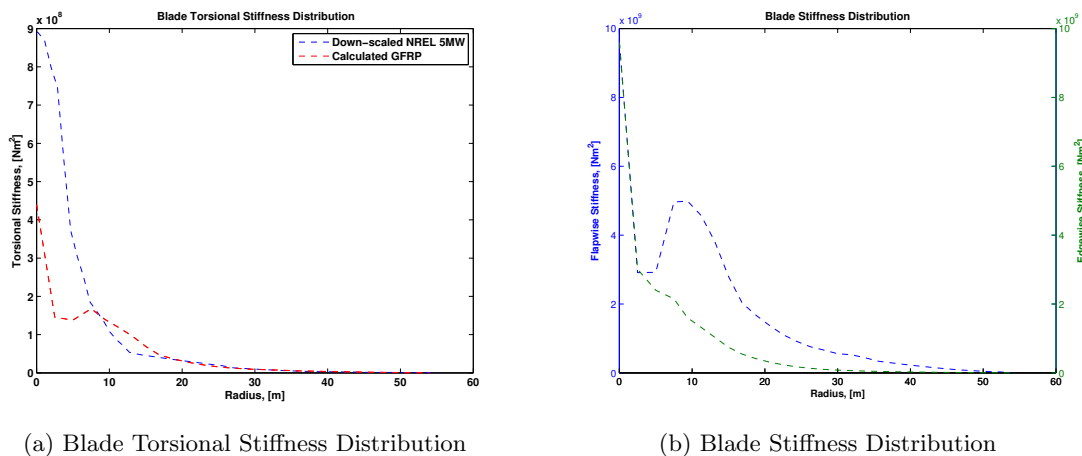


Figure 4.6: Property Distributions of 2.0 MW wind turbine

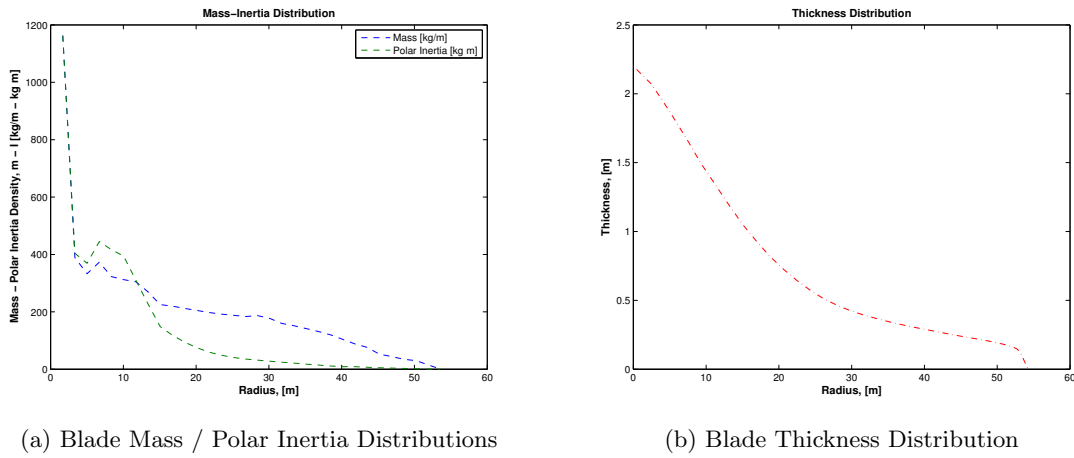


Figure 4.7: Property Distributions of 2.0 MW wind turbine

Figure 4.8, provides a more accurate overview of the blade's planform shape.

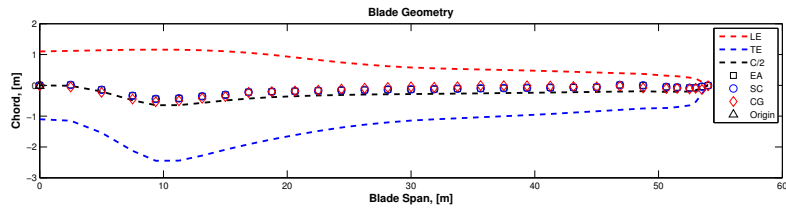


Figure 4.8: Blade Geometry Overview

The torsional stiffness was not provided by MYWP, however with the given structural information and a box beam assumption, the torsional stiffness is estimated for HAWC2. An approximation is also made based on the downscaling of the NREL 5MW wind turbine. Both results are shown in figure 4.6 (a). The method used for the torsional stiffness calculation is included in Appendix D. The blade's mass and bending stiffness properties are critical for the cost estimation of a wind turbine blade, on the other hand, the torsional stiffness is essential for aeroelastic stability purposes.

4.4 Tower Properties

The tower structural properties, provided by MYWP, are included in this section, figures 4.9 and 4.10. As with the blade's structural properties, the tower property distributions remain unchanged.

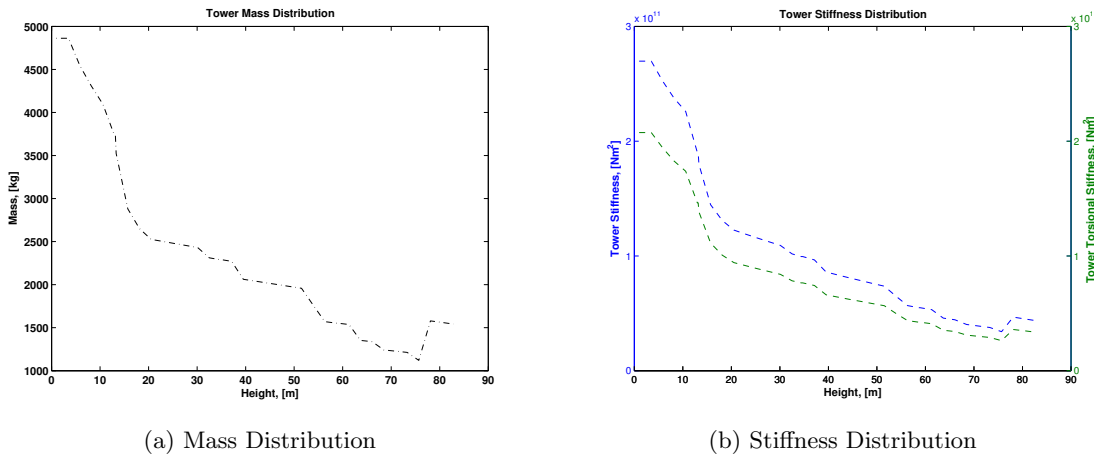


Figure 4.9: Tower Property Distributions of 2.0 MW wind turbine

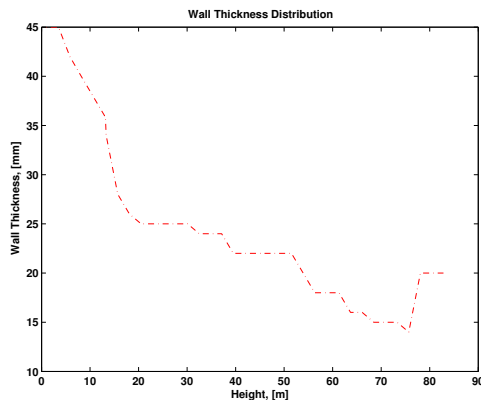


Figure 4.10: Wall Thickness Distribution of 2.0 MW wind turbine

4.4.1 Tower Clearance, Tilt & Cone Angle

The coning and tilt angle are kept the same as the reference wind turbine. The first parameter, θ_{cone} , is commonly used for structural reasons in order to have an acceptable placement of the blade tip with respect to the tower. The second parameter, θ_{tilt} , is the angle between the rotor axis of rotation and the wind direction. Again, this parameter serves for proper displacement with respect to the tower.

These angles are set as follows;

$$C = -r(h) + \cos(\theta_{tilt})A + \sin(\theta_{tilt} + \theta_{cone})(B + R) \quad (4.1)$$

where;

$$h = H + \sin(\theta_{tilt})A - \cos(\theta_{tilt} + \theta_{cone})(B + R) \quad (4.2)$$

No blade structural changes are performed, hence the tower clearance may remain the same at, ≈ 9.6 meters.

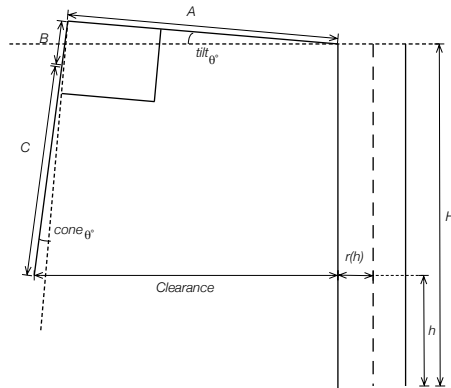


Figure 4.11: Tower Clearance

4.5 Wind Turbine Performance, GH Bladed

The maximum values from the reference wind turbine, serve as a constraint for the new blade design. The maxima, in figure 4.12, are reached at rated speed. Once the wind turbine operates at wind speeds higher than the rated wind speed, blade pitching keeps a constant power output. This causes the reduction of thrust, tip deflection, power coefficient and the bending moments, figures 4.12 to 4.14.

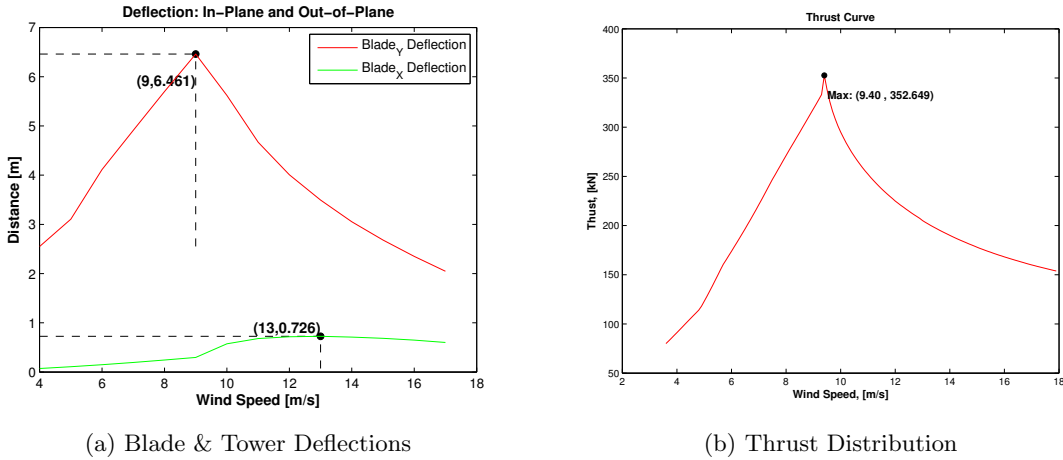


Figure 4.12: Deflections & Thrust Curves, Ref. WT

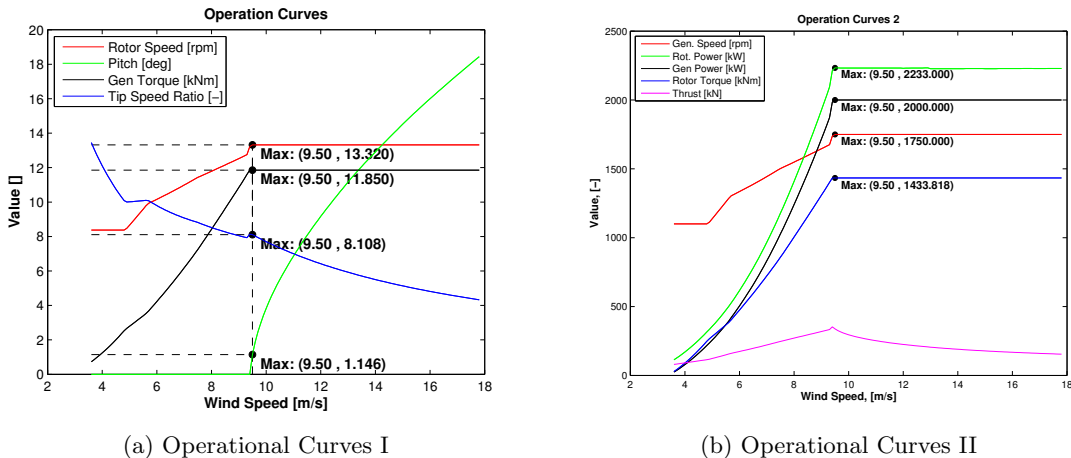


Figure 4.13: Operational Curves, Ref. WT

The rated wind speed of the wind turbine, 9.5 m/s , is quite good for the site, with an average wind speed of $\approx 7 \text{ m/s}$. If the rated wind speed is decreased, the wind turbine operates under full power conditions for a longer period of time. This is an advantage for annual energy production, but not desirable due to fatigue. Fatigue is not only relevant for the blades, but for all wind turbine components. In this case, this is not a constraint, but an aspect to take into consideration.

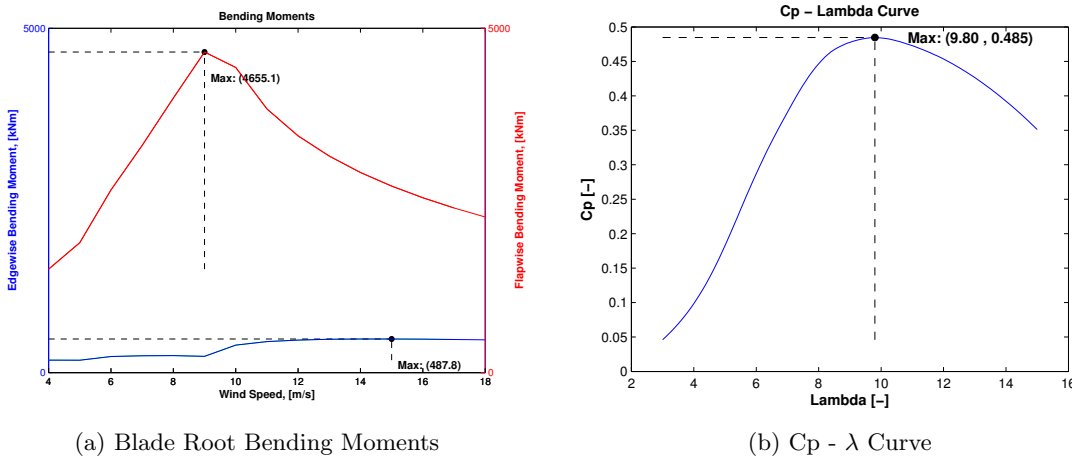


Figure 4.14: Bending Moment, C_p - λ Curves, Ref. WT

From the reference wind turbine's operational curves, a brief summary of the performance indicators is presented, table 4.2. With regards to the aerodynamic performance, it is important to highlight the encryption of airfoil coefficients, in the GH Bladed project file. This means the aerodynamic design of the baseline wind turbine may not be fully implemented in a HAWC2 model. For this reason, the baseline's performance curves for HAWC2 are not included.

Table 4.2: Performance Indicators, 2 MW Reference WT

$C_{P,\max}[-]$	0.485
$\lambda_{\text{opt}}[-]$	-
$\theta_{p,\text{opt}}[\text{deg}]$	0

The behaviour of the reference wind turbine, in Region 2, is explained by the implemented controller, figure 4.15. Usually the tip speed ratio, λ , is kept at a constant value that matches the optimal power coefficient. This is not the case, as the manufacturer uses a C_p look-up table for operation, as a regulation method. The look-up table is dismissed for the new blade design.



Figure 4.15: Controller Look-up Table

4.6 Campbell Diagram

The Campbell diagram, in figure 4.16, shows the rotational speed range during power production. The rotational speed of the rotor is represented by 1P and should usually be 10% below the tower bending frequency. The rotor blades' passage frequency, 3P, should be appropriately spaced from the tower natural frequencies. The reference wind turbine respects these requirements to some extent.

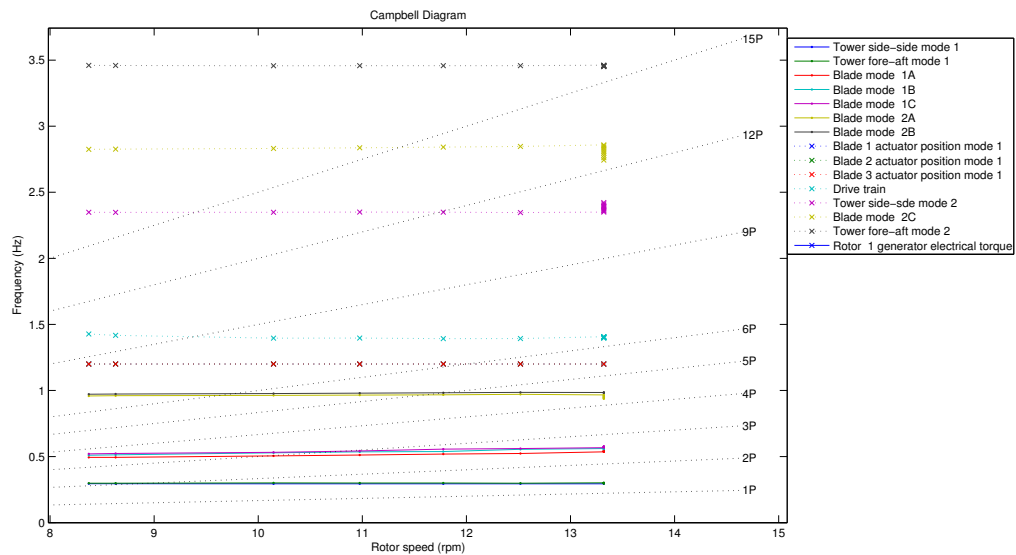


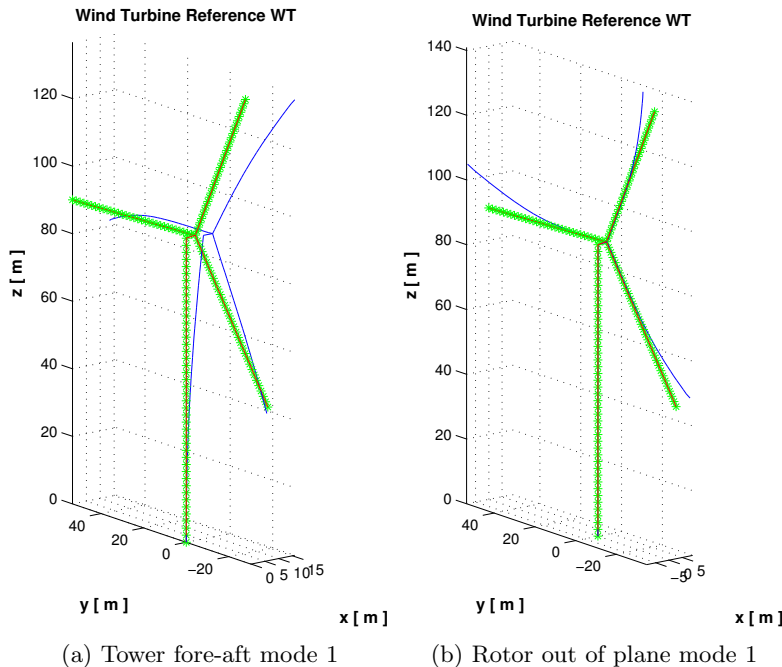
Figure 4.16: Campbell Diagram, Reference Wind Turbine

There is a slight interference of the blade modes with 3P and its harmonic, 6P. Some resonance effects are to be expected. The excitement of these modes occurs at a rotor speed of 9.5 rpm and between 10-11 rpm. Changing the blade stiffness or avoiding this operational regimes is advisable. The blade and tower damping ratios are, $\zeta = 0.007$ and 0.005 . The wind turbine's eigenfrequencies are listed in table 4.3.

Table 4.3: List of the first eigenmodes and their corresponding eigenfrequencies.

Mode	Description	Frequency, [Hz]
1	Tower side-side mode 1	0.295
2	Tower fore-aft mode 1	0.298
3	Rotor out of plane mode 1	0.50
4	Rotor out of plane mode 3	0.53
5	Rotor out of plane mode 2	0.52
6	Rotor in plane mode 1	0.96
7	Rotor in plane mode 2	0.97
8	Drive train	1.43
9	Tower sideside mode 2	2.30
10	Rotor in plane mode 3	1.44
11	Tower fore-aft mode 2	3.40

With the Campbell diagram, some rotational speeds are identified and must be avoided. This may lead to the excitation of some wind turbine eigenfrequencies. The visualization of selected modes is included in figure 4.17, (with support of Ferret Gasch [22]).

**Figure 4.17:** Visualization of Selected Eigenfrequencies

4.7 Summary

Some of the reference wind turbine components serve as the basis for the developed HAWC2 aeroelastic model. To conclude, a complete overview of the reference wind turbine is included in table 4.4.

Table 4.4: Summary of 2 MW reference wind turbine

Dimensions & Masses			
N° Blades	3	Rotor pos.	Upwind
R, D [m]	54.15, 115	m_{rotor} [kg]	55,508
T, C [deg], O [m]	5.0, -3.5, 3.24	I_{rotor} [kgm^2]	20,852,110
H [m]	85	m_{nacelle} [kg]	86,600
m_{blade} [kg]	12,072	m_{tower} [kg]	205,573
I_{blade} [kgm^2]	6,416,862	m_{total} [kg]	347,680
Aerodynamic performance			
Power Output [MW]	2.0	$C_{P,\text{max}}$ [-]	\approx 0.47
U_{rated} [m/s]	9.5	Opt. TSR [-]	9.8
$U_{\text{cut in}}, U_{\text{cut out}}$ [m/s]	4.0, 18.0	Pitch rates [deg/s]	-5.0, 8.5
Ω range [rpm]	8.3 - 13.3	Max ΩR [m/s]	75.0
IEC-Class	III-C	Gross AEP [GWh/yr]	\approx 6.87
Drive train			
Gearbox ratio	131.38	Generator type	-
N° Gear. stages	3	ω_g range [rpm]	1100 - 1750
Shaft torque [Nm]	10,318	Max Q_g [Nm]	11,850
Voltage Output [V]	-	Grid freq. [Hz]	50.0
Control System			
Control type	VSPR	Look-Up Table	-
Torque Control	-	MYWP	-
Pitch Control	-	MYWP	-

Chapter 5

Aerodynamic Design

The aerodynamic design of a wind turbine blade involves a broad range of technical aspects. With the study of the reference wind turbine blade, a set of limitations for the proposed design are established. This reduces the number of free variables. Although the aerodynamic and aeroelastic performance of the reference is assessed, the reference's airfoil geometries or characteristics are not discussed. The design proposed in this chapter, consists of DU airfoils, however a direct comparison to MYWP airfoils cannot be made.

The process begins with a brief rotor diameter analysis, followed by the analysis of DU airfoils under rough and clean conditions. The blade geometry optimization is introduced and the optimal twist / chord distributions are found. Finally, the aerodynamic performance of the blade is assessed and verification follows, with the set of limitations in mind.

5.1 Objective Function

The optimization algorithm targets the minimization of the objective function, delimited by a set of constraints. As the output is minimized, this function determines whether an evaluation step is acceptable or not. An optimization may target different aspects of rotor design, however the objective function is chosen with care to reduce computational time. With respect to this objective function, the wind turbine's aerodynamic blade design takes the spotlight. Being responsible for power transmission to the shaft, the aerodynamic design of the blades is the primary focus.

The structure is not part of the optimization. Whether the blade geometry is compatible with the structural properties given or not, is an important assumption tested in Appendix B. Nevertheless, the aerodynamic optimization respects the constraints set by the structure. This aspect reduces the number of design variables.

To start the optimization and reduce computational time, a proper aerodynamic design guess is beneficial. Section 5.3, covers this aspect.

The optimization method accounts for the cost of the rotor, with respect to its total mass, Eq. (5.2). Transportation, operation and maintenance, manufacturing and material costs are assigned the constant, b_{rotor} . The variable part of the cost is proportional to the rotor's weight. In Eq. (5.1), the fixed costs of the rotor are represented by the subscript, b_{rotor} , and the rotor's mass is represented by the subscript, w_{rotor} . The fixed costs constant, b_{rotor} , is assigned a value of 0.1, Fuglsang et al., Wang et al. [26, 70].

$$C_{rotor} = b_{rotor} + (1 - b_{rotor})w_{rotor} \quad (5.1)$$

$$w_{rotor} = \sum \frac{m_i \times c_{i,opt}}{M_{tot} \times c_{i,or}} \quad (5.2)$$

Based on the formulation above, the new rotor's mass is approximated for the cost model, with respect to the baseline's mass. The twist and chord distribution, resulting from the optimization, influence the blade's mass. Although an interesting aspect to incorporate, the blade's structural properties are not modified and remain fixed for this study. The cost of energy is known with Eq. 5.3, where the total costs are represented by the rotor's cost, C_{rotor} , and the energy produced is the annual energy yield.

$$\text{Cost of energy} = (\text{Total costs}) / (\text{Energy produced}) \quad (5.3)$$

$$f(x) = COE = \frac{C_{rotor}}{AEP} \quad (5.4)$$

With the COE's relative percentage change, comparisons between the two wind turbine rotors are made. With the performance characteristics of the wind turbine and the site's wind data from Chapter 3, the wind turbine's annual energy production is determined as part of the objective function, Eq. (5.4).

In figure 5.1, the Weibull distribution, from figure 3.7, at the wind turbine site, is overlapped on the reference wind turbine's power curve. The overall energy yield curve of the wind turbine is a product of the aerodynamic power and wind speed probability. The annual energy production is defined as;

$$AEP = \sum_{i=1}^{N-1} (P(V_{i+1}) + P(V_i)) \cdot f(V_i < V_o < V_{i+1}) \cdot 8760 \quad (5.5)$$

where, N is the number of velocity segments and $P(V_i)$, denotes the power in kW for each velocity segment. Power is expressed as $P = 0.5\rho AV^3C_P$. This results in the

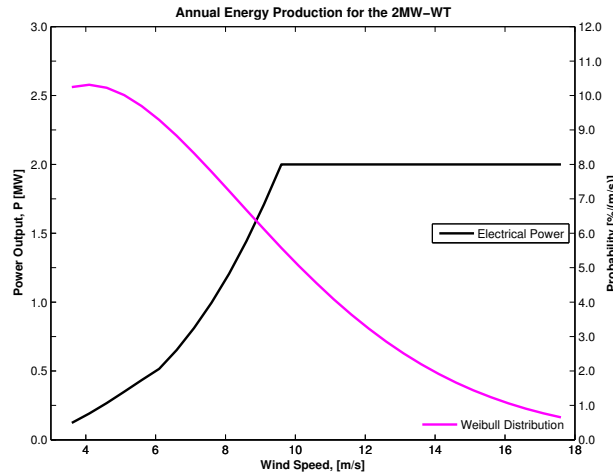


Figure 5.1: Power and site Weibull distribution

annual energy production for the wind turbine rotor. The wind speed probability is determined as follows:

$$f(V_i < V_o < V_{i+1}) = \exp\left(-\left(\frac{V_i}{A}\right)^k\right) - \exp\left(-\left(\frac{V_{i+1}}{A}\right)^k\right) \quad (5.6)$$

The resultant AEP does not consider electrical losses and possible stops due to maintenance operations or emergency stops. In order to account for this, a value for availability of the wind turbine is needed. With respect to the wind resource, MYWP concludes the availability of wind speeds between 3 m/s and 25 m/s is of 7796 hours. Having both the AEP and the rotor's cost formulation, the objective function (COE) is used in the optimization process.

5.2 Constraints

The optimization must remain under feasible limits and constraints are responsible for this. In return, there is a reduction in computational domain. In this section, the chosen constraints are explained.

5.2.1 Rotor Diameter

The first constraint, is the rotor's diameter. Although the rotor diameter, D , is fixed to 115 m, using the well-known blade mass scaling laws, can provide a general overview of the minimal cost of energy ratio to rotor diameter.

$$COE = \frac{C}{AEP} = \frac{(R/R_{ref})^{2.7}}{CF} \quad (5.7)$$

; where the capacity factor, CF , is approximated with the reference wind turbine's AEP and the year round energy production. No operation or maintenance stops are taken into consideration.

$$CF = \frac{AEP}{8760 \times P_{rated}} \quad (5.8)$$

With this relation, one may obtain a rough estimate of the relative change in rotor diameter to match a minimal cost of energy. In this thesis, the diameter remains unchanged. Nevertheless, it is important to mention that blade mass grows with the cube of the rotor's radius, which affects the rotor's cost or the implemented cost of energy model. In figure 5.2, the blade mass versus rotor diameter trend is included.

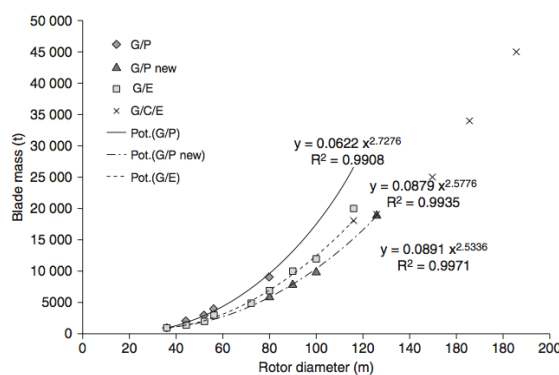


Figure 5.2: Blade Mass versus Rotor Diameter. Taken from Graue H. [30]

MYWP's wind turbine blade has a weight of approximately 12 tons, which certainly matches the mass versus rotor diameter trend line.

5.2.2 Airfoil Family

An airfoil family is chosen as a second constraint. DU airfoils have a specific designation (DUyy-W-xxx), which represent Delft University, the airfoil design date (last two digits of the year), the application type (W - wind energy) and the airfoil maximum thickness, given by the last three numbers divided by 10. DU airfoils come in a wide range of relative thicknesses and are used by many wind turbine manufacturers for rotor diameters that exceed 100 m, Timmer and van Rooij [68].

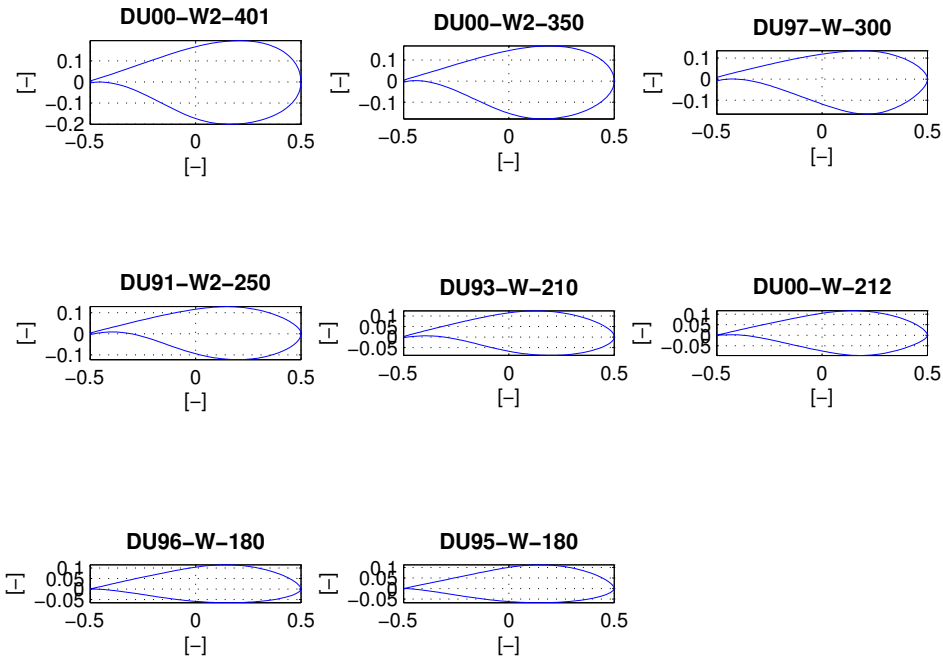


Figure 5.3: DU Wind Turbine Airfoils

Two airfoils from the NACA 63 / 64 six-digit series are also considered, figure 5.4. The NACA six-digit series designation is described in the following manner. The first digit, 6, indicates it is designed for a greater laminar flow than earlier x-digit series. The second digit, 3 or 4, indicates the minimum pressure location ($0.4c$). The digit, after the dash, specifies the design lift coefficient times 10. Finally, the last two digits represent the thickness in percentage of the chord. Some NACA six-digit series airfoils are still used for wind turbine blades, however the NACA four & five-digit series have been discarded for this application due to their sensitivity to roughness, Timmer [67].

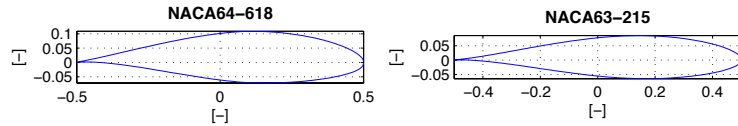


Figure 5.4: NACA 6-Series Airfoils, Wind Turbine Application

The airfoil coefficients and geometries, used by MYWP, for their reference blade design, are not available for this thesis work. This means a direct airfoil comparison cannot be made. DU and NACA airfoils matching the $\frac{t}{c}$ ratio characteristics of the reference wind turbine blade, are used instead. Airfoils with a reliable source of polar data are used i.e. NREL 5MW. For this reason, only some of the airfoils shown in figures 5.3 and 5.4, are used.

The proposed blade follows the same thickness distribution as the reference wind turbine blade. This reference thickness distribution and other specific requirements, table 5.1, are taken into account for the wind turbine's airfoil layout.

Table 5.1: Airfoil Requirement w.r.t. Blade Region

Parameter	Blade Position		
	Root	Mid Span	Tip
Thickness to chord ratio	>28%	28 - 21%	21% >
Structural requirement	High	Med	Low
Geometrical compatibility	Med	Med	Med
Maximum lift insensitive to LER	Low	Med	High
High maximum lift-to-drag ratio		Low	Med
Low max / Post stall behaviour			Med
Low airfoil noise		Low	High

Re Number Effect

Experimental data sets at specific Reynolds numbers are not readily available. To have appropriate airfoil data sets, Rfoil is used. Rfoil, derivating from Xfoil, was developed by TU Delft, National Aerospace Laboratory (NLR) and the Energy Research Centre of the Netherlands (ECN).

The current methodology does not account for Reynolds number effects. However, with the first initial guess or reference chord, the Reynolds numbers along the blade are assessed. This is important, as having the right data completes the HAWC2 model. Therefore, the local Reynolds numbers are obtained as follows:

$$Re = \frac{V_{rel,i} \times c_i}{\nu} \quad (5.9)$$

where c is the chord length, ν is the dynamic air viscosity and V_{rel} is the relative velocity. A rule of thumb for Reynolds number range also exists, Eq. 5.10. Taken from Bak [4].

$$75,000 \cdot R < Re < 150,000 \cdot R \quad (5.10)$$

Figure 5.5 below, shows the Reynolds number experienced along the wind turbine blade with respect to the local relative velocity. The percentage shown refers to the airfoil's t/c ratio. The colours refer to the part of the blade an airfoil is placed at.

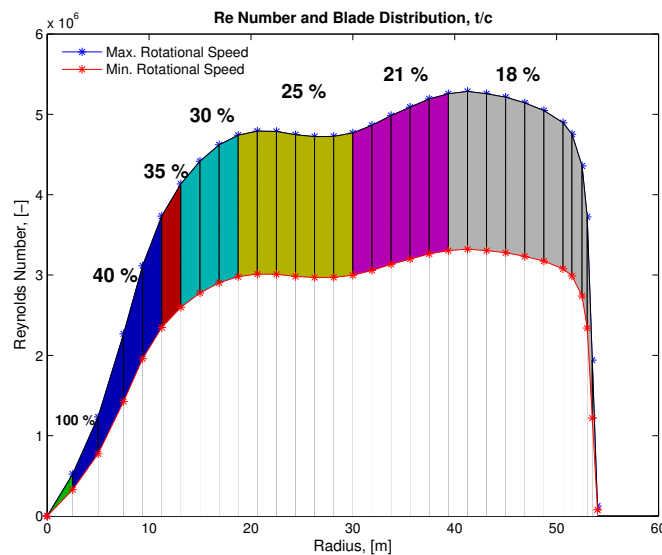


Figure 5.5: Re Number, w.r.t. Radius

Airfoil Characterization, Free & Fixed Transition

As roughness measurements at the desired Reynolds numbers are not available. The rough airfoil surface data sets are calculated by fixing transition, as one of the alternatives. This is done by forcing transition at 5% suction surface chord location and 10% pressure surface chord location, causing transition from laminar to turbulent flow. This is a way of simulating leading edge roughness, as the airfoil is tested under turbulent conditions. The effects of roughness are essential to rotor performance assessment and for the current study, fixing transition is enough, although the effects of leading edge roughness are more severe, Bak and Timmer [5]. The clean airfoil surface data sets are created by using the $e - to - the - n_{th}$ method. The N factor, required as an input, is set to 9 for low turbulent flow. Turbulence, in this case, refers to the turbulence at a boundary layer scale. Near the root, the separation of the boundary layer after stall is affected by Coriolis and centrifugal forces. While this separation occurs, the centrifugal force experienced by the flow is considerably larger than its velocity, causing the flow to displace in the span-wise direction. This effect, as depicted in figure 5.6, influences airfoil behaviour after stall, 2D data. Corrections for three dimensional flow effects, due to centrifugal and Coriolis forces, are required. This is done by adjusting the span-wise solidity factor, c/r , which is the ratio between the local chord length and radius at a specific span-wise blade location. With Rfoil, it has been documented that $\frac{2}{3}$ of the c/r factor gives the best approximation, R.P.J.O.M. van Rooij [59].

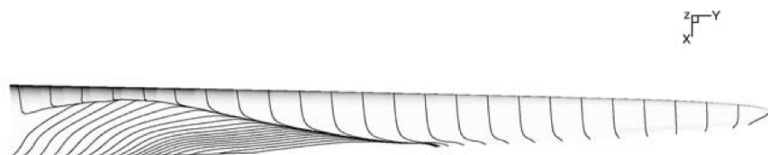


Figure 5.6: Computed limiting streamlines on a stall regulated wind turbine blade at a moderately high wind speed. Taken from Hansen [35]

The correction method implemented in RFoil, solves the boundary layer equations in radial flow, based on an extension of the Snel-Houwink model, R.P.J.O.M. van Rooij [59]. Other 3D correction models exist and are mentioned in, Bak and Timmer [5]. Correction for rotational effects are essential, and are beneficial near the blade root, where much separation occurs. The reduction of lift at the root is significant, however rotational effects compensate for the separation effect. In figures A.1 & A.2, this effect is observed on the lift coefficient curves. In the Appendix, A, polar plots for other DU airfoils, implemented in the design, are included. Corrections to all airfoils are applied. Nevertheless, towards the tip of the blade, airfoils are less influenced by rotational effects and no significant changes should be expected with respect to the 2D airfoil characteristics.

Below, in figures 5.7 and 5.8, the NREL measured airfoil characteristics and the ones obtained with Rfoil are compared. According to NREL's airfoil measurement's notes, the airfoil data holds for Reynolds numbers of $4e6$ to $6e6$.

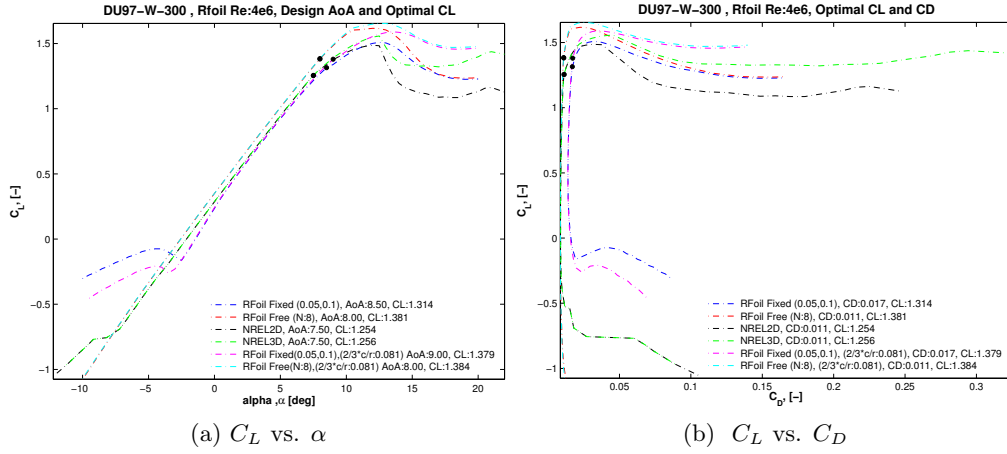


Figure 5.7: DU97-W-300

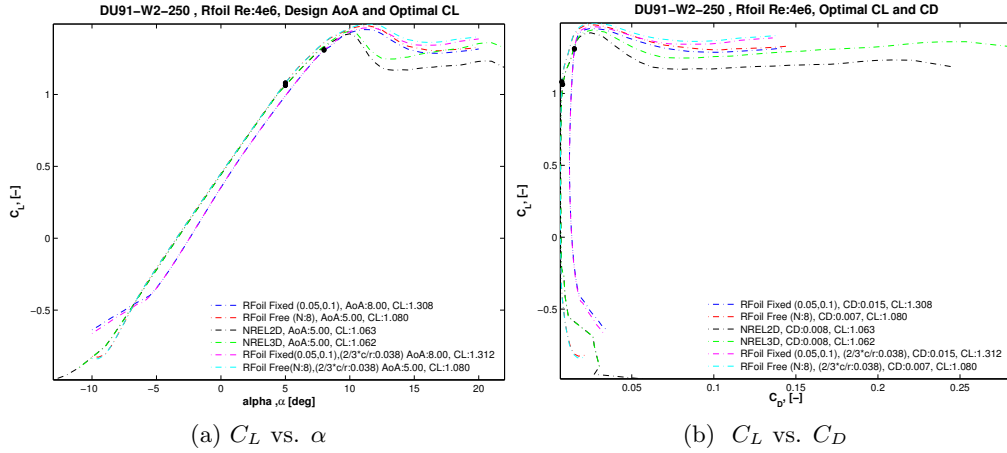


Figure 5.8: DU91-W2-250

It is worth mentioning HAWC2 fails to run, if the full 360° range of angles of attack for the airfoils are not included. In this thesis, the airfoil data sets generated cover an angle of attack range from -10° to 20° . The 360° range is completed with the Viterna method, Hansen [32]. Flat-plate theory may also be used. It is important to have reliable sets of airfoil static characteristics, where roughness effects, 3D-corrections and a full range of angles of attack are considered. Aside from these concerns, dynamic stall effects are equally important and play a critical role in aeroelastic simulations.

Several dynamic stall models exist, Pereira et al. [56] . The dynamic stall model implemented, in HAWC2, is an extension of the Beddoes-Leishman dynamic stall model, the MHH-Beddoes, Hansen et al. [34]. Unlike the static case, the dynamic

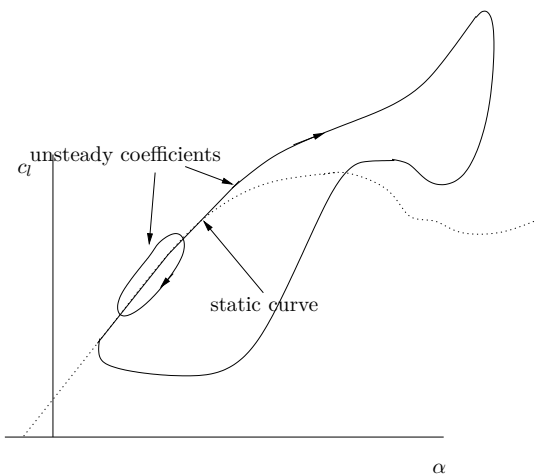


Figure 5.9: Static and dynamic values of lift w.r.t angle of attack. Taken from Holierhoek [39]

case predicts the lift coefficient curve under dynamic effects. This means the lift coefficient differs from the static case, as the angle of attack increases or decreases, figure 5.9. The use of this unsteady aerodynamics model is essential for the aeroelastic simulations.

This brief airfoil analysis demonstrates how turbulent and clean conditions provide both conservative and optimistic airfoil data. A wind turbine does not operate with clean blades during its lifetime. The new blade takes the clean airfoil conditions into account for the design, however, for further assessment, one considers the blade to operate 25% of its lifetime in clean conditions and 75% under rough conditions. This impacts the annual energy production and the cost of energy. As seen above, figure 5.7, both of these conditions modify the airfoil's stall region and affect its design angle of attack. Towards the tip, airfoil stall characteristics are very important due to their contribution to blade aeroelastic instabilities. With the airfoil datasets, obtained in this section, the blade design's performance is assessed later on.

Distributions w.r.t Relative Thickness

From each airfoil's characteristics, distributions of optimum angle of attack, α_{opt} , and lift/drag coefficients with respect to the airfoils' relative thickness, are created. A relative thickness of 100% is assumed at the root (cylinder).

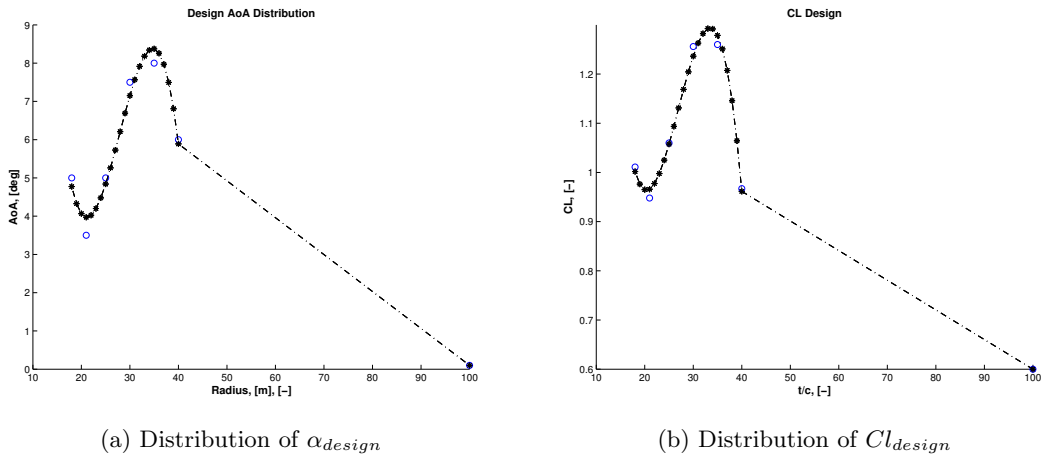


Figure 5.10: Distribution Description

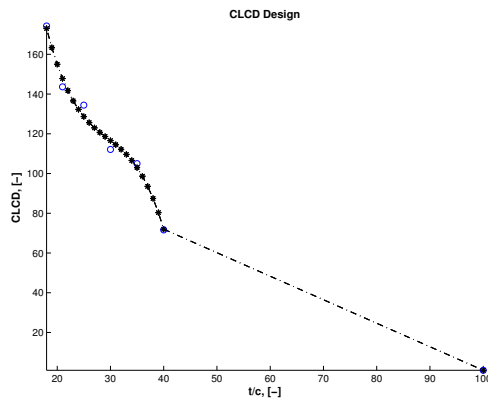


Figure 5.11: Distribution of Cl/Cd_{design}

5.2.3 Other Constraints, w.r.t. Reference WT

From Chapter 4, reference operational constraints are also taken. The maximum blade tip deflection, flapwise/edgewise bending moments and thrust are kept below or at least within an acceptable range of these reference values. These constraints are also important with regards to the fatigue loads, which influence the structural design of the blade.

Most of the constraints are inequality constraints, where the reference values are compared to those of the new design. Apart from these, there are other constraints

such as a rotational speed range of 8 to 13 *rpm*, rated power of *2MW*, and a blade tip speed of *75m/s*. Increasing blade tip speed may increases energy capture, however noise and blade erosion are some limitations to be aware of. This is an inland wind turbine, which means there are acoustic constraints to be kept.

5.3 Design Variables

The design variables describe the blade's shape, i.e. chord, twist. As a limitation, the design variables are given maximum and minimum boundaries. These are $\pm 50\%$ of the initial chord and twist distributions, which are set to vary in a decreasing manner. Such boundaries also aim to reduce computational time.

As mentioned before, the main goal is to reduce the cost of energy. This means, that with respect to the baseline, the annual energy production must increase, while keeping rotor cost and other constraints, within a reasonable level.

To achieve this, it is important to operate at the appropriate design tip speed ratio, λ , in the wind speed range below V_{rated} . In other words, while in operation, the wind turbine operates at a design point which follows the maximum power coefficient, C_p .

$$P = \frac{1}{2} \rho A C_p(\lambda, \theta) v^3 \quad (5.11)$$

Before reaching rated wind speed, the rotational speed increases with the wind speed, in order to, keep the tip speed ratio λ at a constant design value. As the region below rated wind speed is the main focus, one may disregard the pitch angle θ . In return, the degrees of freedom and computational time are reduced.

In the expression above, there is a direct relation between the design tip speed ratio λ and the blade's geometry. It is important to understand that the blades' area, relative to the rotor swept area, decreases with an increasing design tip speed ratio (with constant radius). This blade to swept area ratio is the rotor's solidity σ , as mentioned earlier in Eq. 2.6.

Now, as the tip speed ratio increases, the inflow angle ϕ is affected as well, Eq. 5.12. This means a change in tip speed ratio λ , affects the angle of attack α .

$$\phi = \text{atan}\left(\frac{1 - a}{1 + a' \frac{r}{R} \lambda}\right) \quad (5.12)$$

For the inflow angle ϕ to remain unchanged, the twist angle β is implemented, Eq. 5.13. Consequently, below V_{rated} , the power coefficient C_p is unchanged, as the $\frac{C_l}{C_d}$ ratio also remains unchanged.

$$\phi = \alpha + (\theta + \beta) \quad (5.13)$$

All design variables are coupled together. A change in tip speed ratio λ affects solidity σ , which also affects the inflow angle ϕ . These also have an effect on the twist angle β . Overall, these all impact the power coefficient, C_p , in the region below rated wind.

Aiming to be within the baseline's cost and annual energy production range, the expressions above review the design variables' importance. These variables have a major impact on the blade's design. They determine the COE reduction possibilities a new blade design might have, with respect to the baseline.

5.3.1 Bézier Chord & Twist Distribution

During the optimization, the varying chord and twist distributions are described by a cubic Bezier curve. The curve is assigned 4 control points, where two points lie at both ends of the curve. The other two points change the curve's shape. The formulation for the cubic Bézier curve is provided in Eq. 5.14.

$$P(t) = (1-t)^3 P_0 + 3t(1-t)^2 P_1 + 3t^2(1-t) P_2 + t^3 P_3 \quad t \in (0, 1) \quad (5.14)$$

; where P_0 , P_1 , P_2 and P_3 are the control points and t , the time varying coefficient. This coefficient arises from the binomial expansion of $(s+t)^3$, which results in four functions of t , known as the Bernstein polynomials, Baker [7]. These are the basis for the formulation in Eq. 5.14.

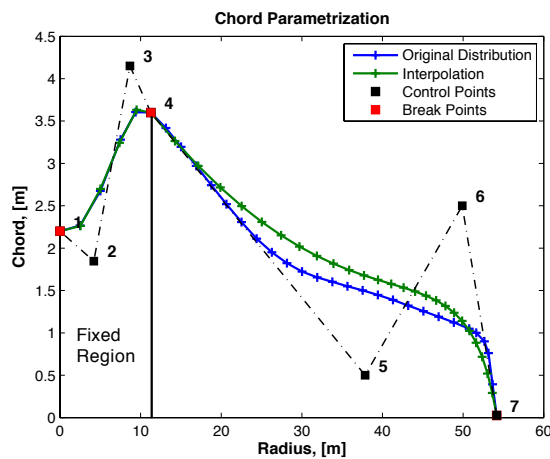


Figure 5.12: Cubic Bézier Curve Representation

Figure 5.12, illustrates the chord representation with a cubic Bézier curve. There are four control points, one at a location 11 m from the root, one at the blade's tip and two intermediate control points. Regarding the root section, this does not contribute significantly to power and a structural constraint exists. For this reason, changes take place from the maximum chord's location to the tip. The twist distribution is defined using a Bézier curve, in the same manner as with the chord distribution.

The control points chosen and the chord/twist definition used, reduce the amount of time required for the analysis. Although other definitions exist, like polynomial functions or splines [2], a cubic Bézier curve representation is chosen. This provides less wavy results, but also restricts the distribution to change in a decreasing monotonic manner.

5.4 HAWC2 Simulation Setup

Preparing the initial model for HAWC2 is an important step. Ming Yang Wind Power provided many of the turbine's components' geometrical and structural properties required to complete the wind turbine model. Parting from a GH Bladed project file, a first step is the conversion of the inputs from one software to another. The conversion tool, developed by Taeseong Kim (DTU Riso A&D group) is used at this stage, figure 5.13.



Figure 5.13: GH Bladed to HAWC2 Converter

Unfortunately, encrypted project files cannot be converted. With the available data, a new project file is set and additional modifications are done to the converter. As seen in figure 5.14, the converter uses data fitting to adjust the GH Bladed project file data to a chosen number of sections. The tool also provides some important blade features, figure 4.8. The optimization phase uses the HAWC2 model, as a set of functions to reproduce it.

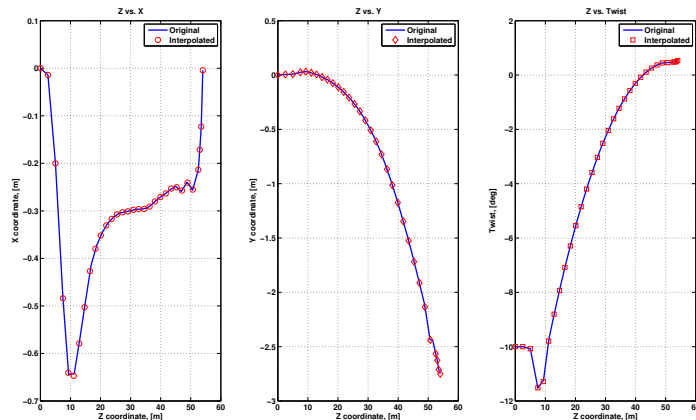


Figure 5.14: Blade Data Fitting

As the optimization takes place, structural, aerodynamic and geometrical inputs are assigned to the model. Some of these are changed within a Matlab routine. To speed up the model build-up process, all necessary files for the HAWC2 simulation are created with Matlab (*.ae, *.st, *.pc, *.htc), figure 5.15. In this manner, modifications consume less time, than the amount of time user modifications take, for each of the mentioned text files.

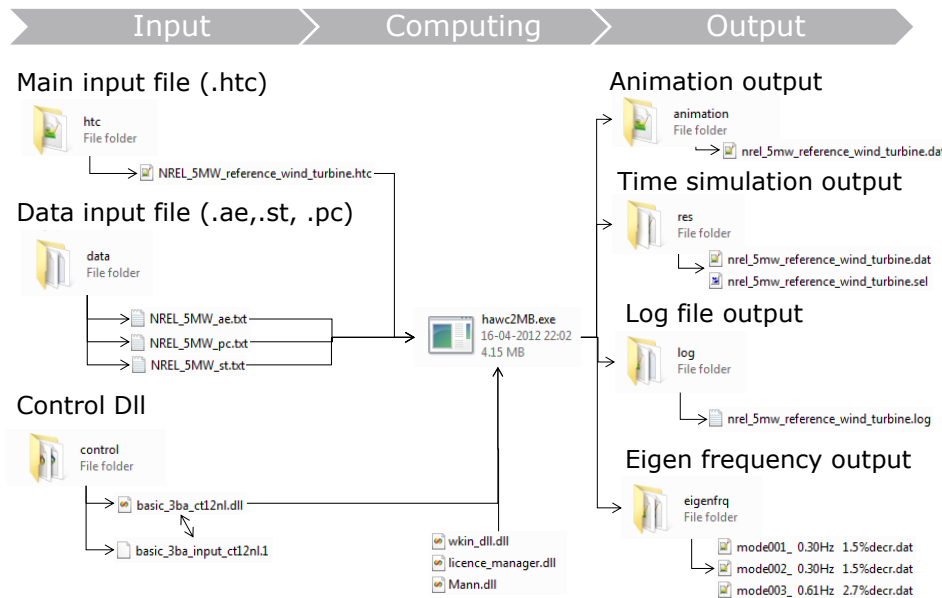


Figure 5.15: HAWC2 Program Structure. Taken from DTU [18]

HAWC2's time simulation outputs are post-processed with Matlab. There are various output file types. These are used to verify the progress and correct execution of all input files/commands, figure 5.16. Other post-processing tools are available and complement each other for a detailed wind turbine analysis.

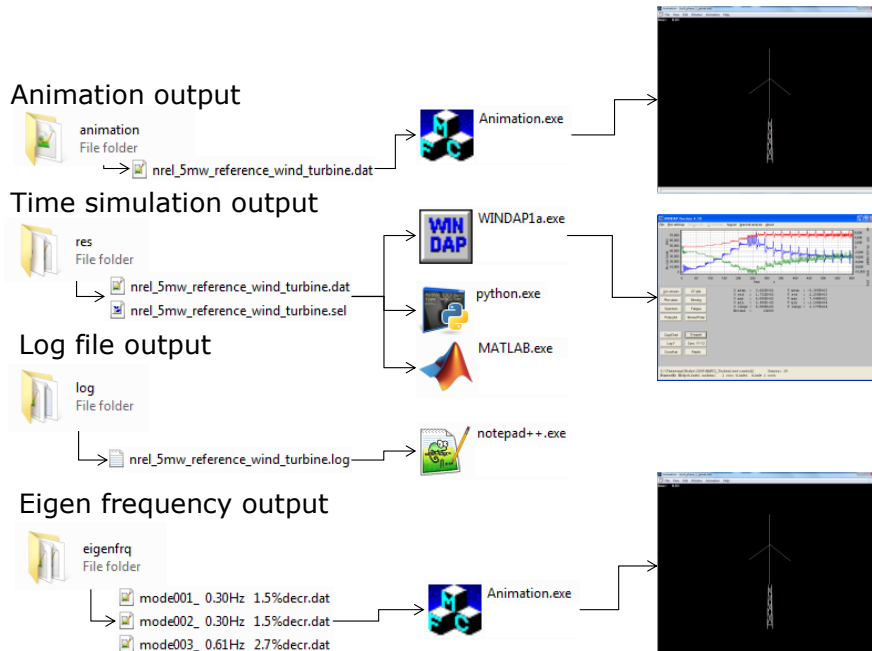


Figure 5.16: HAWC2 Output Structure. Taken from DTU [18]

5.5 Optimization Algorithm

It is important to state the optimization does not target the design of a new wind turbine, but the design of a new blade for the wind turbine's rotor, which adapts to existing wind turbine components. The algorithm begins by building different parts necessary for the wind turbine's aeroelastic simulation. The first part comprises the wind turbine's geometrical and structural design, which includes tower, shaft, hub, tower-top and blades. The wind site data is used for the wind model setup, where a turbulence model and other modules are available. In this step, the aerodynamics of the wind turbine are specified too. Structural properties are called as each component is assigned to the HAWC2 model. The reference wind turbine provides the building blocks and the constraints for the optimization.

To start the algorithm a design angle of attack distribution is defined. For this reason, the airfoil characteristics, mentioned in section 5.2.2 and Appendix A, are important. The principle behind a pitch regulated variable speed (PRVS) wind turbine reviewed in Chapter 4 is equally important. This helps one understand how the angle of attack behaves at different wind speeds. The relative thickness distribution from the reference wind turbine is kept the same, to ensure the structural integrity of the blade, figure 4.7. From this first step, an initial chord and twist distributions are defined.

During the procedure, the chord and twist are varied in a decreasing manner, where some upper and lower boundaries are settled. To asses the cost of energy or annual energy yield of each design iteration, the simulations are performed for a range of relevant wind speeds, from 4 m/s to 9.5 m/s . The wind speed steps used are of 0.5 m/s and 1.0 m/s with a simulation time of 80 seconds per wind step. Longer simulation periods are used as well, to verify no mayor changes occur to the steady state value. After reaching rated wind speed, a steady power output is assumed for successive wind steps, V_{rated} to $V_{\text{cut out}}$. Annual energy production is then determined as described in Eq. 5.5.

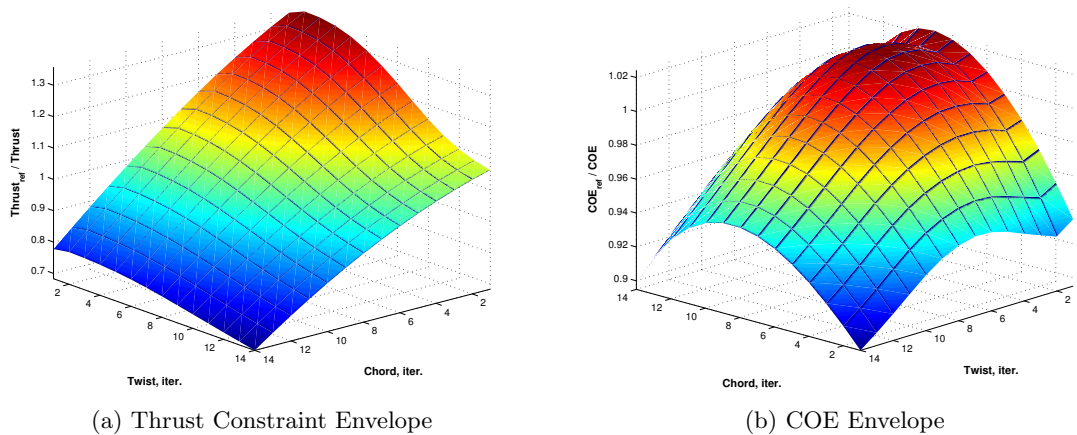


Figure 5.17: HAWC2, Constraint check: examples

Finally, the objective function is evaluated and compared to the relative cost of energy from the baseline. The constraints, mentioned in Section 5.2, are also verified, in order for the iterations to continue or to stop. The algorithm's duration is dependent on the boundaries specified for the chord and twist distributions, and of course, the wind step number and their duration. By assessing the objective function and the constraints from successive iterations, the algorithm stops and the chord/twist distributions, satisfying the conditions set, are found. Figure 5.18 contains the method's block diagram.

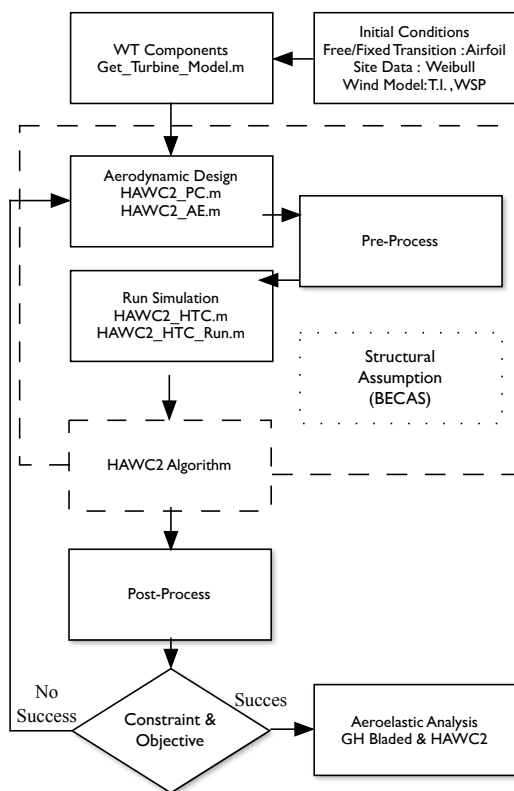


Figure 5.18: Flow Diagram

To implement such a method, an important design assumption is made. This means that the wind turbine information, provided by MYWP, is the product of an initial engineering design process. For this reason, one assumes design load cases (DLC) are not required, if the loads are kept within an acceptable range with respect to the baseline.

5.5.1 Controller: Assumption

Another important aspect to be mentioned is the controller. Being the brain of the wind turbine dynamics, this part needs to be properly tuned. This allows one to operate the wind turbine in a desired manner at a given wind condition. The controller is crucial for the proper operation of the wind turbine and is provided by

MYWP, for the GH Bladed model. Nevertheless, this controller only remains valid for the baseline blade. In HAWC2's case, a controller was tuned using HAWCStab2, a program which works with the same inputs as HAWC2.

Tuned controllers are used during the comparison process, but the performance or proper tuning of the controller is not studied or improved, as this lies out of the scope of this thesis. One is only interested in the steady state conditions reached after the controller transient occurs. In the optimization process, no controller is used. A constant pitch is used and the rotational speed is assigned in the optimization algorithm, by using a HAWC2 bearing3 constraint.

5.6 Results Overview

Power curves are important to wind turbine manufacturers and in this case, a comparison between the baseline and the two blade designs are included, figure 5.19 (a). Some regions show an increase in power capture, specifically from cut in to 6 m/s and from 8 m/s to rated wind speed. Rated wind speed is now reached at $\approx 9.2 \text{ m/s}$ and 9.35 m/s respectively. The change in rated wind speed is small and for it to be considered significant, 9 m/s would have been a considerable change.

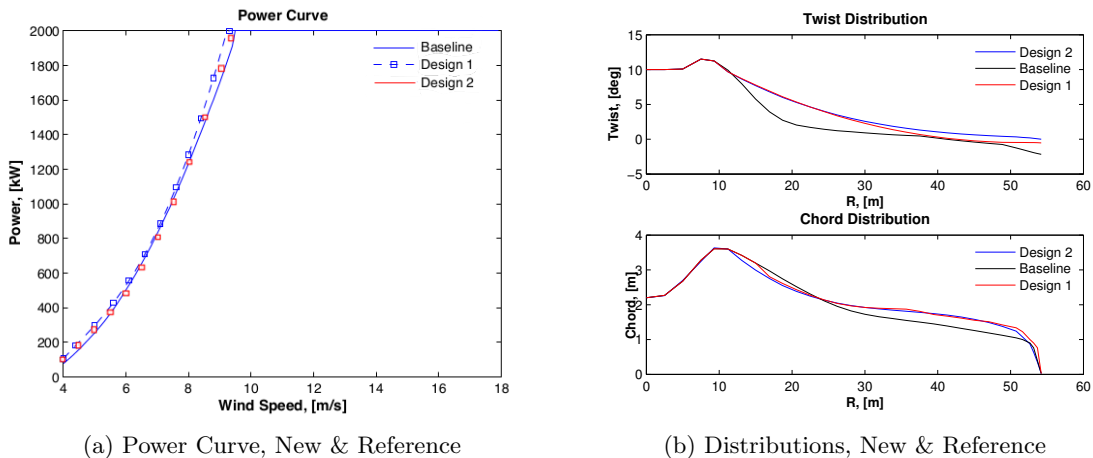


Figure 5.19: HAWC2 Results

In figure 5.19(b), one appreciates the changes in chord, which indeed affect the $c \cdot C_l$ factor. This is responsible for the increased energy production. However, the change in chord is not only responsible for this, but also the airfoil family and the design angle of attack distribution. Considering design #1, the updated blade's planform shape is displayed, figure 5.20.

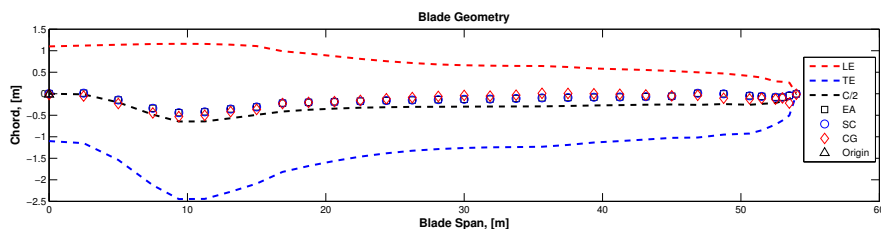


Figure 5.20: Blade Layout: Design # 1

With regards to MYWP's airfoils, it is a possibility that their maximum lift is not as high as those from the DU family. This is tested by using MYWP's exact chord and twist distributions, in the GH Bladed project file, with the DU family instead. The results of this test are included in Appendix E.

5.6.1 Blade Design #1 and #2

Once the blade design is obtained, the assessment of the blade design and its performance follows. It is important to verify and validate the results with other codes as well. The rotor's performance, under different blade roughness conditions, and the blade's in-plane and out-of-plane deflections, for a range of wind steps, are also taken into consideration. The geometry of the initial blade, with MYWP's distributions, and the final wind turbine blades are provided below, figure 5.21 and 5.22. All are depicted with DU airfoils, as MYWP's airfoil geometries are not known. The blade sketches include twist and prebend.

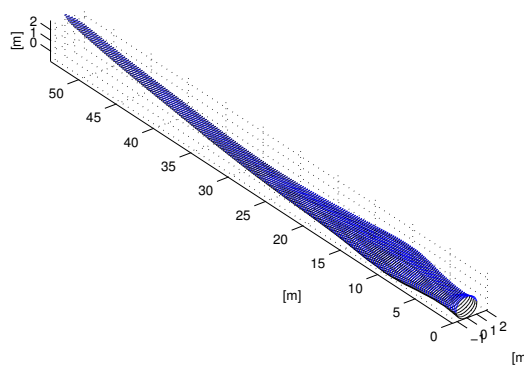


Figure 5.21: Blade, Before Procedure

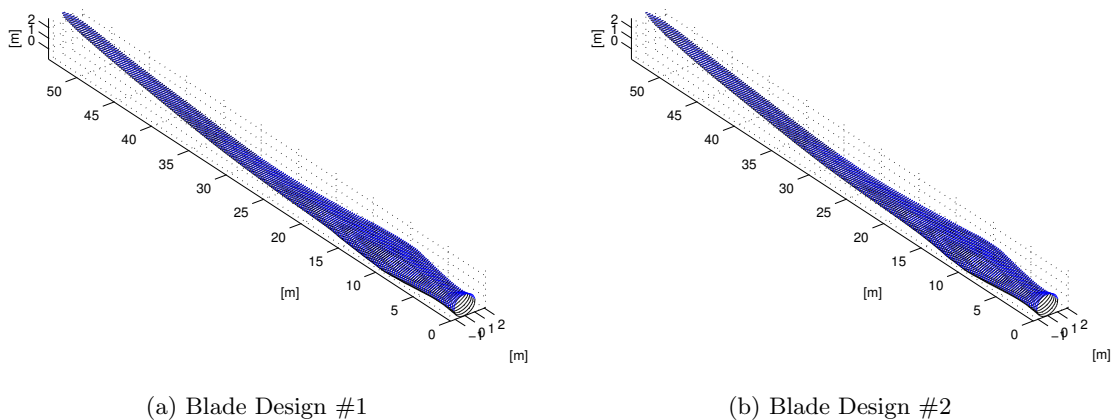


Figure 5.22: Blades, After Procedure

5.7 Design Assessment

Additional wind turbine operational curves give a better insight into the difference between designs. It is important to mention that the operational curves, obtained from GH Bladed, refer to the steady case, whereas the curves resulting from HAWC2 are averaged values. For this reason, some constraints are allowed a small variation. With respect to the averaging, transients are carefully discarded. It is standard procedure to run several simulations in order to come up with a wind turbine power curve. This indeed allows an objective comparison to be made. In this thesis, it is assumed that once the transient occurs in HAWC2, the averaged value approximates the steady case, figure 5.23.

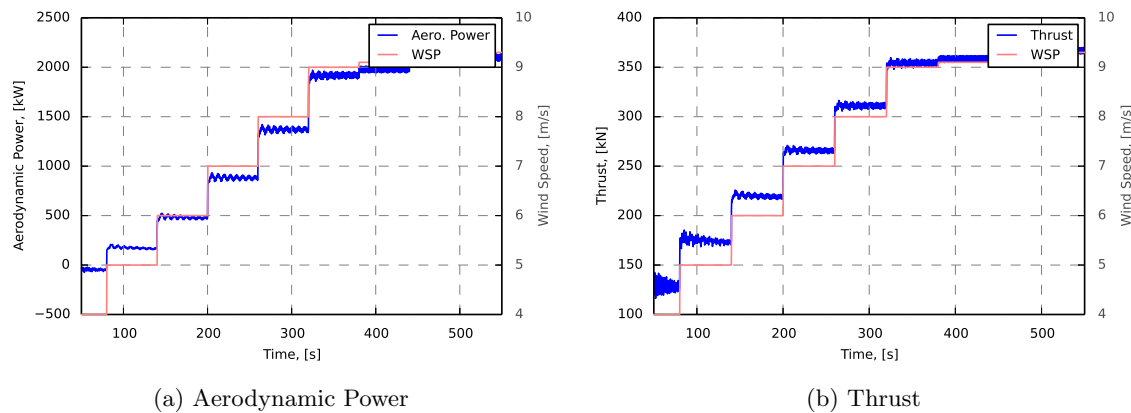


Figure 5.23: Power and Thrust Response. HAWC2

5.7.1 Performance

The operational curves, figure 5.24, show how the tip speed ratio, equal to 8, is kept constant in Region 2. In this region, the wind turbine reaches a C_p of 0.47. The differences with respect to the baseline are notorious, as a look up table is no longer used. The effect of reaching rated power sooner, is clearly appreciated by the change in pitch angle and maximum thrust. In the figures below, **D1** and **D2** refer to the blade design case.

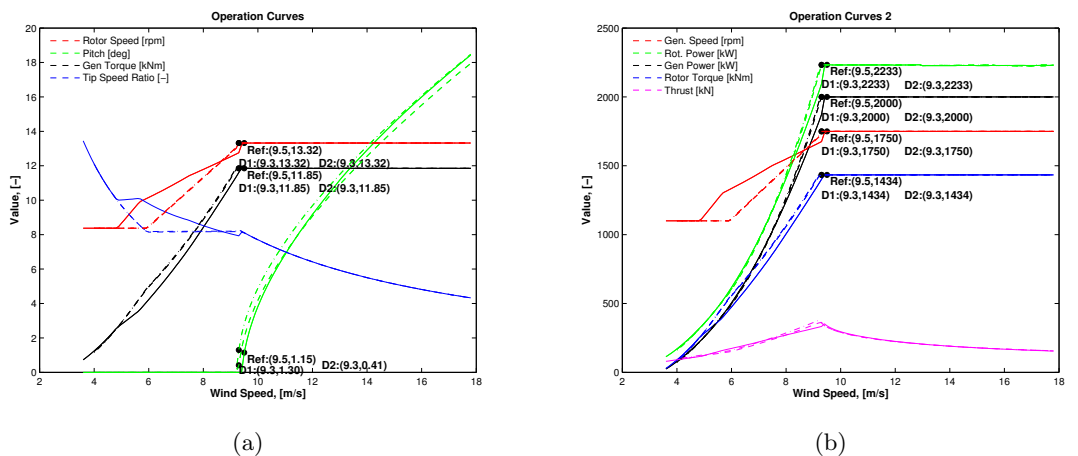


Figure 5.24: Wind Turbine, Operational Curves

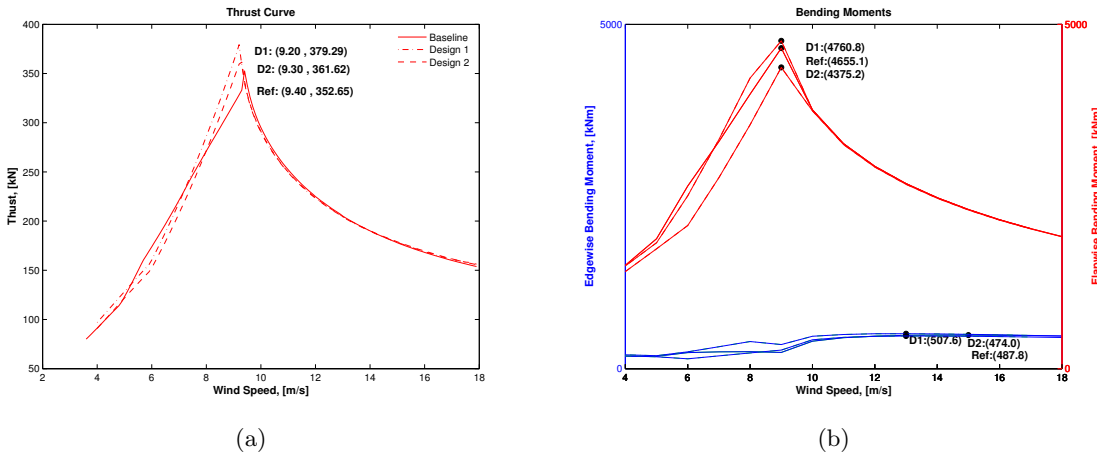


Figure 5.25: Wind Turbine, Thrust and Bending Moments

Above, in figure 5.25, the thrust and bending moment show the expected trend. After rated wind speed is reached, thrust decreases and hence the bending moments are expected to do so as well. The maximum values are relatively close to the baseline, as desired.

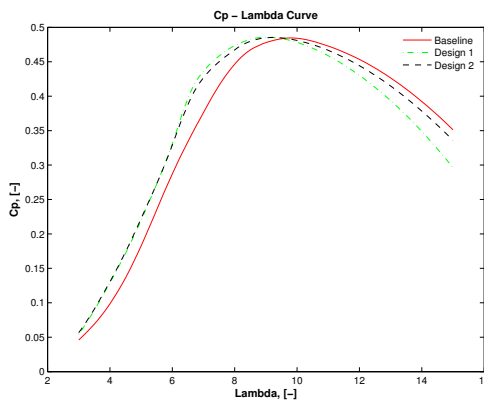


Figure 5.26: C_p - λ Curve

5.7.2 Design Comparison, HAWC2 & GH Bladed

The difference between power curves also has an effect in annual energy production and the cost of energy. This effect and some other maximum values are included in tables 5.2 and 5.3. For the comparisons below, design #1 and #2 are both implemented in GH Bladed and HAWC2. The same settings as the reference wind turbine are implemented (if applicable). In this manner, differences between designs are assessed, but also the variations that are present when using a different aeroelastic code. Besides this aspect, some results may prove to be more conservative, than the ones obtained with a different code. This has effects in the final evaluation and conclusions, with respect to the annual energy production and consequently, the cost of energy. Below, the design comparison of the results obtained with HAWC2. The values, referring to the baseline, are taken from GH Bladed.

Table 5.2: Constraint Comparison, Averaged Values. **HAWC2**

Parameter	Baseline	Design #1	Design #2
AEP , [GWh/yr]	6.81	7.28	7.06
Relative Cost of Energy , [-]	1.468	1.435	1.462
Relative Rotor Cost, [-]	1.000	1.0453	1.0321
Thrust, [kN]	352.6	385	357
Rated Wind Speed , [m/s]	9.5	9.2	9.35

Although the HAWC2 simulation does comply with the constraints, with respect to a tolerance setting, it is more objective to implement the new blade designs in the same code as the baseline, GH Bladed. In HAWC2's case, the unavailability of MYWP's airfoil data, is an obstacle for the comparison of both the baseline and the new design. Both aeroelastic codes may import DU airfoil characteristics, but MYWP's airfoil characteristics are only included in the GH Bladed project file (*encrypted*). Below, the design comparison of the results obtained with GH Bladed.

Tables 5.2 and 5.3, show the cost of energy decreases in one case (HAWC2) and

Table 5.3: Constraint Comparison, Steady Values. **GH Bladed**

Parameter	Baseline	Design #1	Design #2
AEP , [GWh/yr]	6.87	6.95	6.92
Relative Cost of Energy , [-]	1.456	1.503	1.491
Relative Rotor Cost, [-]	1.000	1.0453	1.0321
Thrust, [kN]	352.6	379.2	361.6
Mb Flap, [kNm]	4655.1	4760.8	4705.2
Tip Deflection, [m]	3.75	4.75	4.05
Rated Wind Speed , [m/s]	9.5	9.3	9.3

increases in the other (GH Bladed). The results obtained with GH Bladed are conservative and suggest the benefit is very low or perhaps nonexistent. Of course, with a fixed rotor cost, the cost of energy would decrease by 1.25 %. Nevertheless, a possibility is the over prediction of power with HAWC2. Additionally, by inspecting the AEP, one also notices that the AEP model, implemented in Matlab, under-predicts the annual energy production, by 0.88%, for the same baseline's power curve, analyzed with GH Bladed. In both tools, availability is considered to be of 100%.

From the comparisons, it is clear the constraints are still kept within a certain range. The increase in AEP is certainly a positive and desired result. Nevertheless, there are slight changes, of about 2% to 7%, for some other parameters, i.e. thrust and moments. This translates into additional fatigue damage and possible reduction of life time. These effects could be negligible due to the added material to the blade. Only with several design load cases (DLC), can the scale of such effects be determined. With respect to the AEP, the increase in production translates into the electricity demand of ≈ 60 additional Chinese households (1308 kWh/yr per household, Enerdata [21]).

In the next section, one compares the production in the rough and clean cases for the baseline and blade design # 1. These cases are only simulated in GH Bladed. The main interest is to find out the effects of roughness on wind turbine performance and its consequences in AEP and COE.

NOTE: It is after this section, that the following studies only apply to **blade design #1**. This design has a considerable effect in the cost of energy and thus is selected as a less conservative choice.

Rough vs. Clean Scenario

The performance of the wind turbine blade is assessed under different blade surface roughness conditions. To do such assessment, the airfoil characteristics derived from Section 5.2.2 are taken into account. Table 5.4, gives an overall estimate on how annual energy production is affected and its consequences on the relative COE, in comparison to the baseline.

Table 5.4: Blade Scenarios: Clean, Mixed & Rough

Flow Condition	$COE_{rel.}, [-]$	AEP, [GWh]
Free transition flow, (clean)	1.495	6.99
Mixed, (25 %/75 %)	+1.61 %	6.88
Turbulent flow, (rough)	+2.01 %	6.85

There is a 2% loss of AEP in comparison to the clean case, when the turbine operates with contaminated blades. Although a mixed case is more realistic, the effects of roughness prove to be severe and the annual energy production still decreases with respect to the clean case. As mentioned before, fixed transition is a conservative approach, when simulating leading edge roughness. In reality, the AEP may decrease by a greater factor.

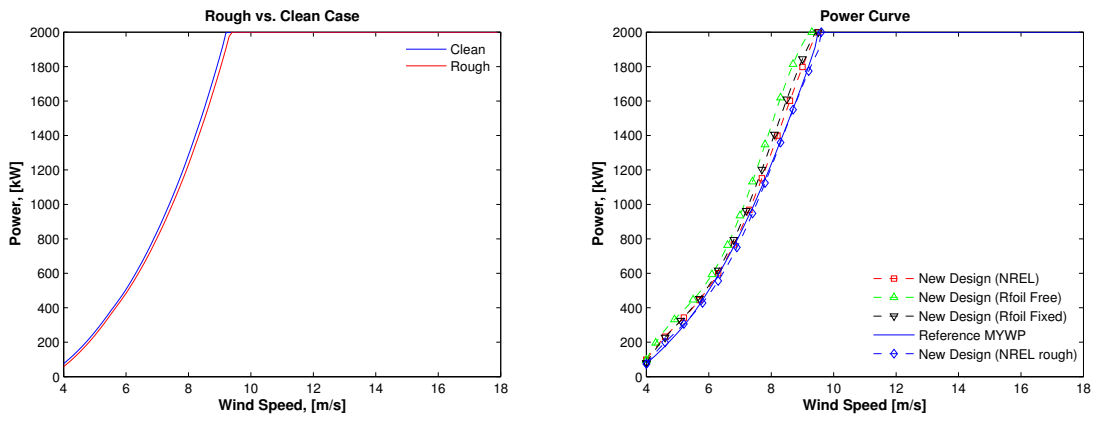


Figure 5.27: Power Curve, Rough & Clean Cases

The power curves for one clean and one contaminated case are portrayed in figure 5.27 (a). Figure 5.27 (b) includes the cases mentioned earlier, plus the baseline's power curve. The rough and clean case, obtained with the Rfoil airfoil coefficients, are compared to those results obtained by the coefficients used in the NREL 5MW reference wind turbine. The offset observed between the Rfoil clean and rough case, is applied to the NREL clean case. This to have an approximate of a NREL rough blade case. In total four power-curves are compared to the baseline. Such cases highlight the importance of the existing uncertainty, when doing under- and over-predictions of wind turbine energy production.

These curves also demonstrate how the new blade, in rough conditions, produces about the same energy output as the baseline, in the clean case. Although LER , is more severe, the cost of energy during the 25 year lifetime of the wind turbine may still benefit from this.

5.7.3 Code-Code Comparison

The validation against other codes is also important. The wind turbine, equipped with the new blade, is simulated for a single wind speed case. Table 5.5 includes the results from a simulation with a wind speed of 8 m/s. BEM does not include unsteady effects. As for Bladed and HAWC2, tower shadow, wind shear and turbulence intensity effects are included. This indeed are possible sources of aeroelastic instabilities.

Table 5.5: Code Comparison, GH Bladed, BEM & HAWC2 at 8 m/s

Parameter	HAWC2 (avg.)	BEM	Bladed(avg./steady)
Power, [MW]	1.446	1.435	1.240 / 1.319
Flapwise M_B , [kNm]	3500	2559	4300 / 4200
Thrust, [kN]	298	259	333 / 286
Tip Deflection, [m]	4.5	3.7	3.95 / 4.05

There are certainly some differences in table 5.5. It is important to mention a controller is tuned for GH Bladed, by using the auto-tuning options, for wind speeds beyond rated. For HAWC2, one uses HAWCStab2. For Region 2, one determines the optimal mode gain factor, defined as:

$$K_{opt} = \eta \cdot \frac{\frac{1}{2}\rho\pi R^5 C_p^{max}}{\lambda_{opt}^3} \quad (5.15)$$

Besides this, the mean values are taken once the controller transient effects have faded. From this comparison, one understands how the different add-ons, within each of these codes, play an important role. Bladed shows higher thrust and blade loads, but a lower power production than the other codes. HAWC2 shows a higher production and a lower thrust. BEM is not as complex as the other codes and does provide lower values, with exception of the power output, where generator efficiency is not taken into account. With respect to BEM, beam theory is used to approximate blade tip deflection, giving fair results. The differences observed may be attributed to the different input files, used by the codes, and the different computational models implemented into them. Nevertheless from the cases studied above, over prediction of power in HAWC2 is also observed.

5.8 Discussion

To develop the blade design, choosing the right constraints is important. There is a direct relation between thrust, bending moments and blade tip deflection, which facilitates the comparisons done in the design algorithm. The chosen airfoils are responsible for these loads and power, and implementing DU airfoils in the design is one of the requirements set by MYWP. The feasibility of implementing DU airfoils with MYWP's baseline components cannot only be evaluated based on the reduction of cost of energy. Aeroelastic instabilities are a risk when it comes to the interaction of dynamics, aerodynamics and elasticity. The importance of this must be highlighted, as for this project no structural verifications are performed. It is assumed that MYWP has done a proper structural assessment of the structural properties for all of the provided components.

The present algorithm targets energy production and then assesses the cost of energy, while keeping the loads within a certain range. The differences the cost of energy experiences, when using a fixed and variable rotor cost, are also interesting. The rotor cost model considers the reference mass and the new and old chord distributions. This provides a non-dimensional cost value. With such a cost model, substantial changes to the cost of energy are observed, but these changes also vary depending on the aeroelastic code used. The estimations done with GH Bladed are more conservative than HAWC2. This causes the cost of energy to vary by about 5 %, between both codes. The results from HAWC2, suggest the COE is reduced by about 2.3 %, whereas the results from GH Bladed suggest the COE has actually increased by 3 %. The AEP calculation has a small influence in these results. The difference, in these COE approximations, is attributed to two things: the possible over-prediction of power in HAWC2 and the use of the steady state power values from GH Bladed. In the code-to-code comparison, it was observed the power output varied in GH Bladed, when a time domain simulation is performed. In the case of a fixed rotor cost, in both aeroelastic codes, the growth in annual energy production outweighs the rotor cost.

As mentioned before, determining appropriate chord and twist distributions, that maximize energy production is an important step. Nevertheless, one needs to be aware, that this layout does not translate into the blade's operation in and out of the stall region. With the airfoil characteristics analysis, in both rough and clean conditions, the interest is not only the effects on optimal C_l or the powercurve, but also the behaviour of the airfoil's stall region. If this region is affected and the negative lift slope is relatively high, there is a considerable risk for the occurrence of aeroelastic instabilities.

The assessment of the campbell diagram or the interaction with any aeroelastic frequencies is not evaluated in the algorithm. For this reason, having met the goal of increasing annual energy production, one continues with the aeroelastic analysis of the proposed blade design.

5.9 Full Rotor Geometry

Sketch of the wind turbine's rotor equipped with the proposed blade design.

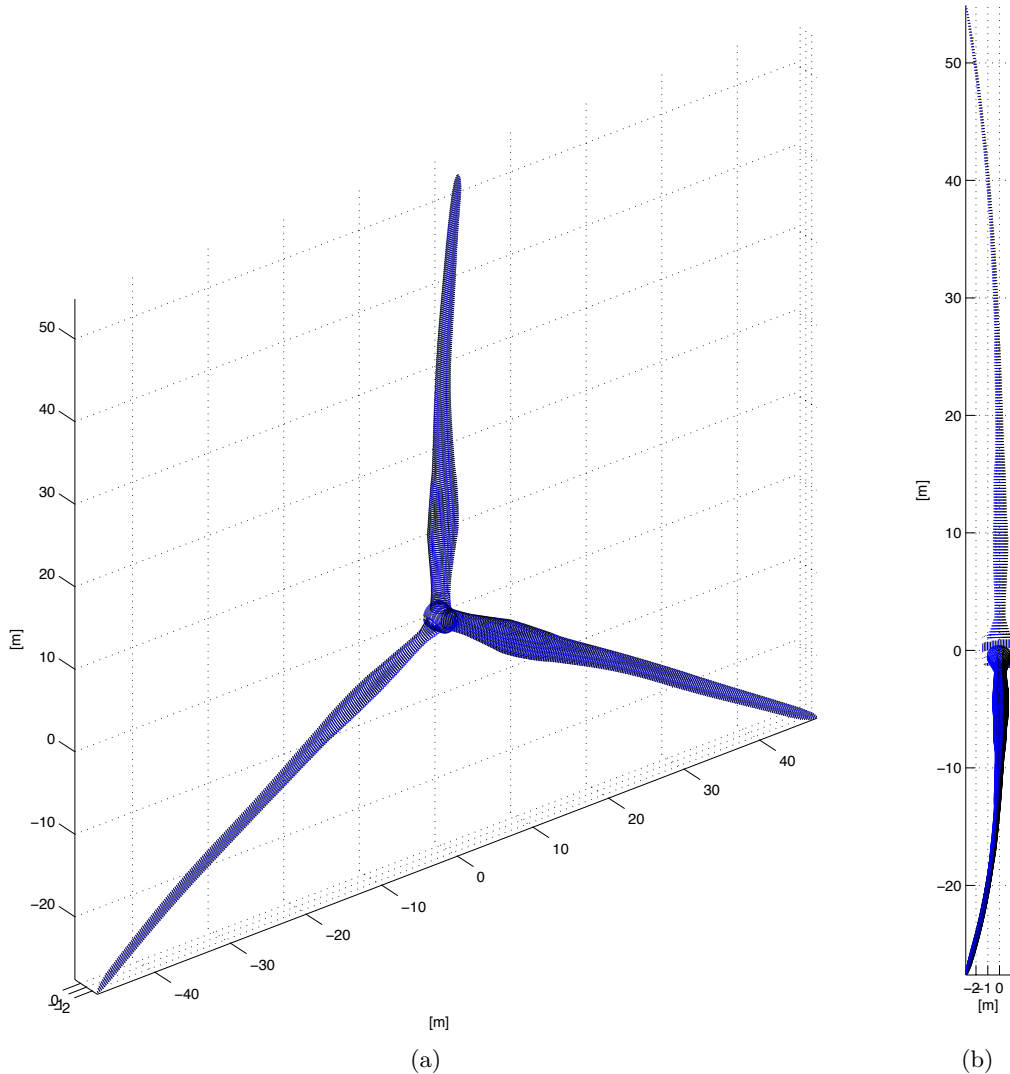


Figure 5.28: Wind Turbine Rotor, with Designed Blades

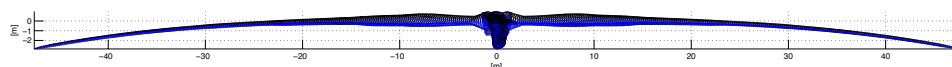


Figure 5.29: Wind Turbine Rotor, Top View

Chapter 6

Aeroelastic Analysis

6.1 Aeroelastic Stability

HAWC2 may also perform an eigenfrequency analysis based on a standstill case, table 6.1. The modes can be viewed with the animation tool, figure 5.16. The estimated logarithmic decrements, in the standstill case, are within an acceptable range.

Table 6.1: Wind Turbine with New Rotor, HAWC2 Eigenanalysis.

Mode	Description	Freq. [Hz]	Log. Dec.
1	1st long. tower bending	0.30	2.3 %
2	1st lat. tower bending	0.31	2.0 %
3	1st shaft torison	0.42	4.3 %
4	1st yawing flapwise	0.44	1.6 %
5	1st tilting flapwise	0.46	1.4 %
6	1st collective flapwise	0.49	1.7 %
7	1st vertical edgewise	0.83	3.4 %
8	1st horizontal edgewise	0.84	3.5 %
9	2nd yawing flapwise	1.09	4.6 %
10	2nd tilting flapwise	1.37	5.1%

The logarithmic decrement describes the change in amplitude of a vibration after an excitation occurs. The logarithmic decrements' magnitude show some vibrations are damped out faster than others. With the logarithmic decrement, the damping, ζ , is identified. A negative damping means the amplitude of a vibration increases, leading to an aeroelastic instability. The damping is determined as follows;

$$\zeta = \frac{\delta}{\sqrt{(2\pi)^2 + \delta^2}} \quad (6.1)$$

where the logarithmic decrement, δ , is defined as, [62]:

$$\delta = \frac{1}{n} \ln \frac{x_1}{x_2} \quad (6.2)$$

Now, that the damping terms are found to be suitable in the standstill case. One can assess whether an aeroelastic instability exists. Some ways of doing this are: through the analysis of blade deflections and root bending moments, as a function of time, and through the Campbell diagram. Before taking these approaches, the structural and aeroelastic modal analysis is performed in HAWCStab2. The modes, during operation, are then identified and displayed with the 1P and 3P frequencies (green lines), figure 6.1.

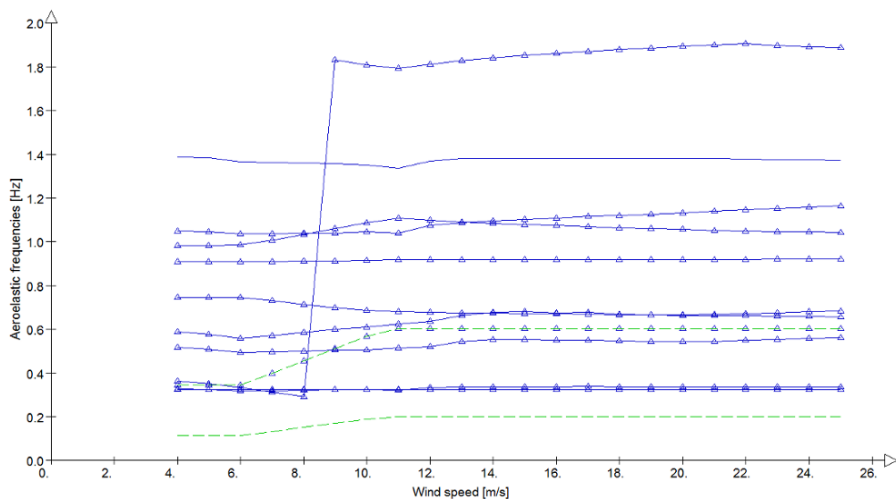


Figure 6.1: Aeroelastic frequencies, MYWP- 2MW

One observes how 3P is not crossing the tower modes, but it is very close to them, at 4-6 m/s. In this case, increasing the tower's thickness (mass) to reduce the tower modes' frequencies, is an option. Nevertheless, 3P does cross the 3rd and 4th modes, where the 3rd mode is clearly excited. Here, one is concerned about the blade's elastic properties. This excited 3rd mode is observed in figure 6.2.

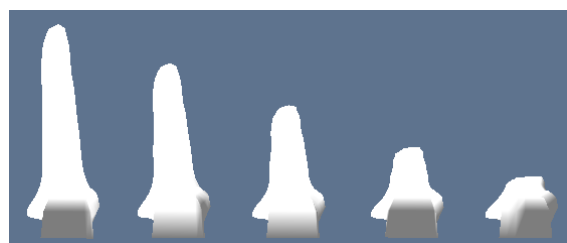


Figure 6.2: Flapwise mode excitation, on blade

In the next section, the Campbell diagram portrays these aeroelastic frequencies as a function of rotational speed.

6.2 Campbell Diagram

The Campbell diagram, for the new wind turbine in both softwares, is compared, figure 6.4. Some coupled frequencies are not quite the same, which may suggest the structural input for the HAWC2 model is not accurate, Appendix C. This is the case for the torsional stiffness, as mentioned in Section 4.3. On the other hand, the method both softwares use to perform an eigenvalue analysis differs, as damping is considered in different manners, Passon et al. [55].

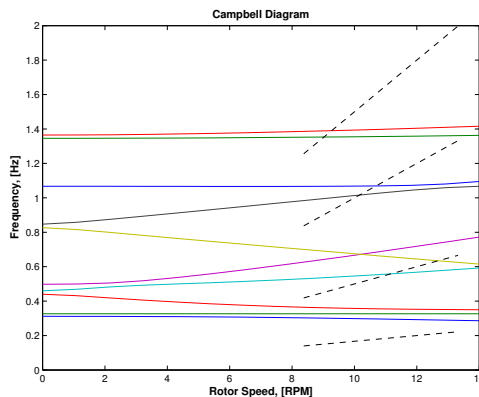


Figure 6.3: Campbell Diagram, HAWC2

In both diagrams, it is seen a rotational speed of 11 rpm is an operational point to be avoided. At this point, the rotational frequency coincides with the first flap-wise forward whirling mode. It is referred to as a whirling mode, due to how the first flap-wise bending mode of the blades couple when the rotor rotates. Refer to figure 2.17, to see how the modes, due to rotation, relate to the standstill case.

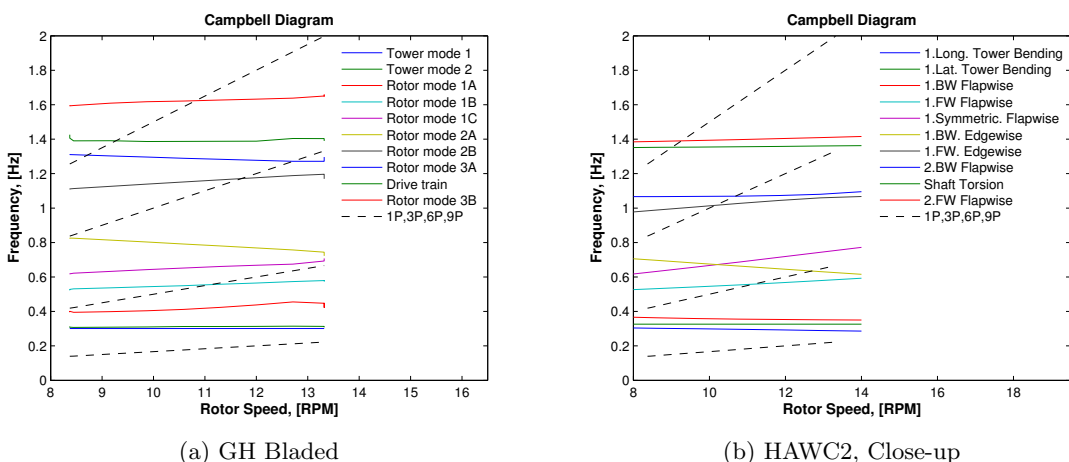


Figure 6.4: Campbell Diagram

One possible alternative to avoid this frequency crossing is to modify the blade's flap-wise stiffness. On the other hand, a proper control method is also capable

of skipping this operational speed. Frequency crossing at 6P is relevant as well. Despite of this, the 6P frequency lies very close to the 11 *rpm* operational point. This highlights the importance of avoiding this rotational speed.

6.2.1 Blade Eigenmodes

Theoretically speaking, there are infinite blade modes, but only the first six are relevant. Although knowing the blade modes is important, these change once the system interacts as a whole. This is observed in the Campbell diagram. Now, before going into the analysis of the deflection time series, important blade eigenfrequencies are identified, figures 6.5 & 6.6.

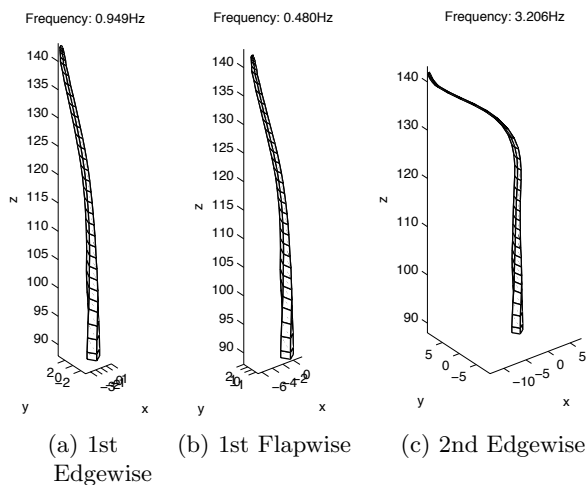


Figure 6.5: Wind Turbine Blade Modes

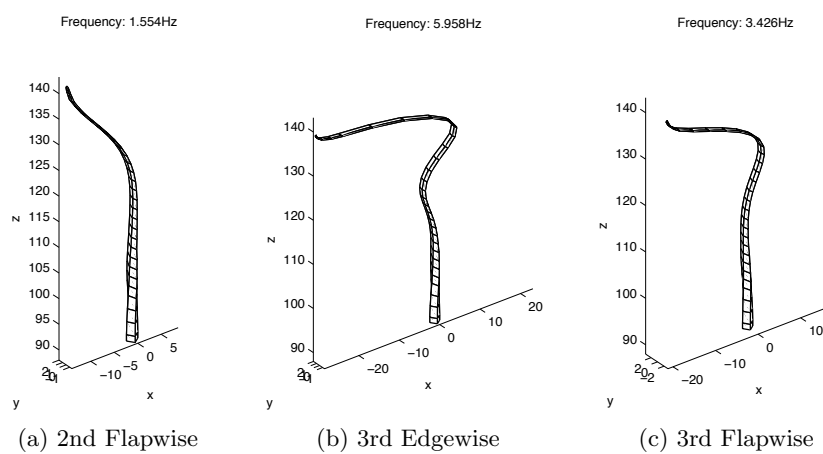


Figure 6.6: Wind Turbine Blade Modes

The sketches above are obtained by using GH Bladed and the prescribed damping ratio of 0.007. These first edgewise and flapwise eigenfrequencies visualizations

and calculations give similar results with HAWC2, figure 6.2. In this case, the damping ratios K_x , K_y , K_z , as labeled in HAWC2, are tuned to keep the logarithmic decrements of the first modes within 10%. The damping ratios used are: 1.11E-03, 7.7E-04 and 5.36E-04.

Table 6.2: HAWC2 Blade Modal Analysis

Mode	Freq. [Hz]	Log. Dec.
1	0.47	0.7 %
2	0.85	1.8 %
3	1.45	2.3 %
4	2.51	4.9 %
5	3.00	4.8 %
6	4.86	8.8 %

From both aeroelastic codes, one observes some matching eigenfrequencies, which means the structural properties are correctly transferred into the HAWC2 model, to some extent. Other higher order blade modes present some slight differences.

In this thesis, no structural changes are done to the blade's cross-sectional properties which are responsible for the blade frequencies described above. It is important that these frequencies do not overlap with each other and with multiples of the rotational frequency, figure 6.4 (b). These frequencies are relevant for the analysis in the next section.

6.3 Blade Deflection Analysis, HAWC2

To further assess the aeroelastic stability of the blade, the blade tip deflection, as a function of time, is studied for selected wind speeds. Additionally, the use of a FFT analysis of the tip deflection and root bending moment time series, allows one to observe relevant blade frequencies. One does know the rotor frequency at a given wind speed and the blade eigenfrequencies, mentioned earlier. These are useful for the analysis. It is easier to distinguish frequencies that are known, from those that are not yet identified.

6.3.1 Runaway Case

First, an aeroelastic instability of the blade is also identified by selecting a wind speed of 9 m/s and allowing the rotor to rotate freely during the simulation. Such a case is valid when the generator has zero torque, known as the runaway case. It is observed a blade aeroelastic instability occurs at a tip relative wind speed of approximately 140 m/s. The blade deflections confirm that indeed an aeroelastic instability takes place, as the amplitude of the deflection increases in a sudden manner. This amplitude increases due to the increasing/decreasing angle of attack,

which is then limited when these reach the stall region. This effect is also due to the coupling of blade modes.

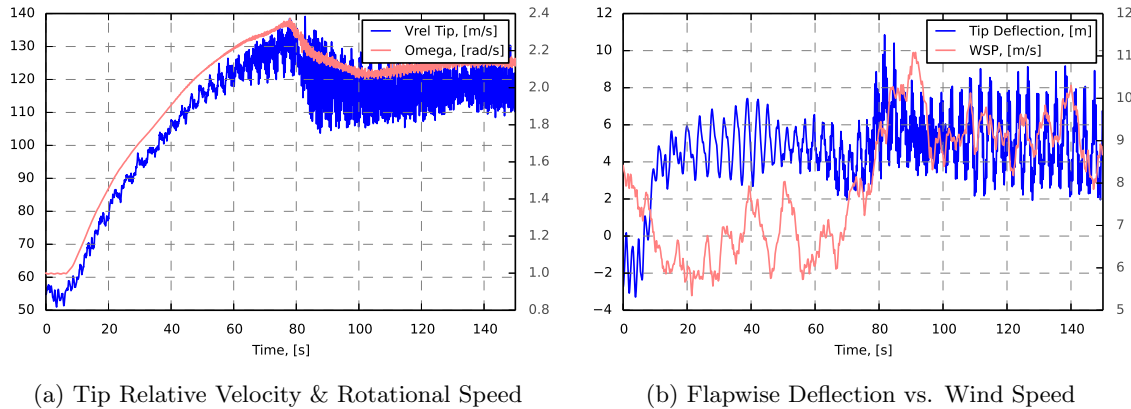


Figure 6.7: Free Rotation

Figure 6.8, demonstrates the aeroelastic twist's behaviour as the aeroelastic instability takes place.

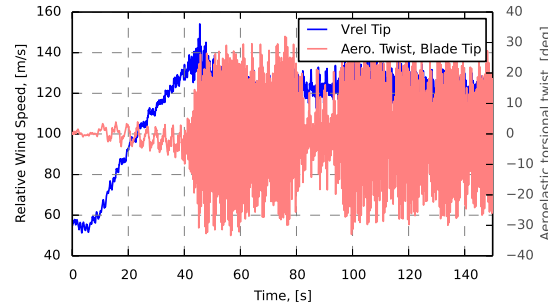


Figure 6.8: Tip Relative Velocity & Aeroelastic Twist

Tower shadow, wind shear and a turbulence intensity of 18% are considered. In uniform, but less realistic conditions, this plausible flutter instability occurs at a relative wind speed of approximately 155 m/s , which is far from the operational conditions of the wind turbine. The frequency of this instability is of ≈ 3.27 Hz. The blade's stiffness is key to this analysis. Although the blade's structural properties are not modified, it is important to highlight how decreasing stiffness lowers the natural frequencies and increases deflection. This influences which blade modes are involved in the occurrence of an aeroelastic instability.

6.3.2 Frequency Domain

The frequency analysis of the deflections and root bending moments in time, do show some clear peaks, describing the occurrence of a specific frequencies. The power

spectra analysis is included in figure 6.9 to 6.12. For the first peaks, one expects to see the rotational frequency of the rotor. This frequency varies with wind speed and thus a displacement must be seen with the change of wind speed. The smaller groups of peaks, appearing after the first ones, are the harmonics of the rotational frequency. Nevertheless, some other peaks are appreciated, in this case, the blade's eigenfrequencies. The coupling of blade frequencies with rotational frequencies and other rotor frequencies, may create the appearance of peaks at higher frequencies, which suggests that an aeroelastic instability may be present and thus lead to failure of the blade. When failure does not occur, hitting the tower is also a possibility.

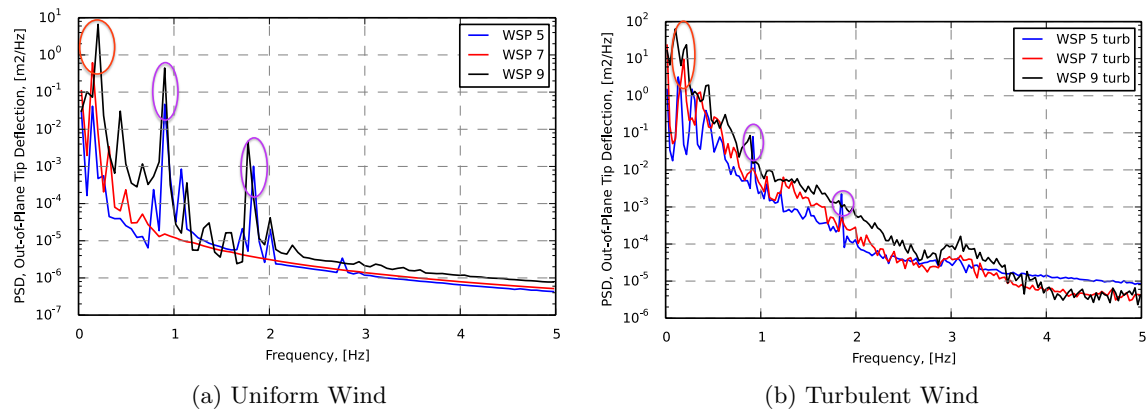


Figure 6.9: Out-of-Plane Tip Deflection

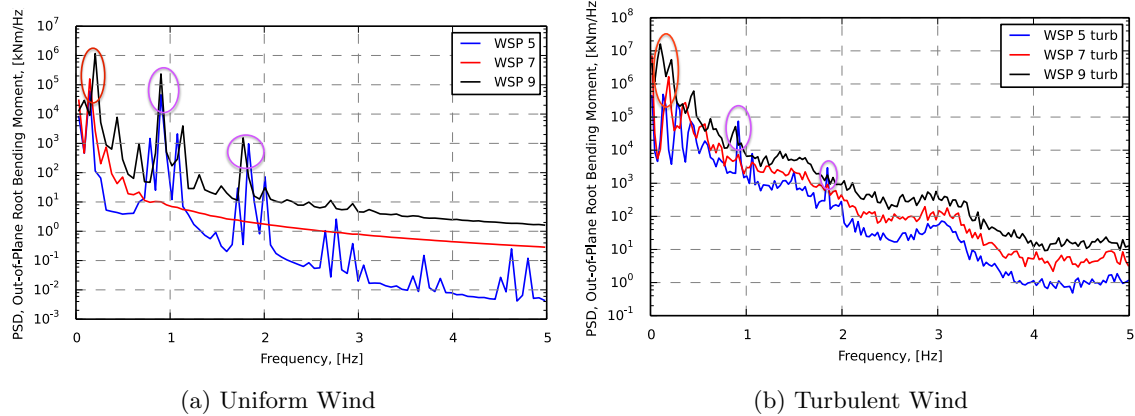
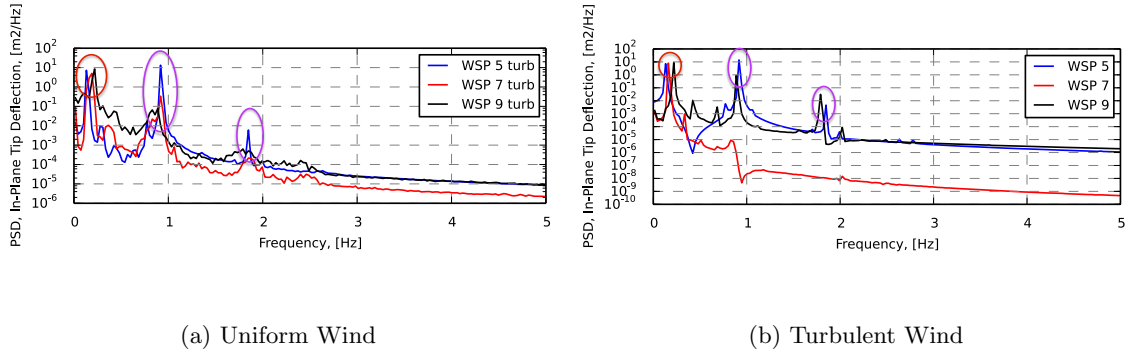
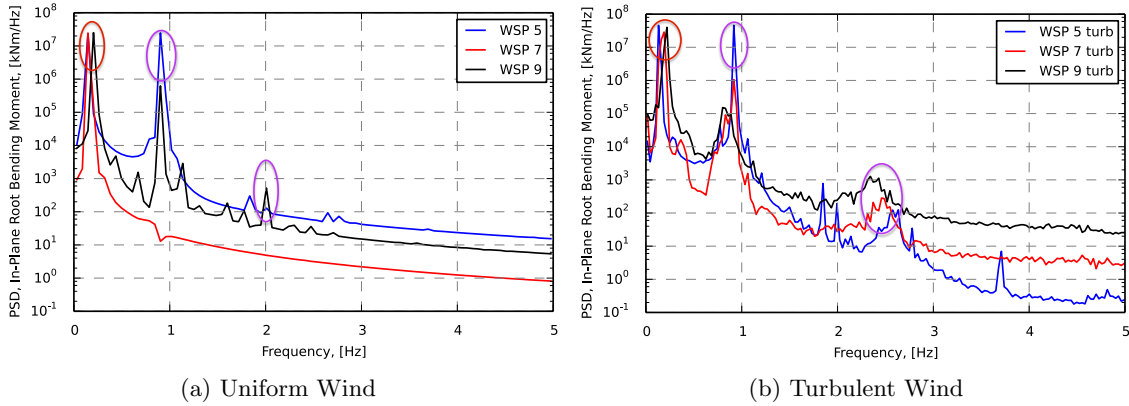


Figure 6.10: Out-of-Plane Root Bending Moment

**Figure 6.11: In-Plane Tip Deflection****Figure 6.12: In-Plane Root Bending Moment**

From these graphs, one can identify the blade modes (encircled in purple) in table 6.2. The rotational speed of 11 rpm, mentioned earlier, occurs at a wind speed close to 7 m/s. With respect to the rotational speed harmonics, these are also observed, but are not encircled. The peak due to the rotational speed (encircled in red) or its harmonics and the interaction of the blade frequencies may lead to resonance, as noted earlier in the Campbell diagram. Consequently, this may lead to the coupling of certain blade modes, into an aeroelastic instability, as observed in the aeroelastic frequency analysis.

6.3.3 Time Domain

The root bending moments and tip deflections, as a function of time, are included below, figures 6.13 to 6.14. The oscillations are uniform. In the turbulent case, it is expected for the signal to vary. However, it is also of interest to observe whether the turbulence excites or amplifies the deflection in an unstable manner. This effect is not observed.

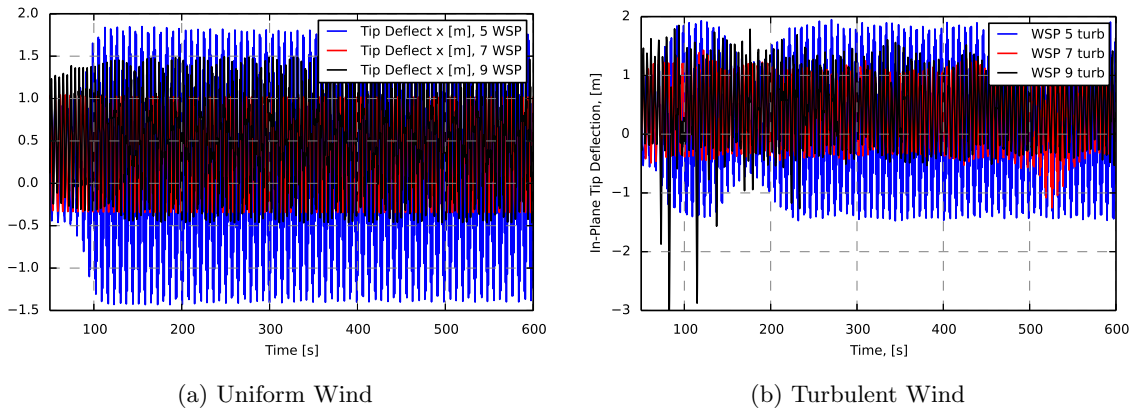


Figure 6.13: In-Plane Tip Deflection

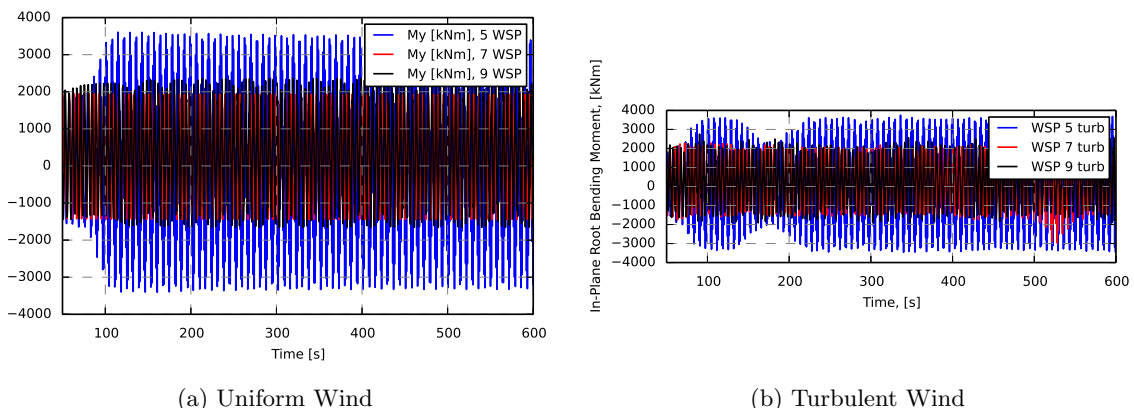


Figure 6.14: In-Plane Root Bending Moment

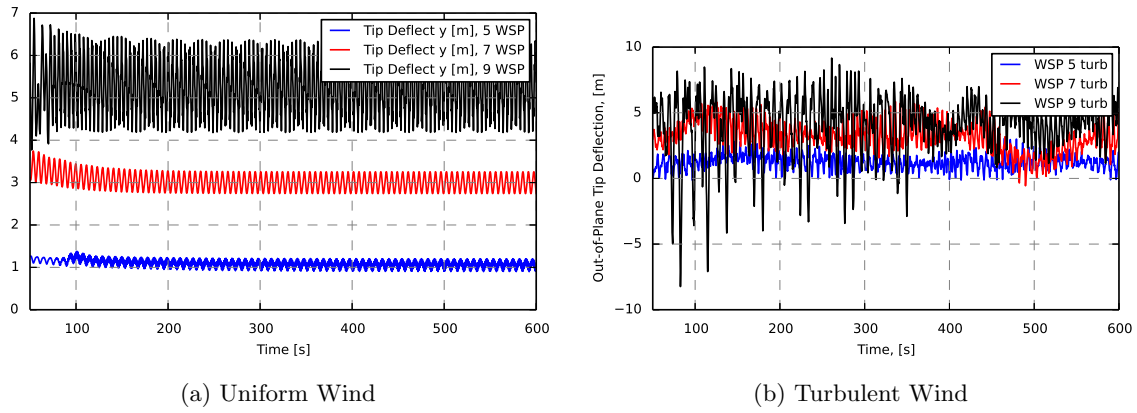


Figure 6.15: Out-of-Plane Tip Deflection

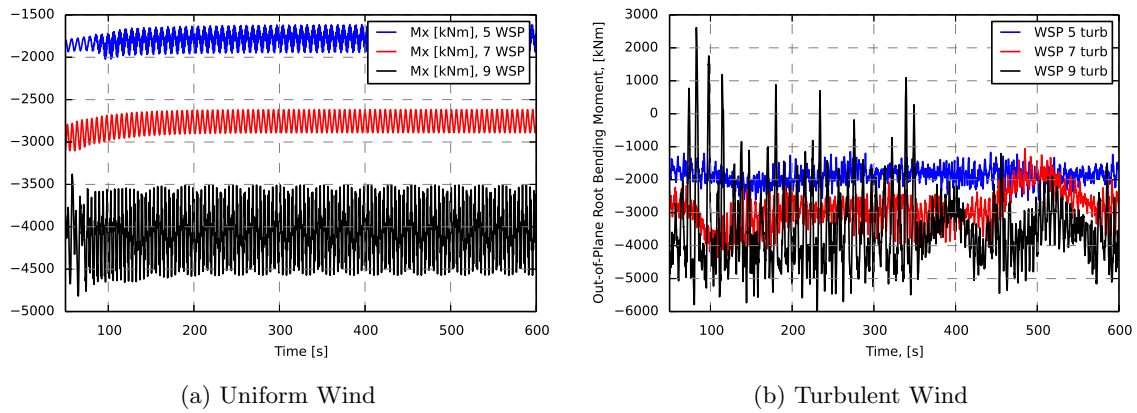


Figure 6.16: Out-of-Plane Root Bending Moment

6.4 Blade Deflection Analysis, GH Bladed

In-plane and out-of-plane deflection data series, obtained with GH Bladed, are analyzed and included in figures 6.17 and 6.18. In these figures, one observes the first peaks which belong to the rotational frequency. There are some other smaller peaks, which are the harmonics of the rotational frequency. In some cases, the first blade eigenfrequencies close to 0.5 and 1 Hz may be observed. The results match what one observes in the previous section.

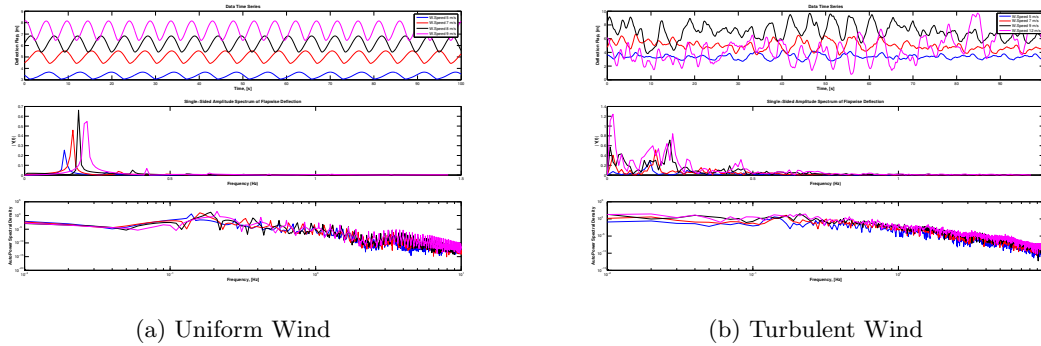


Figure 6.17: Out-of-Plane Deflections

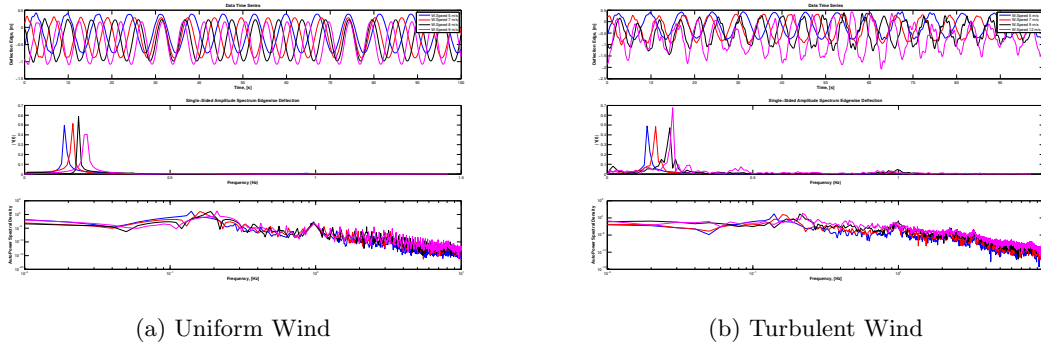


Figure 6.18: In-Plane Deflections

6.5 Discussion

The aeroelastic analysis of the isolated blade is relevant in this study, however once the system interacts as a whole, the shaft, the tower and the other blades influence the presence of aeroelastic instabilities. This means the isolated blade eigenfrequency analysis is relevant to a certain point.

From the aeroelastic analysis of the wind turbine, important blade frequencies are identified. The use of the Campbell diagram also helps identifying problematic rotational speeds and thus possible resonance effects on the wind turbine. In this case, it is advised to avoid a rotational speed of 11 *rpm*. On the contrary, by performing an analysis of the aeroelastic frequencies, with respect to wind speed, the interaction of the 3rd mode with 3P is identified, at low wind speeds. Whether the blade's elastic properties are enough to handle such an effect, is however not determined. The comparison of both analysis, proves that avoiding frequency crossings in the Campbell diagram, is not enough to ensure a wind turbine is safe from any aeroelastic instabilities.

Chapter 7

Large Rotor Study

A case with a larger rotor diameter for a lower rated wind speed is also studied. For this study, the blade length is increased to 66 meters. However, increasing the blade length does involve other aspects, like upscaling the blade structural properties, presented in Chapter 4.3. Therefore, in table 7.1, a review of some relevant blade scaling laws is included, DTU [18]. The blade's tip speed limitation is also changed to 80 m/s.

Table 7.1: Scale Laws for Blades, Structural Properties

Symbol	Defining Formula	Description	Size Dep.
$A(x)$	$= R^2 \int ds = R^2 \cdot A(x)$	Effective Area	R^2
$I_{\approx}(x)$	$= R^4 \cdot I_{\approx}(x)$	Moments of Inertia	R^4
$I_p(x)$	$= R^4 \cdot I_p(x)$	Polar Moment of Inertia	R^4
$J(x)$	$= R^4 \cdot J(x)$	Torsion Constant	R^4
$\bar{\rho}(x)$	$= \bar{\rho}_m(x) \cdot A(x)$	Linear Density	R^2
$\bar{E}(x)$	-	Mean Young's Modulus	Indep.
$\bar{G}(x)$	-	Mean Rigidity Modulus	Indep.

Although scaling the properties is an option, one is mainly interested in the cost of energy and not the structural properties. For this reason, one stiffens the blade by increasing the bending and torsional stiffness, by about ten orders of magnitude. For the cost of energy model, rotor cost is assessed as previously done. Figure 7.1 includes two blade cases, a stiff blade case and a soft blade case. This proves scaling the aerodynamics is beneficial, but also demonstrates the key role the blade's structural properties play. Therefore, using MYWP's structural properties for this longer blade is no longer valid. Other wind turbine components remain the same, which indeed has consequences. The conditions, the components are designed for, change with a larger rotor diameter.

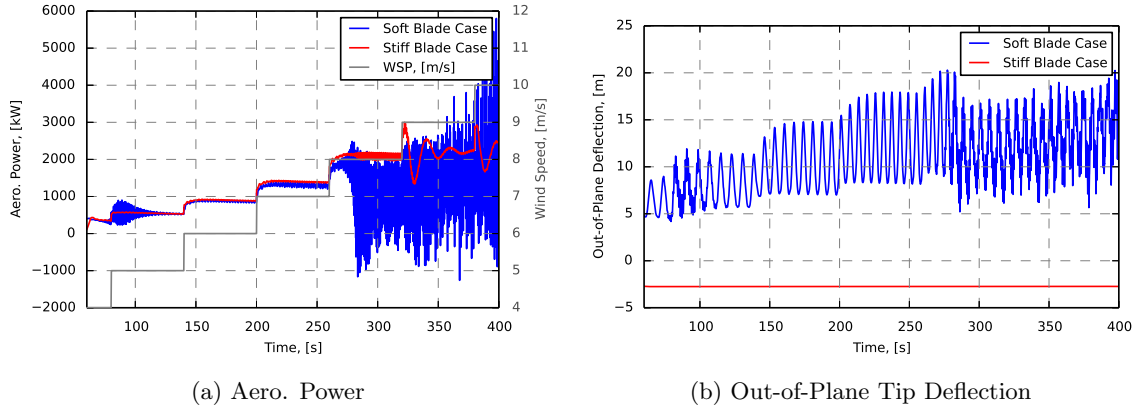


Figure 7.1: Stiff and Soft Blade Cases

Now rated power is reached at a wind speed of $\approx 8 \text{ m/s}$. However, the soft blade case hits the tower and the simulation fails. This is confirmed through the error message in HAWC2's log file, figure 5.16. One may also appreciate how power fluctuates with blade deflections. As expected, the stiffer blade handles deflections much better, translating into less power fluctuations. This case is important in order to highlight the importance of upscaling structural properties when upscaling the blade's length. To handle tower clearance, increasing tilt and coning angle, as defined in Section 4.4.1, are also possible options.

7.1 Results Overview

As in Section 5.5, one obtains chord and twist distributions, which minimize the cost of energy. Nevertheless, a larger rotor means more mass due to the increase in blade length and chord length. With a larger rotor, one reaches rated power at a lower wind speed and annual energy production increases as a consequence of this.

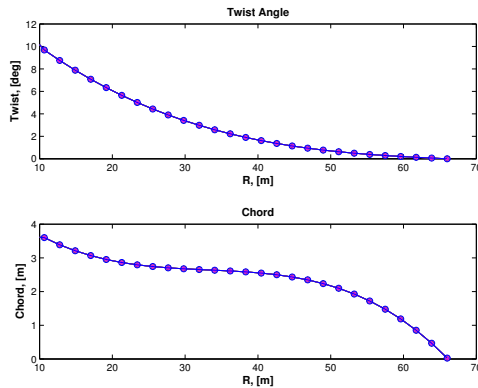


Figure 7.2: Blade Distribution

Table 7.2 compares the results obtained to those of the baseline. In this case, the thrust and bending moment constraint is not kept.

Table 7.2: Blade Scenario: Baseline & Large Blade

Parameter	Baseline	Blade Design
$COE_{rel.}$, [-]	1.456	1.458
AEP, [GWh]	6.87	8.01
Relative Rotor Cost, [-]	1.000	1.167
Thrust, [kN]	352	550

Below, figure 7.3, the wind turbine's aerodynamic power and thrust curve, simulated up to V_{rated} , are compared to the baseline.

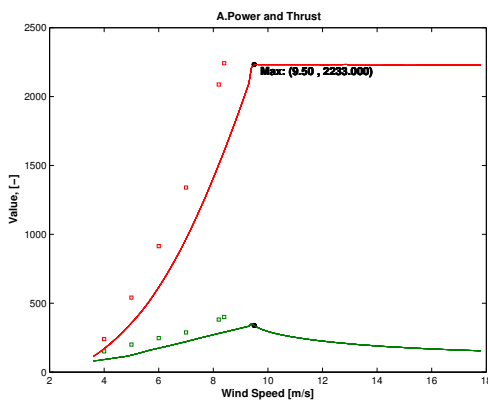


Figure 7.3: Power and Thrust Curves

7.2 Discussion

The results from a longer blade are clear. The increase in rotor cost is quite significant and the annual energy production, at this specific site, is not enough to outweigh the rotor's cost. This keeps the cost of energy unchanged. Annual energy production increases by about 14.5 %, however the rotor's cost is increased by about 17%.

It is important to mention this design is far from optimal. The structural properties are overestimated. This means constraints, like tip deflection or tower clearance, are neglected. Nevertheless, the blade's structural properties cannot remain the same as the baseline. For this reason, it is expected that the structural properties scale up with blade length. This would allow such a long blade to withstand the increase in thrust and blade root bending moments.

Chapter 8

Conclusions

As stated in the introduction, this thesis focuses in the design of a wind turbine blade for a specific site in China. Although the site possesses a wind speed of 7 m/s , it is still considered a low wind speed for wind power production. The assigned wind turbine site and reference wind turbine are studied. This pointed out the turbulence intensity level to be higher, than the one considered by the baseline's class. This is relevant for the wind turbine's blades, but also for other wind turbine components and their design specifications. During the aeroelastic simulations, this turbulence intensity level is used. Only with a proper number of DLC's, one can confirm if the wind turbine system remains fit for this higher turbulence level.

Results show the new blade design increases annual energy production at a higher rotor cost. This is due to the increase of the chord length at the blade's outboard section. The cost of energy is reduced by 2%, nevertheless the results vary with each aeroelastic code. Perhaps the combined implementation of DU airfoils and those developed by MYWP, could have decreased costs. Whether MYWP uses DU airfoils is unknown. However, a test is done by replacing the baseline's airfoils with the DU family, Appendix E. Some differences are observed, indicating DU airfoils may have higher lift characteristics. The C_p - λ curve, figure E.2, differs from the baseline as well. These curves, prove one cannot assume MYWP uses the DU airfoils, considered in this thesis.

Besides the effects on AEP and COE, the effects of leading edge roughness on wind turbine performance are also of interest. Leading edge roughness was simulated by the fixation of transition points at the pressure and suction sides of the airfoil. The change to the annual energy production of the wind turbine is clear. Including the effects of roughness, provides a more realistic power curve as well.

Besides the COE, the aeroelastic behaviour of the blade is also important. The aeroelastic stability analysis highlights some key operational speeds by means of the Campbell diagram. The identification of operational points may be of use for the development of a controller or for tower/blade structural modifications, which

directly affect their natural frequencies. With the use of HAWC Stab2, the aeroelastic frequencies versus wind speed are assessed. The coupling of the third aeroelastic mode with the rotational frequency 3P, is identified as a notorious aeroelastic instability. A runaway case and root bending moment / deflection time series are also inspected for the identification and the occurrence of such instabilities. With the runaway case, a plausible flutter instability is identified. The flutter speed and frequency are noted. With the analysis of the moment and deflection time series, in the frequency domain, the rotational frequencies and the blade eigenfrequencies are identified. Other high level frequencies are observed as well. Nevertheless, by visually inspecting the deflection signals, one cannot observe an amplitude change that would suggest the occurrence of an aeroelastic instability. Nevertheless, a sustained oscillation might also suggest that perhaps the wind turbine blade operates at a boundary, before an instability occurs. Despite this fact, by identifying the rotational speeds or wind speeds, at which the instabilities occur, one must take a step back and use this information in the re-design phase.

To target a lower rated wind speed, a study is performed for the case of a wind turbine with a larger rotor. A larger rotor captures more energy from the wind, thus it increases the annual energy production and reduces the cost of energy. For this rotor, no aeroelastic analysis is done as the blade's structural stiffness is overestimated. The cost of energy is the main driver in this case.

The wind turbine blade resulting from this work, is considered an iteration of one of the design phases, a blade undergoes. Final blade designs need to be thoroughly verified. As further work, the inclusion of the aeroelastic instabilities during the design algorithm could be an alternative. Nevertheless, this also requires the optimization of the blade's structural properties, which may be targeted with BECAS. It is beneficial to minimize the COE, but there are various elements that have to be considered. Perhaps a proper controller may avoid the undesired operational regimes, but then an aeroservoelastic analysis (DLC's) is required. This will assess the overall wind turbine performance, before stating whether the blade is fit for its main purpose: energy extraction.

Appendix A

Airfoil Polar Data

In this section, the additional polar data for DU airfoil family is included. The sets were obtained from RFoil, by setting Reynolds number to $6 \cdot 10^6$ and an angle of attack range of -10° to 20° . This range is the typical operating range for wind turbines.

A.0.1 DU00-W2-401

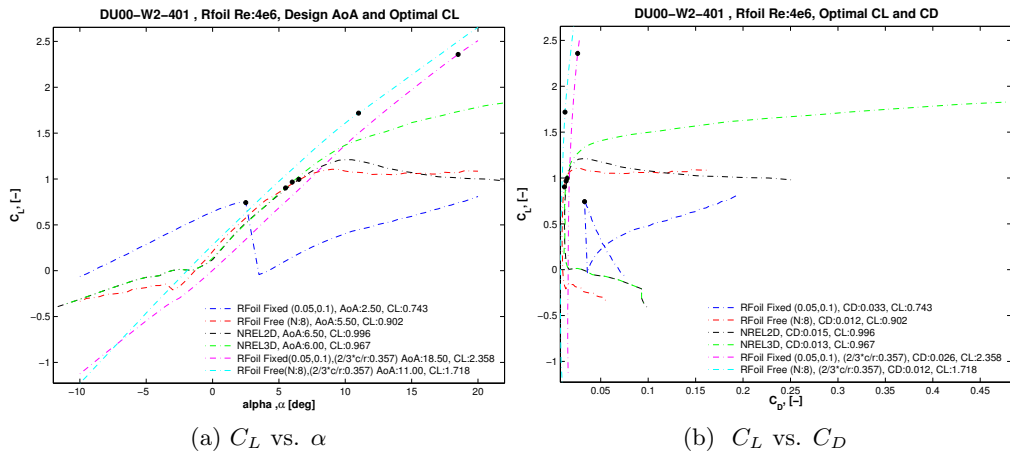


Figure A.1: DU00-W2-401 RFOIL

A.0.2 DU00-W2-350

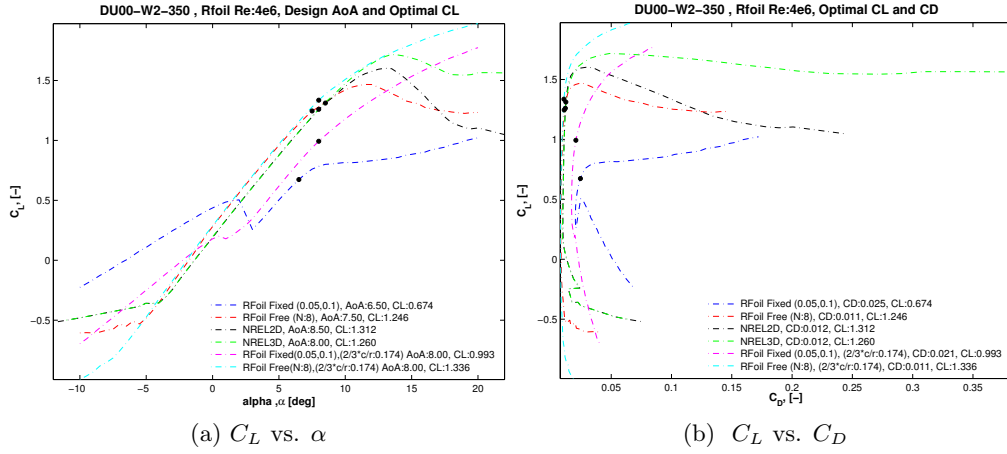


Figure A.2: DU00-W2-350 RFOIL

A.0.3 DU93-W-210

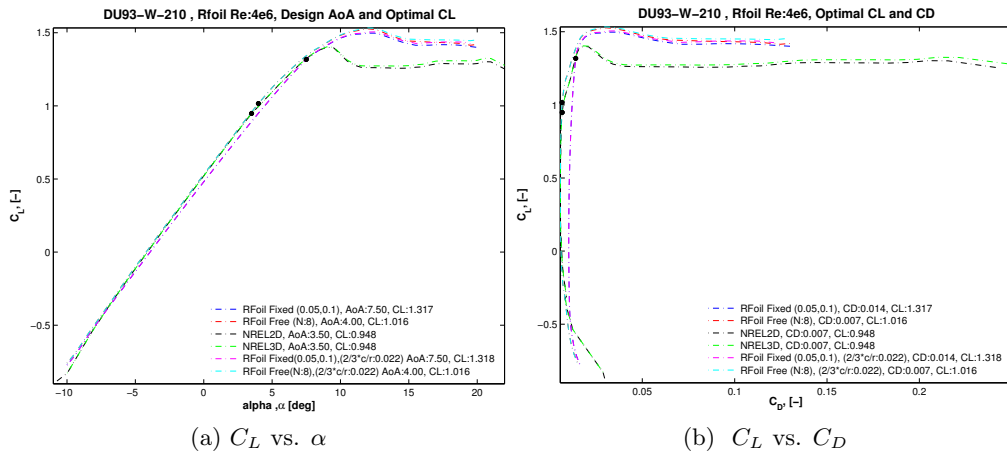


Figure A.3: DU93-W-210

A.0.4 DU00-W-212

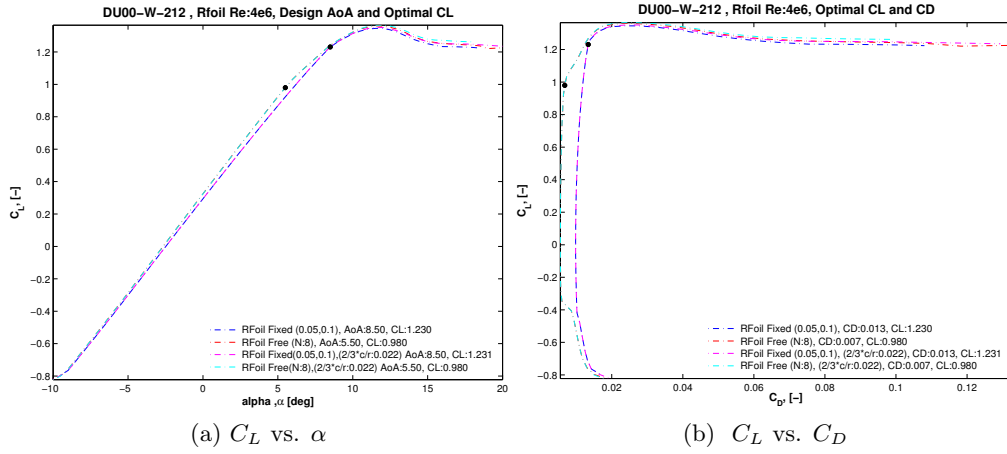


Figure A.4: DU00-W-212

A.0.5 DU96-W-180

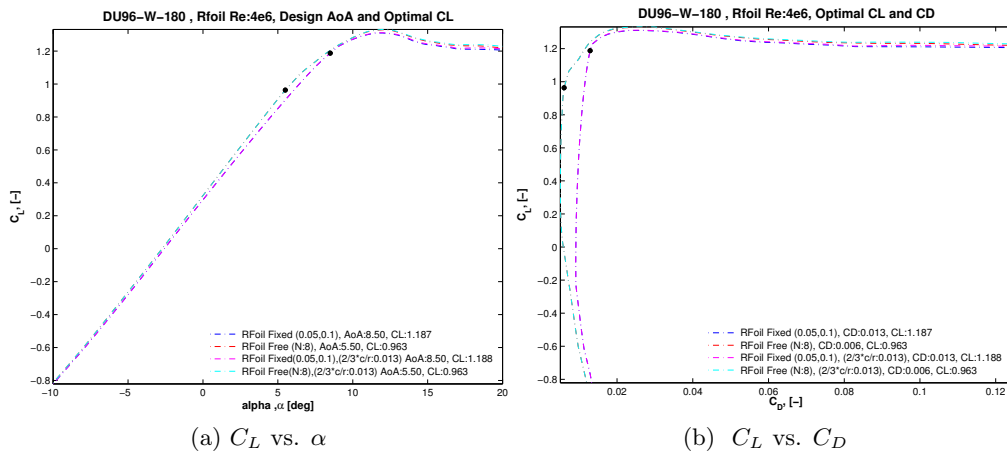


Figure A.5: DU96-W-180

A.0.6 NACA-64618

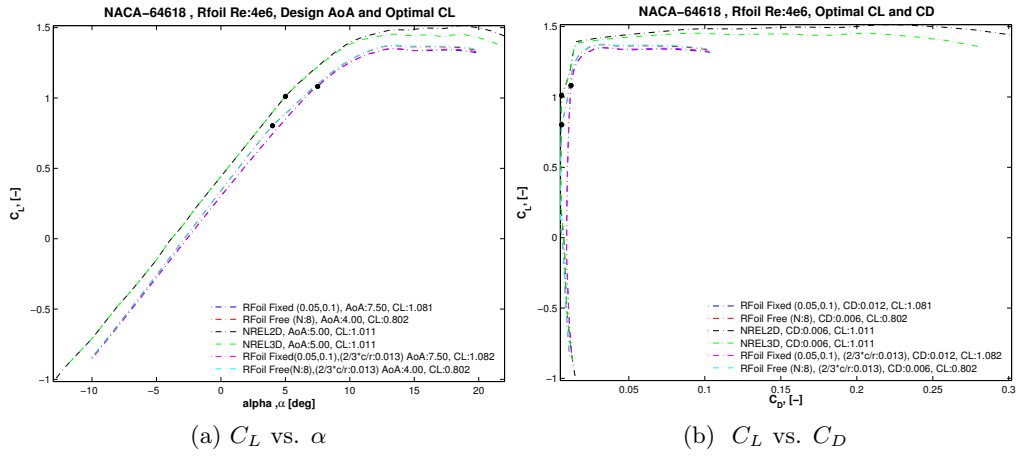


Figure A.6: NACA-64618

A.0.7 NACA-63215

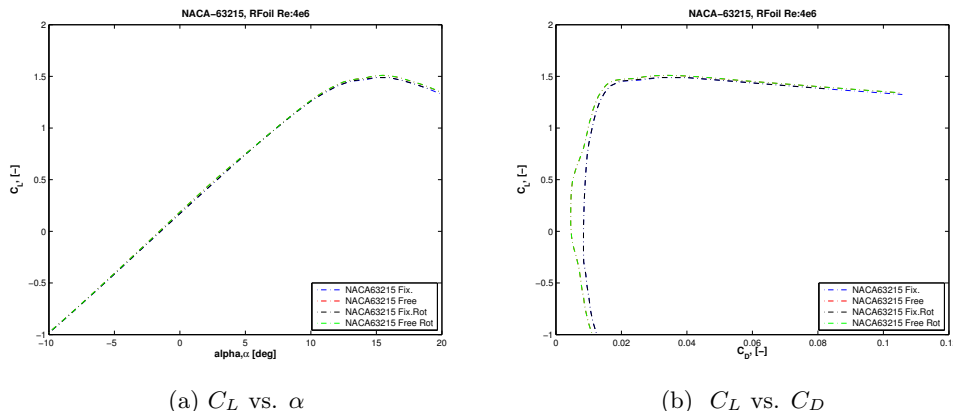


Figure A.7: NACA-63215

A.0.8 CL/CD All Airfoils

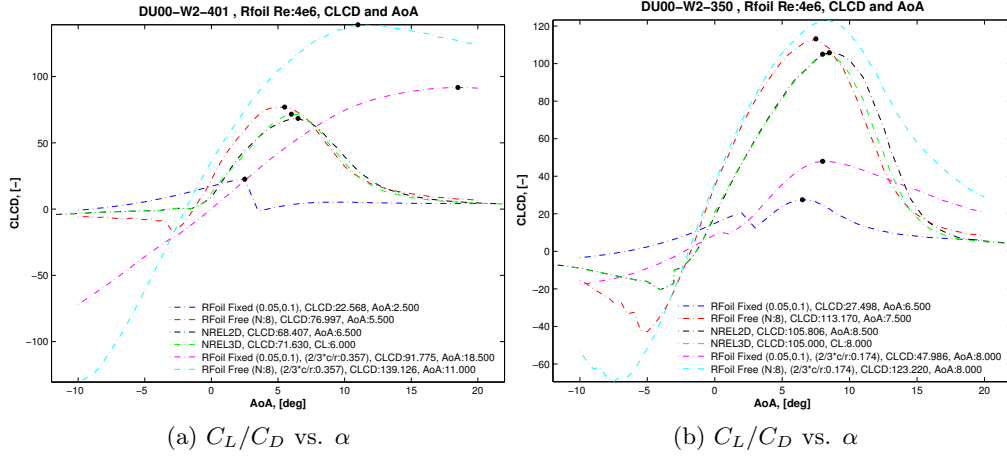


Figure A.8: DU00-W2-401, DU00-W2-350

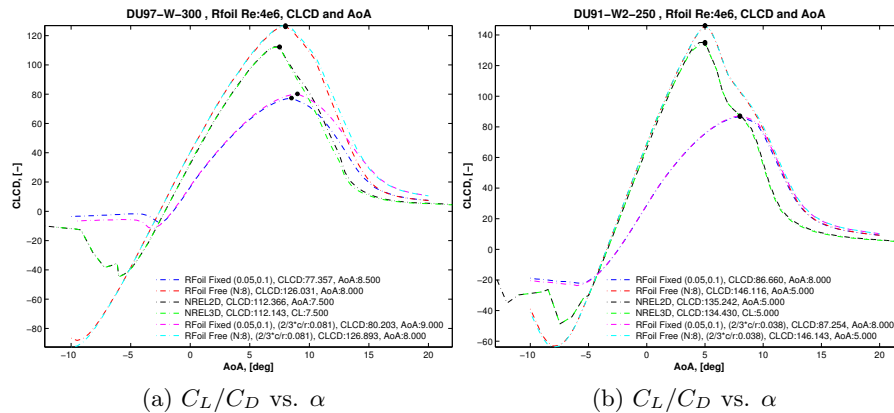
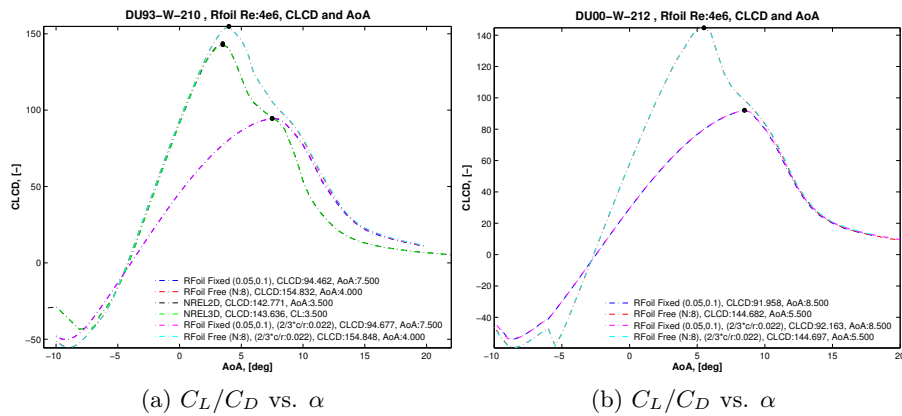
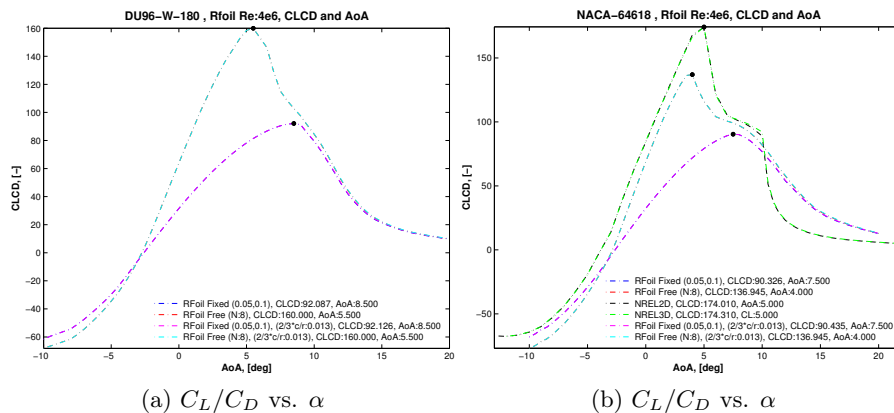
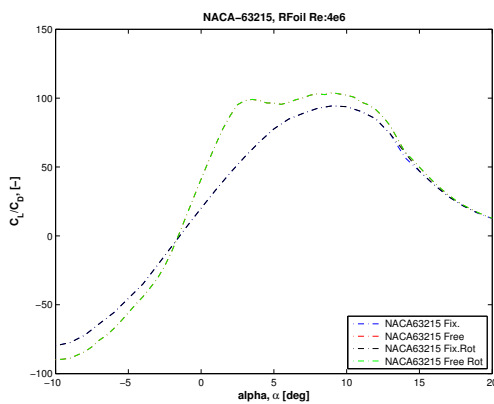


Figure A.9: DU97-W-300, DU91-W2-250

**Figure A.10:** DU93-W-210, DU00-W-212**Figure A.11:** DU96-W-180, NACA-64618**Figure A.12:** NACA-63215 RFOIL

Appendix B

Structural Design Test

B.1 Structural Blade Design, BECAS

The structural properties of the reference wind turbine blade are known and so are the materials used for its construction. Whether the new aerodynamic blade geometry remains compatible with the structural properties of the reference wind turbine blade, is an important and necessary assumption. For this reason, this assumption is tested with the beam cross section analysis software. BECAS is a cross sectional analysis tool for beam sections of arbitrary geometry, DTU [17]. This tool exists as a group of Matlab functions for the analysis of beam cross sections, with respect to their stiffness and mass properties.

```
: . . . . .
:     Structural      .
:     Assumption    .
:     (BECAS)       .
: . . . . .
```

Figure B.1: BECAS Algorithm

B.1.1 BECAS Input

With the use of BECAS, an algorithm is created to target the structural properties of the reference blade and generate a possible structural match per radial cross section of the blade. The main objective is to test whether the airfoils can allocate a structure, with the structural properties defined by the reference blade. BECAS may also provide the structural parameters required for a HAWC2 simulation. This is not done for this thesis, as the created structural model is not optimal (i.e. beam box dimensions, material thicknesses, layout, etc.). The reference blade is made of glass fibre reinforced plastic (GFRP). Consequently, the BECAS algorithm uses this material's typical properties in table B.1.

Table B.1: Typical Effective Material Properties for E-Glass / Carbon

Multidirectional Ply	Uniax	Biax	Triax	Balsa	Carbon	[-]
0° fibers	95	0	30	0	100	%
90° fibers	5	0	0	0	0	%
+45° fibers	0	50	35	0	0	%
-45° fibers	0	50	35	0	0	%
Young's Modulus, E_1	41.63	13.92	21.79	0.05	126	GPA
Young's Modulus, E_2	14.93	13.92	14.67	0.05	11	GPA
Shear Modulus, G_{12}	5.047	11.5	9.413	0.016	6.6	GPA
Poisson's ratio, ν_{12}	0.241	0.533	0.478	0.5	0.28	-
Shear Modulus, G_{13}	5.046	4.538	4.538	0.15	5.5	GPA
Mass Density, ρ	1915.5	1845.0	1845.0	110	1580	kg/m^3

Complementary to the material input, the airfoil coordinates, for the BECAS analysis, are processed. Interpolation between airfoil sections is done and the geometries are scaled with the appropriate chord and twist values. Figure B.2, portraits the beginning of the process, involving airfoil geometry preparation.

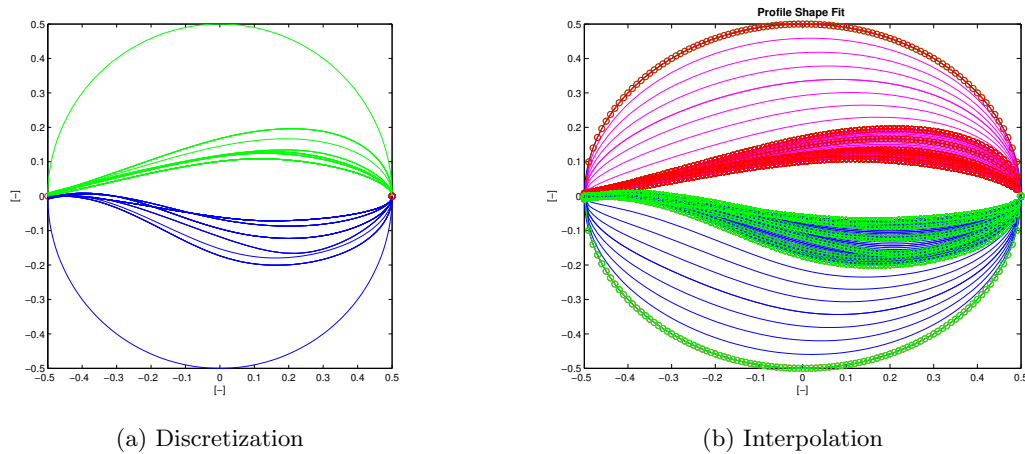


Figure B.2: Airfoil Geometry Preparation

B.1.2 Region Layout

With respect to the cross sectional layout, this one is defined by a number of key points (black circles) and nine regions delimited by them. With these regions and key points defined, the shear webs, spar caps and the blade's shell/skin are prepared for the cross sectional analysis. Below, in Figure B.4, an example of the regions and key points defined for a cross section, are shown.

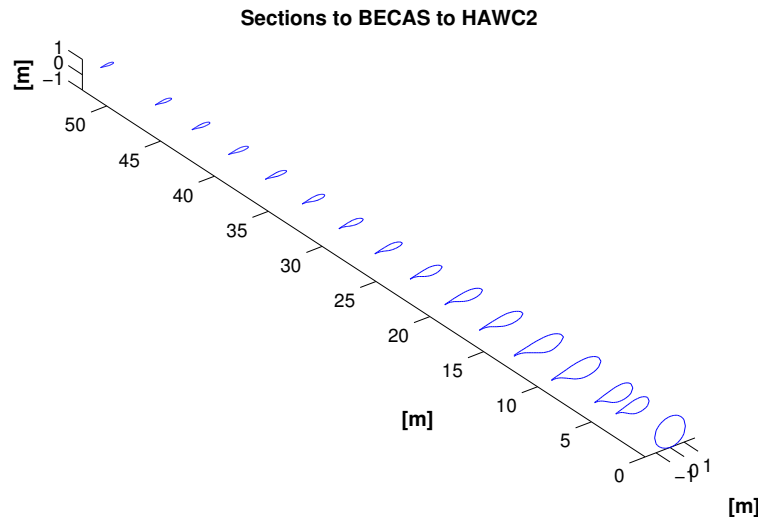


Figure B.3: BECAS Region Layout

Each of the multidirectional/unidirectional plies are region specific. This ensures the structural integrity of the blade, when subject to loads in different directions.

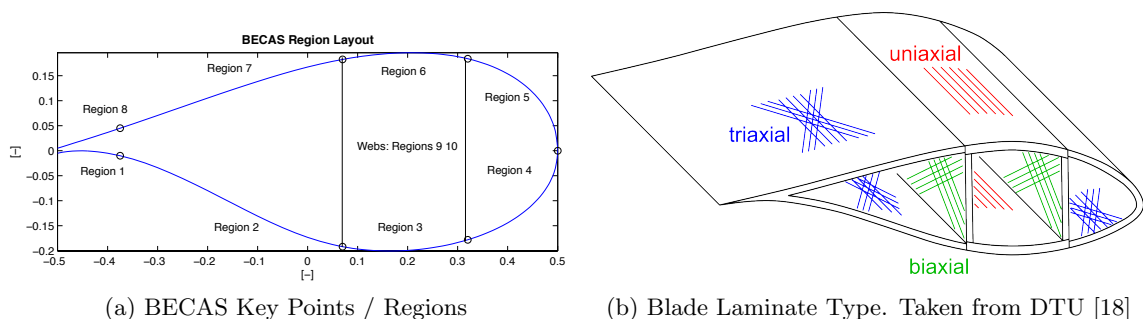


Figure B.4: BECAS Region Layout

B.1.3 Layout Results

Once the necessary parameters per radial station are defined, the cross sections are created. The structural properties for each section are saved into a file ready for HAWC2's use. In Figure B.5, the resulting material layout, the centre of mass, elastic axis position and other key features, are shown. The location of the elastic axis, the centre of gravity and the centre of mass affect the aeroelastic behaviour of the blade. It is for this reason that one uses the structural properties defined by the reference blade, since this BECAS structural design is not an optimized one.

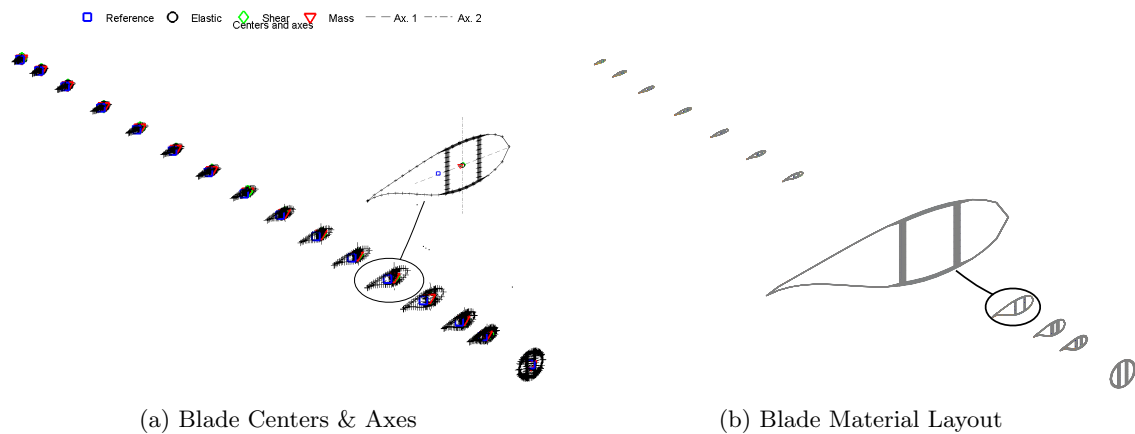


Figure B.5: BECAS Blade Structure Results

The comparison, of the resulting stiffness and mass distributions to those of the reference, is shown in Figure B.6. It is inferred that the proposed layout is structurally feasible, when targeting the distributions set by the reference wind turbine blade.

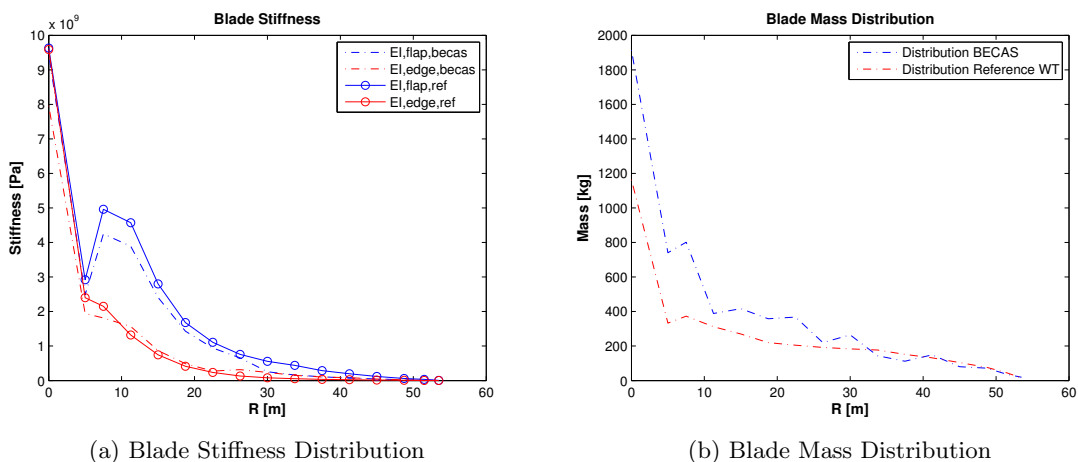


Figure B.6: BECAS Structural Property Distributions

Appendix C

HAWC2 Structural Properties

Appendix D

Blade Torsional Stiffness

D.0.4 Box Thickness

To calculate the torsional property of the blade, the blade structure is modelled as a simple rectangular, thin walled cross section or beam. Assumptions made are: beam box height is equal to blade thickness and the beam box width is equal to 60% of the chord length.

$$t = \frac{M}{\rho \cdot (2 \cdot b + 2 \cdot a)} \quad (\text{D.1})$$

The mass (m), the height of the box (b), the material density ρ and the box width (a) are known. One calculates the thickness with Eq. D.1. It is assumed the thickness is the same everywhere in the box.

D.0.5 Torsional Stiffness

For the calculation of the torsional stiffness of a thin walled rectangle, figure D.1, one can use Eq. D.2, taken from, Megson [51].

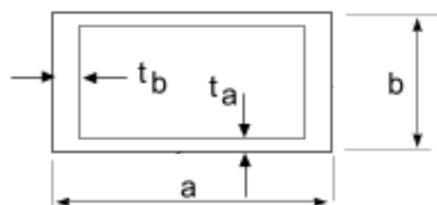


Figure D.1: Crossectional Box Section

$$J = \frac{4 \cdot (b \cdot a)^2}{\frac{2 \cdot a}{t} + \frac{2 \cdot b}{t}} \quad (\text{D.2})$$

By multiplying the torsional moment of inertia times the shear modulus, G , the torsional stiffness is found. The results are presented in Chapter 4, section 4.3.

Appendix E

Baseline Test: DU Airfoils

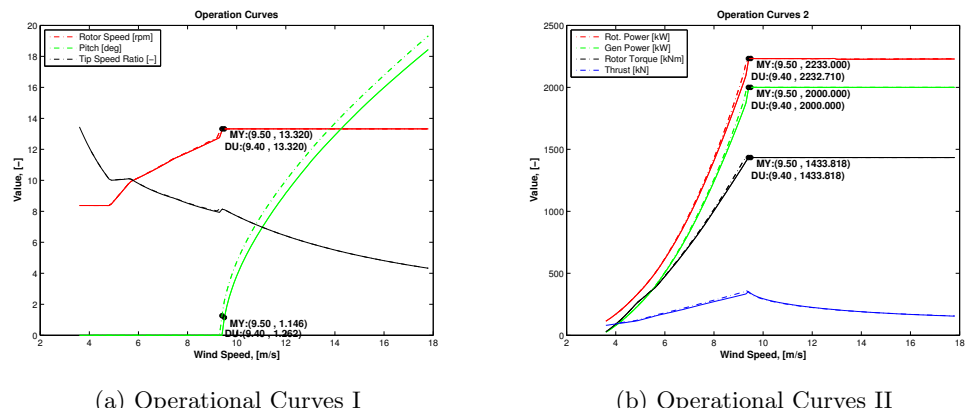


Figure E.1: MYWP Baseline & Baseline with DU Airfoils

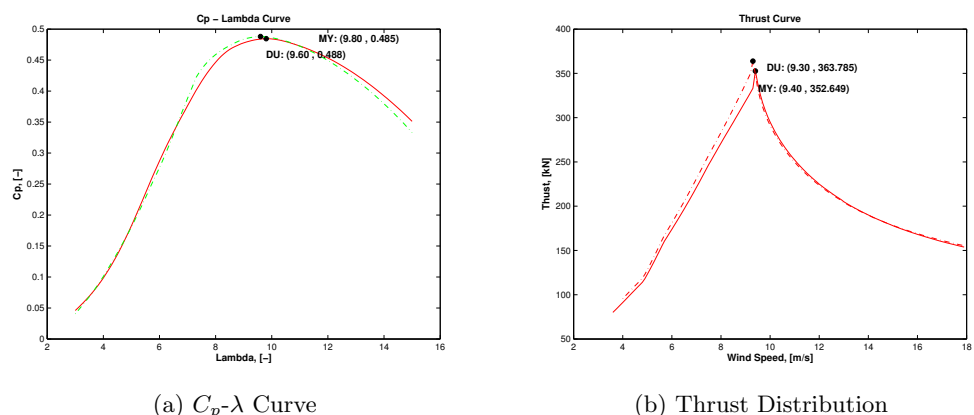


Figure E.2: MYWP Baseline & Baseline with DU Airfoils

References

- [1] A. Ahlström. *Aeroelastic Simulation of Wind Turbine Dynamics*. Trita-MEK. Department of Mechanics, Royal Institute of Technology, 2005.
- [2] Emre Alpman. Effect of selection of design parameters on the optimization of a horizontal axis wind turbine via genetic algorithm. *Journal of Physics: Conference Series*, 524(1):012044, 2014. ISSN 17426588, 17426596.
- [3] Jasbir S. Arora, editor. *Introduction to Optimum Design*. Academic Press, Boston, third edition edition, 2012. ISBN 978-0-12-381375-6.
- [4] Christian Bak. Aerodynamic design of wind turbine rotors. *Advances in Wind Turbine Blade Design and Materials*, 2013.
- [5] Christian Bak and W.A. Timmer. *Aerodynamic characteristics of wind turbine blade airfoils*, chapter 4, pages 109 – 149. Woodhead Publishing Series in Energy. Woodhead Publishing, 2013. ISBN 978 0 85709 426 1. 2013; Part 1.
- [6] Christian Bak, Nicholas Gaudern, Frederik Zahle, and Tomas Vronsky. Airfoil design: Finding the balance between design lift and structural stiffness. *Journal of Physics: Conference Series (Online)*, 524(1):012017, 2014. ISSN 17426596, 17426588.
- [7] Kirby A. Baker. *The Mathematics of Computer Graphics Course Notes*, 2002.
- [8] Thanasis K. Barlas, Frederik Zahle, Niels N. Srensen, Mac Gaunaa, and Leonardo Bergami. *Simulations of a rotor with active deformable trailing edge flaps in half-wake inflow: Comparison of EllipSys 3D with HAWC2*, chapter -. European Wind Energy Association (EWEA), 2012.
- [9] Cameron Beccario. Earth, February 2014. URL <http://earth.nullschool.net>.

- [10] E. Benini and A. Toffolo. Optimal design of horizontal-axis wind turbines using blade-element theory and evolutionary computation. *Journal of Solar Energy Engineering*, 124(4):357 – 363, 2002.
- [11] Jacob Berg, Jacob Mann, and Nielsen Morten. Notes for dtu course 46100: Introduction to micro meteorology for wind energy. Technical report, DTU, 2012.
- [12] E.A. Bossanyi. *GH Bladed - Theory Manual*, September 2007.
- [13] C. L. Bottasso, A. Croce, L. Sartori, and F. Grasso. Free-form design of rotor blades. *Journal of Physics: Conference Series*, 524(1):012041, 2014. ISSN 17426588, 17426596.
- [14] Hamid Sarlak Chivaee, Robert Flemming Mikkelsen, Sasan Sarmast, and Jens Nrkr Sorensen. Aerodynamic behaviour of nrel s826 airfoil at $re=100,000$. *Journal of Physics: Conference Series (Online)*, 524(1):012027, 2014. ISSN 17426596, 17426588.
- [15] CMA. China meteorological administration brochure, climatic resources, 2014. URL <http://www.cma.gov.cn/en/>.
- [16] A. Cordle and J. Jonkman. State of the art in floating wind turbine design tools. *U.S. National Renewable Energy Laboratory*, NREL/CP-5000-50543(0): –, 2011.
- [17] *User Manual for BECAS*. DTU Department of Wind Energy - Technical University of Denmark, v edition, 2012.
- [18] *Lecture Notes: 46320 LAC of WT and HAWC2 Intro Course*. DTU Department of Wind Energy - Technical University of Denmark, v edition, 2014.
- [19] Mads Dssing, Helge Aa. Madsen, and Christian Bak. Aerodynamic optimization of wind turbine rotors using a blade element momentum method with corrections for wake rotation and expansion. *Wind Energy*, 15(4):563–574, 2012. ISSN 1099-1824. doi: 10.1002/we.487.
- [20] D.L. Elliott, National Renewable Energy Laboratory (U.S.), United States. Dept. of Energy, United States. Environmental Protection Agency, American Wind Energy Association, and China Hydropower Planning General Institute. *Wind Energy Resource Atlas of Southeast China*. National Renewable Energy Laboratory, 2002.
- [21] World Energy Council. Enerdata. Average electricity consumption per electrified household, 2013.
- [22] Oriol Ferret Gasch. Wind turbine structural dynamics. Technical report, TU Delft, 2013.

- [23] Lee Jay. Fingersh, M. Maureen. Hand, Alan S. Laxson, and National Renewable Energy Laboratory (U.S.). *Wind turbine design cost and scaling model*. National Renewable Energy Laboratory Golden, Colo, 2006.
- [24] Peter Hauge Madsen Flemming Rasmussen. Wind energy division. riso. system engineering slides., 2008.
- [25] P. Fuglsang and H.A. Madsen. Optimization method for wind turbine rotors. *Journal of Wind Engineering and Industrial Aerodynamics*, 80(12):191 – 206, 1999. ISSN 0167-6105. doi: [http://dx.doi.org/10.1016/S0167-6105\(98\)00191-3](http://dx.doi.org/10.1016/S0167-6105(98)00191-3).
- [26] P. Fuglsang, C. Bak, J. G. Schepers, B. Bulder, T. T. Cockerill, P. Claiden, A. Olesen, and R. van Rossem. Site-specific design optimization of wind turbines. *Wind Energy*, 5(4):261–279, 2002. ISSN 1099-1824. doi: 10.1002/we.61.
- [27] Peter Fuglsang and Kenneth Thomsen. Site-specific design optimization of 1.5-2.0 mw wind turbines. *Journal of Solar Energy Engineering*, 123(4):296(8), 2001-11-01.
- [28] F. Grasso. Genetic algorithms in wind turbine airfoil design. In *EWEA 2011*. ECN, 2011.
- [29] Holierhoek J.G. Grasso F. Enhanced approach for simulation of rotor aerodynamic loads. *Conference Paper: ECN-M-12-003*, 1(1):17, 2012.
- [30] EUROS Graue H. Structural design of wind turbine blades. *Wind Turbine Rotor Blades 3rd Technical Conference*, 2011.
- [31] Giovanni Gualtieri and Sauro Secci. Methods to extrapolate wind resource to the turbine hub height based on power law: A 1-h wind speed vs. weibull distribution extrapolation comparison. *Renewable Energy*, 43(0):183 – 200, 2012. ISSN 0960-1481.
- [32] Dr. Craig Hansen. *NWTC Computer-Aided Engineering Tools. Airfoil Prep*, August 2014.
- [33] M. H. Hansen. Aeroelastic instability problems for wind turbines. *Wind Energy*, 10(6):551–577, 2007. ISSN 1099-1824. doi: 10.1002/we.242.
- [34] M.H. Hansen, Mac Gaunaa, and Helge Aagaard Madsen. *A Beddoes-Leishman type dynamic stall model in state-space and indicial formulations*. Denmark. Forskningscenter Risoe. Risoe-R. Riso, 2004. ISBN 87-550-3090-4.
- [35] M.O.L. Hansen. *Aerodynamics of wind turbines*. Earthscan, 2008. ISBN 1844074382, 9781844074389.
- [36] E. Hau, R. Harrison, T. T. Cockerill, and H. Snel. Conceptual design and costs of large wind turbines. *European Union Wind Energy Conference*, pages 128–131, 1996.

- [37] Dewey H Hodges and G Alvin Pierce. *Introduction to structural dynamics and aeroelasticity*. 2nd ed. Cambridge aerospace series. Cambridge University Press, New York, NY, 2011.
- [38] J. G. Holierhoek. Aeroelastic design of wind turbine blades. *Advances in Wind Turbine Blade Design and Materials*, 2013.
- [39] J.G. Holierhoek. *Aeroelasticity of Large Wind Turbines*. Energy Research Centre of the Netherlands, 2008. ISBN 9789090236278.
- [40] IEC-61400-1. *Wind Turbines - Part 1: Design requirements*. International Electrotechnical Commission, IEC, thrid edition, 2005.
- [41] Inc. IntraSearch. Mapmart, February 2014. URL <http://www.mapmart.com>.
- [42] Cohen J., Schweizer T., Laxson A., Butterfield S., Schreck S., Fingersh L., Veers P., and Ashwill T. Technology improvement opportunities for low wind speed turbines and implications for cost of energy reduction: July 9, 2005 – july 8, 2006. Technical report, National Renewable Energy Laboratory. Technical Report No. NREL/TP-500-41036, 2008.
- [43] Gareth Jones. *Genetic and Evolutionary Algorithms*, chapter 1. John Wiley and Sons, Ltd, 2002. ISBN 9780470845011.
- [44] M. Jureczko, M. Pawlak, and A. Myk. Optimisation of wind turbine blades. *Journal of Materials Processing Technology*, 167(2003):463 – 471, 2005. ISSN 0924-0136. *jce:title*;2005 International Forum on the Advances in Materials Processing Technology*/ce:title*.
- [45] Taeseong Kim, Anders M. Hansen, and Kim Branner. Development of an anisotropic beam finite element for composite wind turbine blades in multibody system. *Renewable Energy*, 59(0):172 – 183, 2013. ISSN 0960-1481.
- [46] E. Llorente, A. Gorostidi, M. Jacobs, W. A. Timmer, X. Munduate, and O. Pires. Wind tunnel tests of wind turbine airfoils at high reynolds numbers. *Journal of Physics: Conference Series*, 524(1):012012, 2014. ISSN 17426588, 17426596.
- [47] Don W. Lobitz. Aeroelastic stability predictions for a mw-sized blade. *Wind Energy*, 7(3):211–224, 2004. ISSN 1099-1824.
- [48] H. Aa Madsen, V. Riziotis, F. Zahle, M. O. L. Hansen, H. Snel, F. Grasso, T. J. Larsen, E. Politis, and F. Rasmussen. Blade element momentum modeling of inflow with shear in comparison with advanced model results. *Wind Energy*, 15(1):63–81, 2012. ISSN 10954244, 10991824.
- [49] J. F. Manwell, A. L. Rogers, and J. G. McGowan. Wind energy explained: Theory, design and application. *Wind Energy Explained: Theory, Design and Application*, pages –, 2010. doi: 10.1002/9781119994367.
- [50] MathWorks. *MATLAB optimization toolbox user's guide*. MathWorks, 2013.

- [51] T.H.G. Megson. *Chapter 18 - Torsion of beams.* Butterworth-Heinemann, Boston, fifth edition edition, 2013.
- [52] B Mendez, X Munduate, and U San Miguel. Airfoil family design for large offshore wind turbine blades. *Journal of Physics: Conference Series*, 524(1): 012022, 2014.
- [53] NASA. Openmdao, 2014. URL <http://openmdao.org/>.
- [54] NREL. Computer-aided engineering tools, 2014. URL http://wind.nrel.gov/designcodes/simulators/HARP_Opt/.
- [55] P. Passon, M. Kuehn, S. Butterfield, J. Jonkman, T. Camp, and T. J. Larsen. Oc3-benchmark exercise of aero-elastic offshore wind turbine codes. *Science of Making Toruqe From Wind*, 75:–, 2007. ISSN 17426588, 17426596.
- [56] Ricardo Pereira, Gerard Schepers, and Marilena D. Pavel. Validation of the beddoesleishman dynamic stall model for horizontal axis wind turbines using mexicodata. *Wind Energy*, 16(2):207–219, 2013. ISSN 1099-1824.
- [57] M. Preindl and S. Bolognani. Optimization of the generator to rotor ratio of mw wind turbines based on the cost of energy with focus on low wind speeds. In *Industrial Electronics Conference*, pages 906–911, 2011.
- [58] Nstor Ramos-Garca, Jens Nrkr Sorensen, and Wen Zhong Shen. Validation of a three-dimensional viscous?inviscid interactive solver for wind turbine rotors. *Renewable Energy*, 70(0):78 – 92, 2014. ISSN 0960-1481. Special issue on aerodynamics of offshore wind energy systems and wakes.
- [59] J.G. Schepers R.P.J.O.M. van Rooij, A. Bruining. Validation of some rotor stall models by analysis of the iea annex xviii field data. *ECN, TU Delft*, page 9, 2003.
- [60] G. Schepers. Advaned aerodynamic tools for large rotors, 2014. URL <http://www.eera-avatar.eu/>.
- [61] W.Z. Shen, J.N. Srensen, and Christian Bak. Tip loss corrections for wind turbine computations. *Wind Energy*, 8:457–475, 2005. ISSN 1095-4244.
- [62] Clifford B. Smith and Norman M. Wereley. Composite rotorcraft flexbeams with viscoelastic damping layers for aeromechanical stability augmentation. *ASTM Special Technical Publication*, 1304:62–77, 1997.
- [63] H. Snel. Review of aerodynamics for wind turbines. *Wind Energy*, 6(3):203–211, 2003. ISSN 10954244, 10991824.
- [64] SNL. The dakota project, 2014. URL <http://dakota.sandia.gov/>.
- [65] H.H. Song, J.J. Wang, Z.H. Hu, and J. Zhou. Research on low-wind-speed wind power. *Applied Mechanics and Materials*, 448-453:1811–1814, 2014.

- [66] N. N. Sorensen, J. A. Michelsen, and S. Schreck. Navierstokes predictions of the nrel phase vi rotor in the nasa ames 80 ft 120 ft wind tunnel. *Wind Energy*, 5(2-3):151–169, 2002. ISSN 1099-1824. doi: 10.1002/we.64.
- [67] W. A. Timmer. An overview of naca 6-digit airfoil series characteristics with reference to airfoils for large wind turbine blades. *47th AIAA Aerospace Sciences Meeting Including the New Horizons Forum and Aerospace Exposition*, pages –, 2009.
- [68] W.A. Timmer and R. P. J. O. M. van Rooij. Summary of the delft university wind turbine dedicated airfoils. *Journal of Solar Energy Engineering*, 125(part 4):488–496, 2003. ISSN 0199-6231.
- [69] Fabian Vorpahl, Michael Strobel, Jason M. Jonkman, Torben J. Larsen, Patrik Passon, and James Nichols. Verification of aero-elastic offshore wind turbine design codes under iea wind task xxiii. *Wind Energy*, 17(4):519–547, 2014. ISSN 1099-1824. doi: 10.1002/we.1588.
- [70] Xudong Wang, Wen Zhong Shen, Wei Jun Zhu, Jens Nrkr Sorensen, and Jin Chen. Shape optimization of wind turbine blades. *Wind Energy*, 12(8):781–803, 2009. ISSN 1095-4244.
- [71] Frederik Zahle, Christian Bak, Niels N. Sorensen, Tomas Vronsky, and Nicholas Gaudern. Design of the lrp airfoil series using 2d cfd. *Journal of Physics: Conference Series (Online)*, 524(1):012020, 2014. ISSN 17426596, 17426588.
- [72] Wei Jun Zhu and Wen Zhong Shen. *Integrated airfoil and blade design method for large wind turbines*, chapter –, pages –. Technical University of Denmark, 2013.

DTU Wind Energy is a department of the Technical University of Denmark with a unique integration of research, education, innovation and public/private sector consulting in the field of wind energy. Our activities develop new opportunities and technology for the global and Danish exploitation of wind energy. Research focuses on key technical-scientific fields, which are central for the development, innovation and use of wind energy and provides the basis for advanced education at the education.

We have more than 240 staff members of which approximately 60 are PhD students. Research is conducted within nine research programmes organized into three main topics: Wind energy systems, Wind turbine technology and Basics for wind energy.

Danmarks Tekniske Universitet

DTU Vindenergi
Nils Koppels Allé
Bygning 403
2800 Kgs. Lyngby
Telefon 45 25 25 25

info@vindenergi.dtu.dk
www.vindenergi.dtu.dk